Mind over Metabolism:
An Anatomical and Functional Analysis of Dorsal Motor Vagal Neurons Controlling Cardiac and Pancreatic Functions

Nicholas John Conley
Rochester, New York

B.S Behavioral Neuroscience, Northeastern University, 2018

A Dissertation presented to the Graduate Faculty of the University of Virginia in Candidacy for the Degree of Doctor of Philosophy

This dissertation is dedicated to B.Cat, Julia & Michael Conley, and Stella & Nicholas Loverdi

Department of Neuroscience, BIMS
University of Virginia
September 2024

Abstract

The vagus nerve, also known as the 10th cranial nerve, is a critical component of the parasympathetic nervous system, playing a fundamental role in the regulation of various physiological functions, including glucose metabolism and cardiac regulation. Originating in the brainstem, the vagus nerve extends through the neck and thorax to the abdomen, innervating major organs such as the heart, lungs, and digestive tract. Central to its function is the dorsal motor nucleus of the vagus (DMV), located in the medulla oblongata, which serves as a primary source of vagal efferent fibers.

The vagus nerve significantly influences glucose homeostasis. It modulates pancreatic insulin secretion and hepatic glucose production through its efferent and afferent pathways. The efferent fibers of the vagus nerve facilitate the release of insulin from the pancreas, thus promoting glucose uptake by tissues and maintaining blood glucose levels. Additionally, the DMV has been implicated in the feed forward release of insulin prior to meal consumptions known as the cephalic phase insulin response. Dysregulation of vagal activity has been implicated in metabolic disorders such as diabetes mellitus, where impaired vagal signaling can lead to reduced insulin sensitivity and abnormal glucose production.

In addition to its role in metabolic control, the vagus nerve exerts a profound influence on cardiac function. It modulates heart rate, myocardial contractility, and atrioventricular conduction through its extensive innervation of the heart. The vagal efferent fibers, originating from the DMV, release acetylcholine, which binds to muscarinic receptors on cardiac cells, leading to a decrease in heart rate (negative chronotropic effect) and a reduction in the force of contraction (negative inotropic effect). This parasympathetic control counterbalances the sympathetic nervous system, maintaining cardiovascular stability. Furthermore, the effects of the DMV and vagus nerve on the heart are clinically significant for mood disorders such as anxiety and post-traumatic stress disorder (PTSD), where

dysregulated heart rate variability and vagal tone have been observed. Dysfunction in vagal activity has been associated with various cardiac pathologies, including arrhythmias and heart failure, where diminished vagal tone can exacerbate disease progression.

This dissertation aims to explore the intricate roles of the vagus nerve and the DMV in regulating glucose tolerance and cardiac functions. By elucidating the mechanisms underlying vagal control of these vital processes, this research seeks to contribute to a better understanding of how autonomic dysregulation can lead to metabolic and cardiovascular phenotypes and how these systems may be therapeutically targeted for interventions.

Understanding the multifaceted roles of the vagus nerve and the DMV in glucose and cardiac regulation is crucial for developing novel strategies to treat metabolic and cardiovascular disorders. This dissertation will delve into the physiological, cellular, and molecular mechanisms by which the vagus nerve maintains homeostasis, highlighting its importance as a therapeutic target in modern medicine.

Acknowledgements

I would like to thank my mentor, professor John Campbell for his continued guidance, understanding and mentorship. The lab environment that Dr. Campbell cultivated was critical for my success in this program and on the following projects. I am beyond grateful for the discussions and generously kind mentorship style that have allowed me to freely explore and develop the concepts, techniques, and mind-set necessary to learn and grow as a scientist. I have been beyond grateful to work and learn with him.

I would like to thank the professors on my committee; Michael Scott (former), Stephen Abbott, Ali Güler, Heather Ferris, and Mark Beenhakker. Thank you all for your continued time, intellectual contributions, and project feedback throughout this experience. Your advice on my projects has steered it effectively and your questions have helped me to shore up weakness in my projects and in myself as a scientist. Thank you for challenging and helping me through this process and for dealing with all the rescheduling.

I would especially like to thank the very impressive research assistants that have helped make this work possible; Lily Kauffman, Lane VanderVoort, Pati Castro, Ian Irushalmi, Cate Bundon and Chelsea Li. Without your dedicated work and curiosity these projects would not have been achievable. Additional I would like to thank the members of the Campbell Lab, especially Maisie Crook and Addison Webster. Your support, friendship and our discussions have been monumental in getting me through this, thanks for sticking by as long as you did. In a similar vein I would like to thank cohorts in my program, namely Ryan Brown, David Tyus and Katriel Cho for your unending support and friendship. I hope you know how critical you were to me being here today.

I would like to thank the Neuroscience department, Biology Department, and BIMS for supporting me throughout graduate school. Especially Nadia Cempre and Kim Knotts who have been fantastic and understanding program administrators. Finally, a special thank you to my family. Thank you to my mom (Julia) and dad (Michael) for always encouraging me to do what was intellectually compelling, for supporting my career in science both mentally and financially and for helping me get back on my feet when I had lost them. It is because of you that I am here. I would like to thank my sisters for their support through my life and would especially like to thank my grandma Stella and grandpa Nicholas Loverdi for encouraging a love of animals, science, chess, and riddles, at a very young age.

May you always be at peace Nicholas -The other big Nick

B Cat, enjoy chasing the butterflies

Table of Contents

Summary of Figures

Introduction

Figure 1: Schematic of the functional organization of Nerve X- DMV.

Figure 2: Contrasting effects of glucagon and insulin within glucose regulating tissues

Figure 3: Neuronal innervation of the pancreatic nervous system

Vagal Motor Neurons Control Heart Rate and Anxiety

Figure 4. Optogenetic stimulation of DMV elicits bradycardia in male and female mice:

A: Genetic crossbreeding paradigm used to generate transgenic mice harboring loxP-flanked ChR2 in Chat-positive motor neurons

B: Photostimulation-evoked action potentials from DMV motor neurons to 20 Hz stimulation. Representative diagram illustrating confirmed locations of optogenetic probes

D: Representative images of DMV (top) and NA (bottom) stained for the neuronal activation marker, c-Fos (middle panel; red) and GFP (left panel; green) immunoreactivity confirming c-Fos activation in DMV, but not NA, after DMV photostimulation

E: Schematic illustrating time course of optogenetic studies in awake mice

F-G: Representative trace (F) and mean HR (G) showing optogenetic stimulation of DMV produced a bradycardia in mice expressing $Chat^{cre}$;ChR2 but not in $Chat^{cre}$ mice.

H-I: Representative trace (H) and mean HR (I) showing i.p. muscarinic parasympathetic blocker, methyl-scopolamine, eliminated the photostimulation-induced bradycardia, while sympathetic blockage with b-1 receptor blocker atenolol mildly reduced this bradycardia.

J: Representative images of probe site (top) and immunohistochemical staining of NA showing c-Fos activation after stimulation of NA

K-L: Representative trace (K) and mean HR (L) showing the nicotinic antagonist, hexamethonium (i.p.) abolished photostimulation-induced bradycardia in both DMV and NA.

Figure 5. DMV innervates cardiac tissue through the vagus nerve in male mice:

A: Schematic showing injection into the epicardial fat pad and labeling in both CVN brain regions

B: Representative images of DMV and NA after cardiac injection of retrograde tracers, rhodamine (left in red) and cholera toxin subunit B (CT-B; right in green)

C: Both rhodamine and CT-B significantly labeled cardiac projecting neurons in NA and DMV as analyzed by a repeated measure two-way ANOVA with Sıdak's post hoc

D-E: Representative image (D) and mean cell count (E) showing a right cervical vagotomy significantly attenuated CVN^{DMV} numbers ipsilateral to vagotomy as analyzed by a two-tailed paired Student's t test.

Figure 6. Differential electrophysiological properties of CVN^{DMV} compared to CVN^{NA} in male mice:

A: Rhodamine-positive DMV neurons showing pipette (top) and rhodamine (bottom; red)

B: Representative immunofluorescence image of CVN^{DMV} showing biocytin recovered patched cardiac-labeled neurons are cholinergic

C-D: Representative trace (C) and mean firing rate (D) of CVN^{DMV} neurons show significantly higher spontaneous firing rates compared to CVN^{NA}, with the majority of CVN^{DMV} firing as analyzed by a Mann Whitney test.

E: No statistical differences in resting membrane potential were found between CVN^{DMV} and CVN^{NA} using a two-tailed unpaired Student's t test

F: Representative traces of membrane responses from CVN^{NA} (top) and CVN^{DMV} (bottom) to stepped current injections

G: Current-voltage (I-V) relationship graph obtained from CVN^{NA} and CVN^{DMV}

H: R_{input} was higher in CVN^{DMV} compared to CVN^{NA} as analyzed by a two-tailed unpaired Student's t test

J: Representative action potential responses in CVN^{NA} (top) and CVN^{DMV} (bottom) in response to 300 pA injection of direct depolarizing current (I). Action potential response curves were higher in CVN^{DMV} compared to CVN^{NA} in response to 50 pA-step injections of direct depolarizing current as analyzed by a repeated measure two-way ANOVA with Sıdak's post hoc

Figure 7: Chemogenetic Stimulation of the DMV produces bradycardia and reduces anxiety in both male and female mice.

A. Schematic of dorsal vagal complex genetic targeting strategy and virus (AAV1-CreON/FlpON-hM3Dq-HA
B. Representative images of rostral, intermediate, caudal DMV and nAMB stained for HA (magenta) and H2b-GFP (green) immunoreactivity in Chat-Cre;hox2b-Flp;R26-dsHTB mice after DMV injection of AAV1-CreON/ FlpON-hM3Dq-HA
C. Percentage of H2b-GFP+ cells immunoreactive for hM3Dq-HA in the rostral, intermediate, and caudal DMV and nAMB(C). Effect of CNO on HR in DMV-hM3Dq mice over 24-h period. CNO (1 mg/kg, i.p.) injected at time = 0 min. Data analyzed using repeated measure ANOVA with Tukey's post hoc.
D. Effect of i.p. saline, CNO and CNO+MA on HR in DMV-hM3Dq (magenta) and control mice (black); comparisons are to baseline using a repeated measure ANOVA with Tukey's post hoc
E. Effect of i.p. saline, CNO and CNO+MA on HR in DMV-hM3Dq (magenta) and control mice (black); comparisons are to baseline using a repeated measure ANOVA with Tukey's post hoc
F. Schematic of open field experiment
G. Effects of i.p saline and CNO on time in the center
H. Effects of i.p saline and CNO on time spent moving

I. Correlation between changes in HR and center time between saline and CNO conditions in DMV-hM3Dq mice

J. Schematic of elevated plus maze (EPM) experiment

K. Effects of i.p. saline vehicle, CNO and CNO+MA administration on open-arm time

L. Effects of i.p. saline vehicle, CNO and CNO+MA administration on time spent moving

M. Pearson correlation between changes in HR and open-arm time in saline vs. CNO conditions in DMV-hM3Dq mice

N. Effects of i.p. MA and AQ-RA-741 on open-arm time in elevated plus maze, compared to saline; same saline and CNO+MA data as in Figure 7K.

Supplementary Figure 1: Related to Figure 7

A. Representative images of intermediate DMV hemisphere stained for H2b-GFP (green) and fluorogold immunoreactivity (blue) in Chat-Cre;Phox2b-Flp;dsHTB mice after (i.p.) systemic injection of retrograde tracer Fluorogold (136 of 139, 97.8%, Fluorogold+ DMV neurons were also H2b-GFP+); n=4 mice).

B. Representative images of intermediate DMV stained for HA (magenta) and H2b-GFP (green) immunoreactivity in $R26^{ds\text{-}HTB}$ mice (Cre-/Flp-) after DMV injection of AAV1-CreON/FlpON-hM3Dq-HA. (n=3)

C. Effect of saline (white), CNO (magenta) and CNO+MA (green) on HR in DMV-hM3Dq and control mice; comparisons to vehicle. (n=8)

D. Effect of saline or CNO on control mice, which lack hM3Dq expression, open arm time in the elevated plus maze, n=8 mice.

E. Effect of saline, CNO and CNO+MA in DMV- hM3Dq mice on head dip events in the elevated plus maze.

F. Effect of saline, CNO and CNO+MA in DMV- hM3Dq mice on velocity in the elevated plus maze

Vagal Motor Control of Glucose Metabolism

Figure 8. Calb2 expression marks a discrete population of DMV neurons with unique spatial localization

A. Calb2 expression levels in Chat+DMV neurons

B. Representative RNA scope in situ hybridization of Calb2, Grp and Chat

C. Calb2+ DMV spatial localization model

D. Schematic of DMV; intersectional approach for targeting Calb2+ DMV

E. Calb2-Cre;Chat-Flp;dsHTB mouse

F. Chat-Cre;Phox2b-Flp;CaTCh construct,

G. Representative images of CaTCh expression in rostral, intermediate, and caudal DMV.

Figure 9. Calb2+ DMV neurons project to the pancreas

A: Schematic of PLAP anterograde tracing (top) and fluorescence anterograde tracing (bottom)

B: PLAP anterograde tracing in pancreas from Chat-Cre+ DMV cells

C: PLAP anterograde tracing in pancreas from Calb2-Cre+ DMV cells

D: PLAP anterograde tracing in pancreas from Grp-Cre+ DMV cells

E: PLAP anterograde tracing in stomach from Calb2-Cre+ DMV cells

F-H: Fluorescent anterograde tracing in cleared pancreas from Calb2-Cre+ DMV cells

Figure 10. DMV chemogenetic activation improves glucose tolerance

A. Schematic of optogenetic-IPGTT paradigm

B. Optogenetic-IPGTT, Chat-Cre;Phox2b-Flp;CaTCh, absolute values,

C. Optogenetic-IPGTT, Chat-Cre;Phox2b-Flp;CaTCh, % baseline change

D. Optogenetic-IPGTT, Chat-Cre;Phox2b-Flp;CaTCh, area under the curve

E. Schematic of chemogenetic-IPGTT paradigm

F. Chemogenetic-IPGTT, Chat-Cre;Phox2b-Flp;dsHTB, absolute values,

G. Chemogenetic-IPGTT, Chat-Cre;Phox2b-Flp;dsHTB, baseline change,

H. Chemogenetic-IPGTT, Chat-Cre;Phox2b-Flp;dsHTB, area under the curve

I. Chemogenetic-IPGTT, Calb2-Cre;Chat-Flp;dsHTB, absolute values,

J. Chemogenetic-IPGTT, Calb2-Cre;Chat-Flp;dsHTB, % baseline change,

K. Chemogenetic-IPGTT, Calb2-Cre;Chat-Flp;dsHTB, area under the curve

L. Insulin ELISA Calb2-Cre;Chat-Flp;dsHTB; baseline saline and CNO 1.0mg/kg

Supplementary Figure 2 Related to Figure 9,10

A: PLAP anterograde tracing in stomach from Chat-Cre+ DMV cells

B: PLAP anterograde tracing in liver from Chat-Cre+ DMV cells

C: PLAP anterograde tracing in stomach/LES from Grp-Cre+ DMV cells

D: 3.5mg/kg CNO Chemogenetic-IPGTT, Calb2-Cre;Chat-Flp;dsHTB

E: Males 3.5mg/kg CNO Chemogenetic-IPGTT, Calb2-Cre;Chat-Flp;dsHTB

F: Females 3.5mg/kg CNO Chemogenetic-IPGTT, Calb2-Cre;Chat-Flp;dsHTB

Conclusion Figures

Figure 11: DMV-mediated glucose tolerance Model

Figure 12: DMV-mediated anxiolysis schematic

Figure 13: Hypothesized schematic of DMV-mediated pro-foraging behavior

Summary of Acronyms

ACh- Acetylcholine

ANS- Autonomic Nervous System

ARC- Arcuate nucleus

AQ- AQ-RA-741

CaTCh- Cre and Flp dependent excitatory opsin

CeA- Central nucleus of the amygdala

CG- Celiac ganglia

ChAT- Choline-acetyltransferase

CNS-Central Nervous System

CNO- Clozapine-n-oxide

CVN- Cardiovagal neurons

DMV- Dorsal Motor Nucleus of the Vagus

DVC- Dorsal Vagal Complex

ENS- Enteric Nervous System

EPM- Elevated Plus Maze

GLP-1- Glucagon like peptide 1

GRP- Gastrin releasing peptide

GSSG- Glucagon receptor

HFD- High Fat Diet

IC- Insular cortex

ISH- in situ hybridization

I.P.- Intra peritoneal

IPG- Intra pancreatic ganglia

LH- Lateral hypothalamus

MA- Methyl-atropine

mRF- Medullary reticular formation

nAMB- nucleus ambiguous

NE- Noradrenaline

NO- Nitric oxide

NPY- Neuropeptide Y

NRO- Raphe obscurus nucleus

NTS- Nucleus of the solitary tract

OF- Open field maze

PACAP- Pituitary adenylate cyclase activating polypeptide

PB- Parabrachial nucleus

PG- Paravertebral ganglia

PNS- Peripheral Nervous System

PP- Pancreatic Polypeptide

PVH- Paraventricular hypothalamus

SMG- Superior mesenteric ganglia

SP- Substance P

T2D- Type 2 Diabetes

TRH- Thyrotrophin-releasing hormone

VIP- Vaso intestinal peptide

VN- Vagus nerve

VNS- Vagus Nerve stimulation

Chapter 1. Introduction

Functional Organization of the Efferent Vagus Nerve

The vagus nerve (VN) or 10th cranial nerve serves as the parasympathetic conduit between the central nervous system (CNS) and organs of the cardiac, digestive, and immune systems in the abdominal and thoracic cavities. It is the longest nerve in the autonomic nervous system. While generally referred to by the singular 'vagus' it is important to note that the right and left vagal branches have different, and sometimes overlapping innervation of target organs (2). The vagus nerve contains both the efferent motor and parasympathetic fibers from CNS vagal nuclei to visceral organs as well as afferent sensory fibers from those organs back up to the CNS (*1*). Approximately ~80% of the VN's fibers are afferent sensory fibers while only ~20% are efferent motor fibers (*2*). The VN innervates the pharynx, soft palate, larynx, heart, lungs, liver, gallbladder, stomach, pancreas, and intestines. In addition to motor reflexes such as coughing, sneezing, swallowing, and vomiting, the vagus nerve coordinates a host of physiological functions such as cardiovascular activity, respiration, and digestive processes such as gastric acid secretion, insulin secretion, and gastrointestinal motility.

The vagus nerve (VN) innervates various tissues, making it a significant focus of research due to heterogeneity and the multitude of pathological states that can result from its dysfunction. However, this functional complexity and heterogeneity also poses a challenge, as activating the entire VN affects multiple organ systems via efferent pathways and alters afferent signaling, complicating the study of vagal communication between the gut and CNS. This multifunctionality allows for multiple therapeutic avenues but represents a research obstacle. My research focuses on two key functions of the vagus nerve: its role in heart rate and glucose tolerance, with particular emphasis on the Dorsal Motor Nucleus of the Vagus (DMV).

Anatomy, connectivity, and function of the Dorsal Motor Nucleus of the Vagus (DMV)

The dorsal motor nucleus of the vagus (DMV) is one of four major vagal nuclei in the brain. The DMV, first described in 1843 (3), is an asymmetrical bilateral nucleus located within the dorsomedial caudal medulla oblongata of the brainstem. DMV neurons are cholinergic preganglionic motor neurons that provide parasympathetic motor outputs to the heart, esophagus, stomach, intestines, pancreas, portal

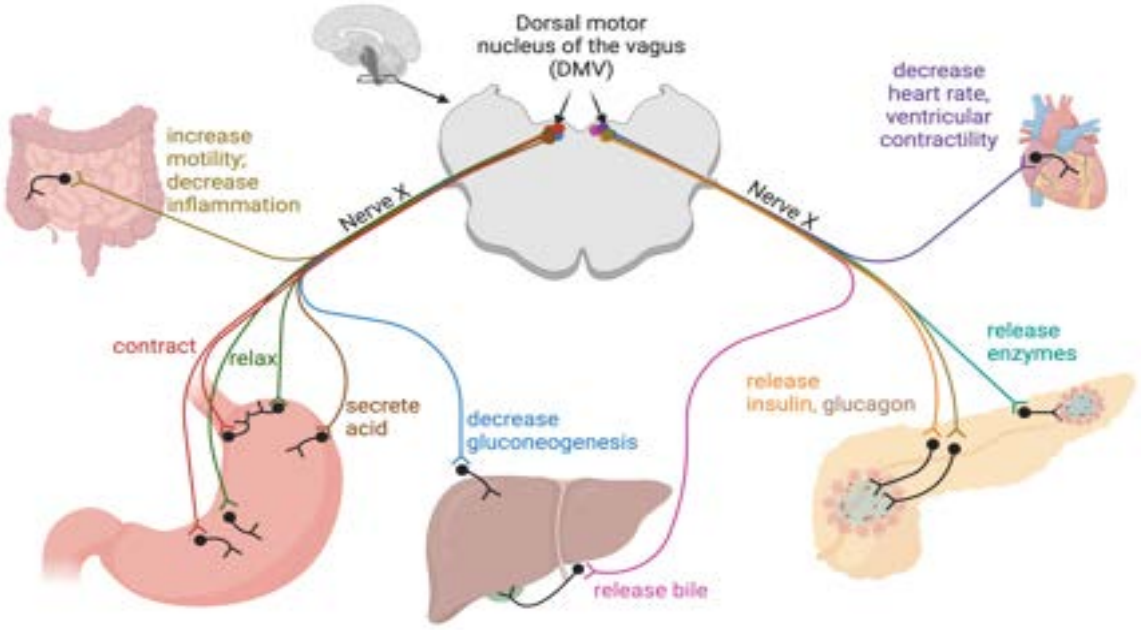

Figure 1: Nerve-X; Functional Targets of the Dorsal Motor Nucleus of the Vagus (DMV). {Modified from 24}

vein, biliary and the liver [Figure 1, modified from 4] (1,4). The preganglionic motor fibers of the DMV synapse onto postganglionic neurons located in or around the targeted organs. In a coronal slice of the brainstem, the DMV lays sandwiched inferior to the NTS (nucleus of the solitary tract) and superior to the XIIth nucleus, running adjacent to the IVth ventricle (*2*). In a horizontal brain section, the DMV makes a Y shape. Anterior to the central canal, both hemispheres of the DMV are bifurcated distally. At the rostral-caudal level of the central canal both hemispheres of DMV converge into a unified midline nucleus just dorsal to the canal. Most, or all these preganglionic parasympathetic motor neurons are cholinergic. However, catecholaminergic and nitrergic neurons projecting subdiaphragmatically have also been categorized (5). Smaller neurons also exist within the DMV that don't project through the

vagus and are thought to be inhibitory interneurons (*6*). In addition to neurons, astrocytes may play a role in vagal regulation as astrocyte depletion in the NTS leads to decreased vagal function such as decreased baroreflex and cardiorespiratory reflex (*7*).

The anatomy of the DMV provides insights into its functional structure. Vagal afferents innervating the NTS form a viscerotropic map of subnuclei organized along the rostro-caudal axis (8). NTS axons and DMV dendrites extend across their common border, this loose border can make spatial stimulation results difficult to interpret (6,*10*). The DMV is also organized viscerotopically but instead along the mediolateral axis. The orthogonal arrangement between the NTS and DMV means that each functional column of the DMV is physically near all of the subnuclei of the NTS (9). This physical proximity and organization mean that all sensory inputs can connect with all motor outputs of the vagal system. Anterograde and retrograde tracing studies have elucidated some of the structural organization within the DMV. Neurons within the DMV are situated in longitudinal columns which lay medial-lateral and run rostral-caudal (12,13). These columns represent a viscerotropic map as these columns correspond to different branches of the vagus. Neurons in the left DMV form columns which represent the hepatic, accessory coeliac, and anterior gastric branches while neurons in the right DMV represent the coeliac and posterior gastric branches (10,11,12). The relationship between spatial position and functional output within the DMV can be shown experimentally. Microinjection of glutamate into the rostral and caudal extents of the DMV typically result in opposing functional outcomes. For example, glutamate injection into the rostral DMV elicited gastric contraction while injection into the caudal DMV increased gastric relaxation (9,13).

Inputs and Outputs of the DMV

DMV neurons receive interoceptive and exteroceptive input from the viscera and CNS, respectively. Sensory information from the viscera travels along vagal afferents to the NTS which in turn densely innervates the DMV. The DMV also receives afferent inputs from other CNS structures. Hypothalamic regions such as the arcuate nucleus (ARC) and lateral hypothalamus (LH) and the paraventricular hypothalamus (PVH) send direct projections to DMV. Indirect inputs from other CNS structures such as the insular cortex (IC), central nucleus of the amygdala (CeA), mesencephalic central grey matter, parabrachial nucleus (PB), medullary reticular formation (mRF), and the raphe obscurus nucleus (NRO) have also been previously described (14,15,16). One of the main inputs to the DMV is the NTS which modulates DMV activity via both inhibitory and excitatory synaptic inputs (14,17,18). As the NTS receives vagal sensory information the DMV-NTS represents a bridge between vagal sensory information and vagal motor output.

Approximately ~80% of DMV neurons give rise to preganglionic parasympathetic fibers which innervate the airways, heart, esophagus, stomach, intestines, pancreas, hepatic portal vein and biliary (2,4). The DMV also projects to the liver, but whether the DMV directly innervates the liver or signals indirectly is still a matter of debate (*20,51,52,166*). Preganglionic parasympathetic motor neurons of the DMV synapse onto postganglionic cells in or around target organs of the digestive system. In the pancreas these postganglionic cells form intrapancreatic ganglia which then synapse onto effector cells such as the beta cell of the islets. In the heart, the target of DMV innervation are cardiac ganglia which go onto the innervate the SA node (19).

In addition to its synaptic inputs, the DMV also receives endocrine signals. Adjacent to the DMV, the area postrema (AP) is one of the select brain regions not enveloped by the blood brain barrier. Dendrites from DMV neurons extend far beyond their regional boundary, reaching out through the NTS and

towards the AP. This proximity of the DMV and AP, coupled with the dendritic morphology of DMV neurons allows the DMV access to circulating signaling molecules not available in most brain regions. Indeed, within the AP, NTS and DMV there exist receptors for GI peptides (ghrelin, TRH, pancreatic polypeptide) which are secreted from digestive organs. In one experiment, ghrelin infusion into the intracerebroventricular space led to an increase in pancreatic secretion, with vagotomy completely removing this effect (21). The contribution of nonneuronal signaling to DMV function is not fully understood.

While the innervation targets and structural organization of the DMV has largely been elucidated, what remains unclear is the molecular composition and functional organization of neuronal cell types within the DMV. Two potential models for the DMV's functional architecture have been proposed. In the "one-to-all" model, neurons of the DMV are all one molecular subtype but innervate different organs. In the second "functional units" model, molecularly distinct subgroups of the DMV carry out different physiological functions (24,25).

In support of the "functional units" theory, at least seven genetically distinct subtypes of neurons were recently found in the mouse DMV. Two of these genetically distinct subgroups (DMV-Cck and DMV-Pdyn) are distinct but both innervate the glandular stomach, where they appear to carry out opposing functions. DMV-Cck neurons preferentially synapse onto $Chat^{+}$ neurons in the stomach while DMV-Pdyn neurons preferentially synapse onto $Nos1^{+}$ neurons in the stomach (*24*). The functionally opposite roles of $Chat^{+}$ and $Nos1^{+}$ neurons in the stomach (e.g., gastric contraction and gastric relaxation respectively) point towards a functional units model of the DMV in which spatially and genetically distinct neurons mediate discrete vagal functions. Recently, this model has received additional support as genetically distinct subpopulations within the nucleus ambiguous have been shown to separately innervate either

the esophagus or pharynx (25,27). If the functional units model of the Dorsal Motor Nucleus of the Vagus (DMV) is correct, we would expect distinct molecular groups within the DMV to control specific target organs, such as the pancreas and heart, thereby regulating functions like glucose and cardiac regulation, respectively.

DMV Modulation of Cardiac Function

Subsets of vagal efferent neurons project from the hindbrain (DMV and nAMB) to the cardiac ganglia via the vagus nerve and are known as cardiovagal neurons (CVNs). Upon activation, CVNs release acetylcholine onto ganglionic nicotinic acetylcholine (ACh) receptors. These cardiac ganglia neurons then release ACh onto muscarinic receptors on cardiac pacemaker cells, primarily located in the sinoatrial (SA) node and atrioventricular (AV) node. This binding inhibits the activity, thereby slowing the heart rate and decreasing ventricular contractility. These CVN projections elicit cardioinhibition at both rest and during homeostatic reflexes. Of the two vagal efferent regions, the nAMB, which contains 80% of CVNs, has been shown to significantly affect heart rate and is thought to be the major, if not the sole, arbiter of parasympathetic modulation of heart rate (5,*28,26*).

Despite anatomical evidence for CVNs in the DMV, conflicting functional data has kept the DMV's control of heart rate as controversial. In previous studies electrical activation of the DMV resulted in no change significant change to HR (28,29). Contrasting these findings, L-glutamate injected into the left DMV causes a significant reduction in both left ventricle contractility and heart rate (30). Recently it has been shown that Vagal nerve stimulation can facilitate CPR in rodents. Animals with CPR+VNS were resuscitated 90.91% rather than 83.33% with CPR alone. Both the increased resuscitation probability and the lower amounts of myocardial ischemia were linked to the decreased use of oxygen as a result of

vagal-bradycardia (31). One major limitation of previous studies was the inability to look at heart rate in awake behaving mice as their protocols required anesthesia which would impact basal heart function. Another critical limitation was the inability to specifically target DMV CVN's without influencing other neuronal populations such as the NTS or potentially inhibitory interneurons of the DMV. Both of which are populations that exert inhibitory effects on the DMV and could significantly influence DMV activity. Therefore, whether DMV neurons are capable of decreasing heart rate remains unclear.

Vagal Control of Emotions

Interest in vagal physiology has surged lately, largely spurred by the expanding therapeutic applications of vagus nerve stimulation (*32*) and the importance of interoception to health and well-being. Beyond its cardiovascular effects, emerging research has highlighted the vagus nerve's involvement in the regulation of emotional states and motivation. Recently, it has been shown that a gut-brain circuit from vagal sensory neurons plays a role in motivation and dopamine release (33). In addition, the vagus nerve serves as a crucial component of the neurobiological pathways underlying the stress response, influencing both the physiological and psychological aspects of anxiety (165).

Notably, vagus nerve stimulation shows promise in treating anxiety and post-traumatic stress disorder (*32*). In studies with rats, vagus nerve stimulation has been shown to hasten the extinction of conditioned fear and reduce anxiety-like behavior (*34,35*). Similarly, in humans, there's evidence suggesting that vagal nerve stimulation could alleviate treatment-resistant anxiety disorders (*36*). However, the precise mechanism behind the anxiolytic effect of vagal stimulation remains elusive. Given that the vagus nerve operates bidirectionally, transmitting sensory information from the body to the brain and motor signals from the brain to the body, it's unclear whether the reduction in anxiety stems

from sensory or motor signaling. It also remains unclear why the DMV, which canonically handles anticipatory gut-brain metabolism would be having such a pronounced effect on heart rate/anxiety.

Glucose Homeostasis

Glucose regulation is essential for maintaining brain function and overall neural health. The brain, despite making up only 2% of body weight, consumes about 20% of the body's glucose supply, reflecting its high energy demands. This energy requirement is crucial but comes with significant risks to survival. The digestion and absorption of nutrients can disrupt internal osmolarity and cause rapid increases in blood glucose levels, which, if not properly controlled, can be harmful. Glucose is vital for numerous neural processes such as synaptic transmission, neurogenesis, and cellular homeostasis. However, excessive circulating glucose can damage the vascular system and impair organ function. Therefore, maintaining blood glucose within a narrow range (4-6 mM) (*108*) is critical for health. This tight regulation is primarily managed by the pancreas, liver, adipose tissue, muscle, and brain, which communicate through neural and endocrine signals to maintain glucose homeostasis. Dysregulation of glucose levels, as observed in conditions such as diabetes and hypoglycemia, can lead to vascular damage, cognitive deficits, mood disorders, and an increased risk of neurodegenerative diseases like Alzheimer's disease.

Glucose tolerance refers to the body's ability to regulate blood glucose levels following the ingestion of glucose, which is vital for maintaining glucose homeostasis. An organism with higher glucose tolerance can consume more glucose before reaching the same blood glucose levels as one with lower tolerance. There are two types of glucose tolerance mechanisms: reactive mechanisms, which activate in response to glucose blood levels, and anticipatory mechanisms, which are triggered before glucose enters

circulation. The brain plays a key role in managing both types of mechanisms by sensing blood glucose changes and activating the appropriate regulatory pathways. This involves a complex interplay of neural circuits, metabolic pathways, and hormonal signals, making it essential to understand these processes for developing interventions that address impaired glucose metabolism.

Glucose, Insulin, Glucagon, Somatostatin, GLP-1

Glucose is monosaccharide, a subset of carbohydrate, and the body's main source of energy. Glucose is broken down through glycolysis to pyruvate and usable energy in the form of adenosine triphosphate (ATP). Prior to meal consumption, glucose levels are low. Glucose levels being to steadily rise shortly after meal consumption (0-10min) and peak (~1hour) after meal ingestion, returning to baseline in (~2-3hours) (40,41). When glucose levels are high, glucose can be converted into glycogen through glycogenesis to be stored for later use. When these glycogen stores are needed, they can be broken down into glucose in a process called glycogenolysis. And finally, in the absence of available stores, glucose can be synthesized in the liver from amino acids and pyruvate in a process called gluconeogenesis. These processes allow glucose to be generated or stored as needed and are subject to regulatory mechanisms which control blood glucose levels. The major molecules involved in glucose homeostasis are glucose, insulin, glucagon, somatostatin, and glucagon-like peptide (GLP-1). These molecules each affect the others in a complex web of regulation.

Insulin is an anabolic peptide hormone produced by the beta cells of the pancreas. Insulin regulates carbohydrate metabolism by facilitating glucose absorption from the blood and into adipose, liver, and skeletal muscle cells. Insulin has tissue specific effects. In skeletal muscles insulin signaling increases glucose uptake and glycogen synthesis while decreasing glycogenolysis and gluconeogenesis. In adipose

tissue, insulin causes an increase in glucose uptake, glycogen synthesis and triglyceride synthesis while decreasing lipolysis. In the liver insulin acts to increase glycogen synthesis while decreasing glycogenolysis. Insulin release occurs in a biphasic manner. The first phase is a rapid, short-term response that uses pre-stored insulin. The second phase is a slower, more sustained response involving newly synthesized insulin. The first phase of insulin release is an initial and rapid release of insulin from the pancreas in response to elevated glucose levels. Lasting ~10min and primarily driven by pre-stored insulin, this phase is crucial for reducing blood glucose levels quickly. The second phase is induced by blood glucose levels rising during nutrient absorption, represents the bulk of insulin released, and reaches a peak after ~2-3 hours (*61*). Interestingly, one of the first beta-cell deficits seen in individuals who develop T2D is the attenuation of first phase insulin secretion (63). The loss of first phase insulin secretion occurs in patients with impaired glucose tolerance or who are in the initial stages of T2D (*63,64)*). Interestingly, while these individuals have decreased first phase secretion, they generally have a higher second phase insulin secretion. Indicating compensation, this increase in second phase insulin secretion represents a net increase in insulin secretion across both phases yet is less effective at limiting post-prandial glycemia.

Glucagon, produced in the alpha cells, is a catabolic peptide hormone that opposes the function of insulin. Glucagon's ultimate effect is to increase available glucose in the blood. Like insulin, glucagon has tissue dependent effects. In adipose tissue glucagon decreases the level of lipolysis. The liver is the main locus of glucagon's glycemic effects. Glucagon signals the liver to increase glycogenolysis, gluconeogenesis, amino acid uptake and fatty acid catabolism. Despite glucagon's canonical role as a catabolic peptide there are, conditions under which glucagon may act to paradoxically potentiate insulin release and decrease glucose levels. Glucagon is known to stimulate insulin secretion indirectly by promoting hepatic glucose output, which elevates blood glucose levels. This rise in blood glucose can

enhance insulin secretion from beta cells. Glucagon has also been shown to directly this process through the beta-cell's glucagon receptor (GCGR) (*44*). In a fed, high glucose state glucagon can also act on beta-cells GLP-1Rs to increase insulin secretion and lower glucose (42). Similarly, ablation of alpha cells or alpha cell secretory products resulted in impaired insulin secretion (43). These studies suggest that glucagon may be an important potentiation mechanism of beta cell insulin secretion. The consequences of glucagon's contrasting functions to glucose regulation will be explored during the summary. The dynamics and relative abundance of these signaling molecules work in concert to modulate blood glucose levels.

Glucagon-like peptide 1 or GLP-1 is the only major glucose-regulating peptide not secreted by the pancreas. Instead, GLP-1 is secreted by enteroendocrine L-cells of the intestine. These L cells act as nutrient sensors, and release GLP-1 in response to sugars. GLP-1 has two major roles in digestion and glucose homeostasis. First at the local environment level GLP-1 activates parasympathetic vagal-vagal reflexes. In the intestine GLP-1 activates vagal afferent fibers that terminate in the brainstem where they initiate efferent vagal activity to target organs such as the liver, pancreas, muscles, and blood vessels. In the pancreas GLP-1 acts directly on the islet cells to suppress glucagon release while stimulating insulin release (44,45). In the liver, it acts to reduce glucose production. Glucose levels must be elevated above fasting levels for GLP-1 to have its reductive effect. Consequentially, the ability for GLP-1 to reduce blood glucose levels is glucose dependent. This property is also dose/concentration dependent. So as post-meal glucose levels fall (partly in response to GLP-1's actions) so too does GLP-1's effectiveness at lowering those levels. The functions and properties of GLP-1 have made it a prime target for diabetic therapies. GLP-1 analogs, GLP-1 receptor agonists and drugs which prevent enzymatic cleavage of GLP-1 are all current therapies used in the treatment of type 2 diabetes.

Somatostatin is produced by delta cells. Unlike both insulin and glucagon, somatostatin does not act on distant targets, instead it is released locally in the islet in response to a range of glucose levels. Somatostatin inhibits both glucagon secretion from alpha cells as well as insulin secretion from beta cells. Because somatostatin negatively regulates both hormones, it can act to fine tune pancreatic hormone secretions and ultimately blood glucose levels.

Pancreas

By volume, most of the pancreas (98%) is exocrine acinar cells, which release the digestive enzymes amylase and lipase through the pancreatic duct into the duodenum of the small intestine to break down starches and fats, respectively. Since amylase breaks down starches into glucose, it directly increases the amount of glucose that can be absorbed into the bloodstream. The relatively scarce endocrine cells form morphologically and spatially distinct islands of endocrine tissue aptly named islets. The islets contain five cell types in varying amounts, each responsible for the production and secretion of various hormone(s):

- Alpha cells constitute 15-20% of the islet cells and produce/secrete glucagon.
- Beta cells, 65-80%, produce C-peptide and insulin.
- Delta cells, 3-10%, produce somatostatin
- Gamma cells, 3-5%, produce pancreatic polypeptide.
- Epsilon cells, <1%, produce ghrelin.

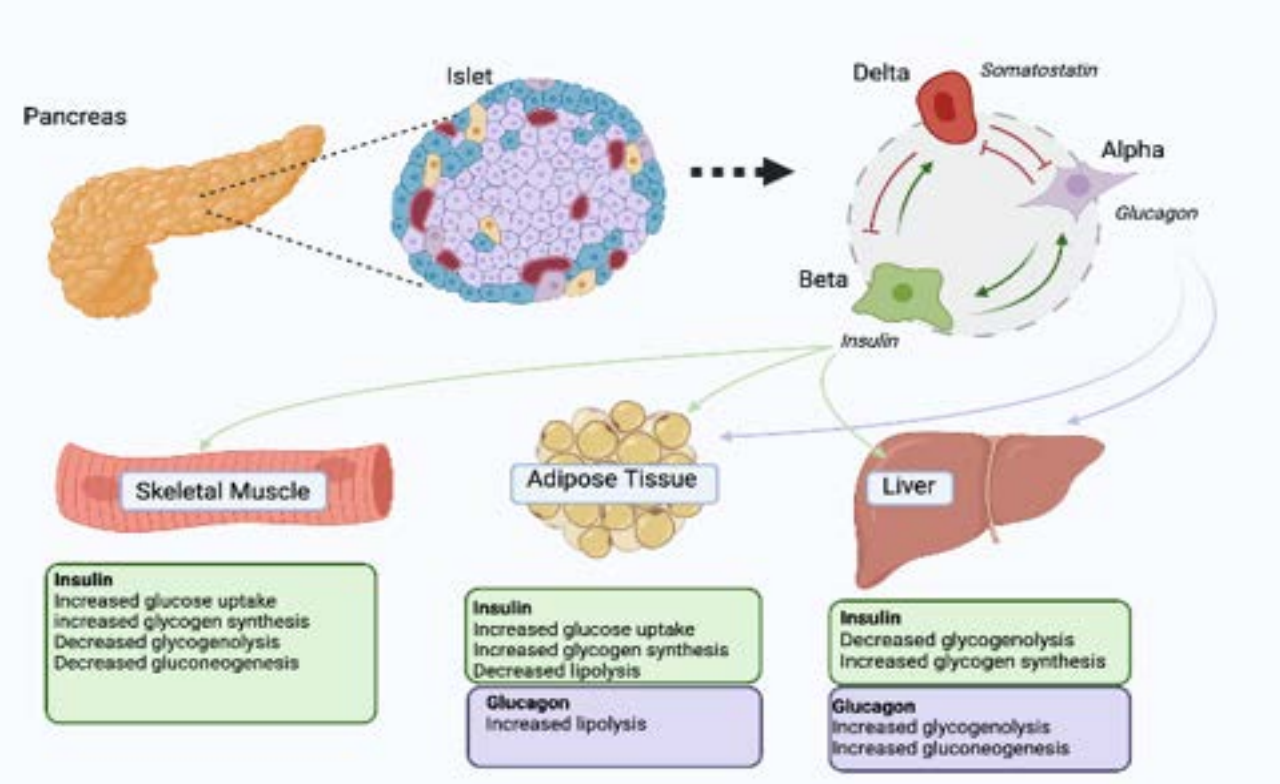

Figure 2: Contrasting functions of insulin and glucagon in glucose regulating tissues, islet-islet interactions {Modified from 46}

The islet cell types, their hormones and their effects on blood glucose are summarized in Figure 2 (46). Vascular innervation of the islets is essential as it allows for the endocrine delivery of these signaling hormones to the blood stream, target organs and peripheral tissue. As such mechanisms that increase or decrease blood flow could have effects on glucose regulation by increasing perfusion of insulin for example. It is the production, secretion, timing, and efficacy of these hormones that is so essential to the regulation of glycemic levels (2,77).

Pancreatic islets are under both direct control from the pancreatic nervous tissue and indirect control from the CNS. The pancreas nervous system consists of extrinsic nerves and intrinsic clusters of neural cells known are intrapancreatic ganglia. These ganglia are made up of neurons, glial cells, and nerve fibers and are found throughout the pancreas, alongside nerve trunks (49,50). They innervate islets and receive innervation from the parasympathetic, sympathetic, and enteric nervous systems as well as other intrapancreatic ganglia [Figure 3]. This interconnectedness allows these ganglia to integrate the sensory/motor information coming from the brain/gut and coordinate islet functions (*20, 28, 29*). The source of synaptic input to these ganglia is understood to some degree. Parasympathetic inputs originate from the dorsal motor nucleus of the vagus (DMV) while sympathetic input originates from the celiac ganglia (CG), superior mesenteric ganglia (SMG), and paravertebral ganglia (PG). Enteric neurons

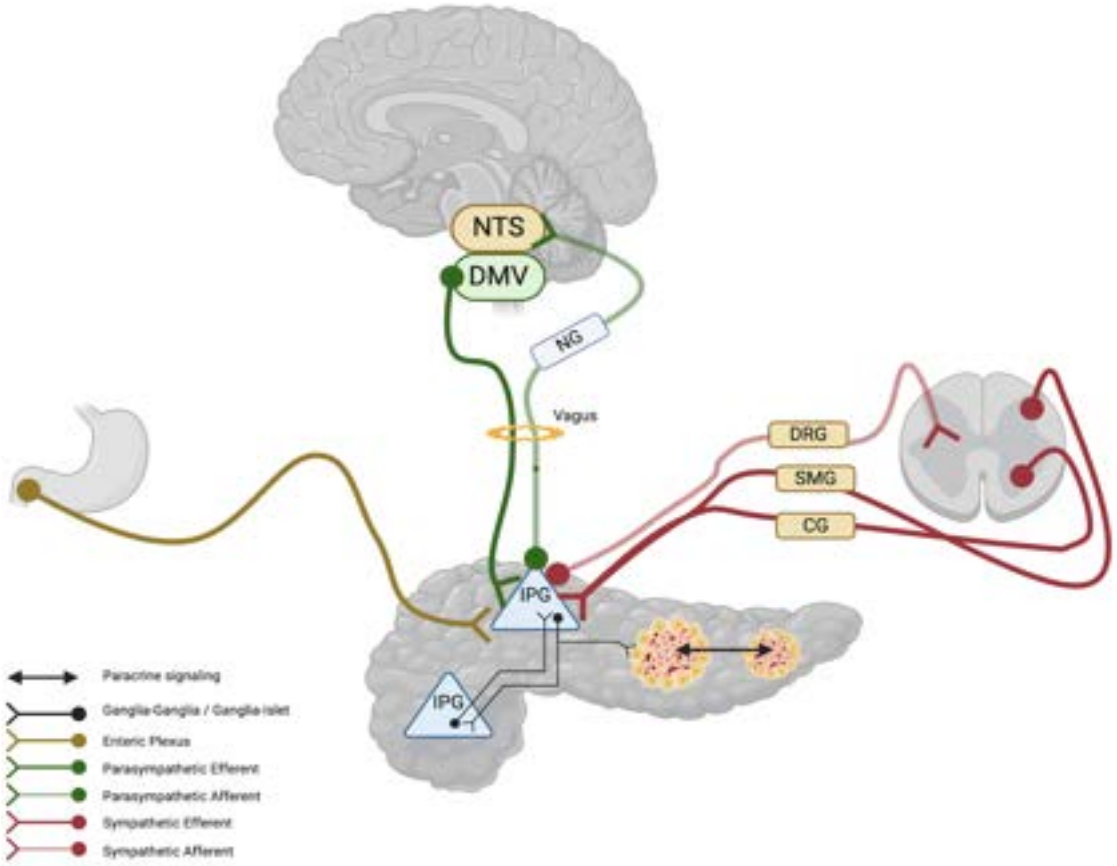

Figure 3: Intrapancreatic ganglia receive input from the PNS, SNS, ENS and other intrapancreatic ganglia (IGP). CG celiac ganglia, SMG superior mesenteric ganglia, DRG dorsal root ganglia, NG nodose ganglia {modified from 28}

in the myenteric plexus also innervate these ganglia, though the effect and functional importance of enteric innervation is not fully understood.

Liver

Claude Bernard was the first to outline the liver's role in glucose production and regulation experimentally, showing vagotomy reduced hepatic glucose production (51,52). Depending on need, the liver can release/synthesize glucose to increase glycemia, or store excess glucose in the form of glycogen, effectively lowering glycemia. Insulin signaling in the liver promotes a decrease in blood glucose via two mechanisms. First, insulin promotes glycolysis by increasing expression of a gene which codes for a crucial enzyme in the conversion of glucose into glucose-6-phosphate. Secondly, insulin acts to downregulate glucose-6-phosphatase and phosphoenolpyruvate expression which promote glycolysis and demote gluconeogenesis, respectively. Through these mechanisms, insulin signaling in the liver decreases blood glucose levels. Opposing insulin, glucagon signaling in the liver promotes an increase in blood glucose via activation of PKA. The effects of PKA activation inhibit glycolysis and glycogenesis and stimulate glycogenolysis and gluconeogenesis (*39*). In addition to hormonal influences, recent studies point to an increasingly key role of neuronal modulation in hepatic glucose production/regulation.

The liver, like the pancreas, receives input from both the parasympathetic and sympathetic branches of the autonomic nervous system (51,52). Activation of the parasympathetic nervous system significantly dampens hepatic gluconeogenesis (53). Additionally, a population of POMC+ neurons in the hypothalamus signal via the DMV to the liver. Activation of melanocortin-4 (Mc4r) receptors inhibits Chat+ DMV neurons and optogenetic inhibition of liver-projecting parasympathetic cholinergic fibers increases blood glucose levels (56). However, the exact role of DMV signaling to the liver remains controversial. Recent studies have shown that chemogenetic activation of cholinergic DMV neurons increased glucose levels via hepatic gene expression in mice (56). The authors note the discrepancy of

DMV neuron activation's effect on liver function, suggesting it may depend on the metabolic state, as the study was conducted under fed- compared to the usual fasted-condition. Communication between the brain and liver, as well as between the pancreas and liver, links glucose sensing and glucose production, which is necessary for proper glycemic regulation.

Anticipatory Glucose Regulation

Prior to and throughout meal consumption the body acts in a feedforward fashion to minimize homeostatic disruptions. For instance, anticipating an increase in blood osmolality due to absorption of solutes, the brain triggers a pre-emptive increase in thirst. Similarly, the brain anticipates an increase in blood glucose levels during a meal and so pre-emptively increases insulin release when a meal begins. These anticipatory responses are essential to maintaining homeostatic variables, such as blood osmolality and glucose, within a narrow range. This is because reactive mechanisms, such as glucose-induced insulin release, tend to produce large oscillations in homeostatic variables. 'Reactive' glucose regulating mechanisms only get activated in response to increasing blood glucose levels. The large variance between internal glucose-states immediately preceding, during, and following a meal represents a challenge for these reactive mechanisms. Primarily in that, feedback-only regulation could result in oscillations that take the organisms outside of healthy glycemic ranges. If, however, an organism can predict the timing and degree of homeostatic disturbance (e.g., large glucose influx) before it occurs, it can make changes that "flatten the curve" in glycemia and so reduce the risk of tissue damage due to hyperglycemia. This anticipatory, or feed forward, mechanism works in conjunction with reactive feedback mechanism (e.g., glucose-induced insulin release) to efficiently maintain glycemic homeostasis (*33*).

Anticipatory responses to feeding were observed and studied as early as 1897. Ivan Pavlov's experiments with dogs introduced classical conditioning and showed that anticipatory digestive responses, such as salivation and gastric secretion, could be conditioned (*58*). For instance, his experiments showed that the presence of food in the mouth is a powerful prompt for gastric secretions. In anticipation of food entering the stomach, the brain, working through the vagus nerve, induces gastric secretions to prepare for digestion (71). Dogs learned to associate an auditory cue with food presentation and eventually would salivate upon hearing the auditory cue, without any food. This demonstrates that anticipatory digestive responses can be cued by a conditioned environmental stimuli, and how, once learned, those stimuli are sufficient to cause the same anticipatory responses as food presentation itself. Pavlov referred to the anticipatory changes in digestive function that occurred at the start of a meal as the cephalic phase of digestion. Cephalic phase responses (CPR) are those anticipatory changes that occur during this pre-digestive state. Innately present but shaped by experience, these cephalic responses use internal and external sensory information to mitigate the homeostatic disruptions of meal consumption (57).

Cephalic Phase Insulin Response

Cephalic responses have been observed for many physiological processes: salivation, gastric acid secretion, release of gastrin, lipase, immunoglobulins, ghrelin, bicarbonate, amylase, trypsin, insulin, and pancreatic polypeptide (16,59). CPIR or the cephalic phase insulin response is defined as the anticipatory release of insulin prior to meal digestion that facilitates post-prandial glucose homeostasis. In other words, CPIR reduces the glucose load, or the extent to which a meal will increase blood glucose. In humans, the peak increase in plasma insulin occurs shortly (4 minutes) after sensory stimulation and

returns to baseline after about 10 minutes. This rapid response accounts for only ~1% of all secreted insulin that occurs during a meal (*37*).

While the amount of insulin released during CPIR is relatively tiny, blocking or circumventing CPIR can have a dramatic effect on periprandial glycemia (61). The physiological significance of CPIR in rodents is well established. Yet the significance of CPIR in humans has remained controversial. Human studies have shown an absent, mild, or strong cephalic phase insulin response across different experimental paradigms (62). The varying procedures, administration methods and analysis may make sense of inter-study differences to some degree. Additionally, differences in prior diet could modulate an individual's response to those stimuli found in their diet. For example, one common discrepancy is whether individuals have CPIR in response to nonnutritive sweeteners. It could be that individuals who always eat lunch with a diet soda would show a significantly different effect when given the nonnutritive sweetener within diet soda, than those who drink diet soda alone. While the CPIR is a clear mechanism for improved glucose homeostasis and is vital in rodents, its importance in humans is mixed and inconclusive.

The importance of anticipatory glucose regulation can be experimentally shown by bypassing or removing the cephalic phase responses from the digestive process (done by injecting nutrients directly into the stomach or bloodstream, bypassing the oral cavity). Without the experience of eating, food entering the body circumvents feedforward control of digestion, decreasing the efficiency of nutrient digestion, absorption, and metabolism (*16*). While not necessary for digestion, the cephalic phase primes both the gastric and intestinal phases and allows for optimal digestion efficiency.

What could be the evolutionary advantage of CPIR? One possibility is that it allows animals to consume larger, less frequent meals. For instance, one study specifically denervated pancreatic beta cells in rats to investigate the importance of CPIR to meal size. First, rats were given a drug (streptozotocin) which destroys beta cells activity and induces a severe diabetic phenotype (*65*). After it was shown that these rats cannot secrete insulin, they were given a beta-cell transplant. Importantly, these transplanted beta cells can react to levels of glucose but are not neuronally innervated. Despite their beta cells still working reactively to manage glycemia, these animals show no cephalic insulin secretion but do behaviorally compensate by reducing their meal size (66,67). Animals who have had their vagus nerve surgical cut (vagotomized) will also have significantly higher levels of blood glucose compared to control animals given the same caloric load (65,66,67). Put another way, without CPIR, animals don't secrete enough insulin early enough to prime metabolic organs and ultimately can't handle the glucose challenge of larger meals. Interestingly, animals and people who have had a vagotomy consume smaller meals, potentially as a means of alleviating the undesirable effects of high blood glucose brought about by their lack of CPIR (65,66). CPIR likely evolved to enable optimal glucose homeostasis and allow for less frequent and larger meals to be consumed (57) The larger the meal, the larger potential increase in blood glucose levels. CPIR reduces the effective glucose load of a meal and therefore allows for larger meals to be consumed at once.

The ability to consume larger meals reduces the energy expenditure and risks associated with extensive foraging (*70*). In environments where food acquisition incurs no significant cost, animals typically mitigate the potential negative effects of large meals by consuming many small meals throughout the day (57). However, as risk or the energetic cost of acquiring food increases, animals tend to consume larger meals less frequently. This behavior reflects a trend towards an equilibrium between the metabolic consequences of larger meals and the costs associated with food acquisition. Mechanisms

such as the cephalic phase, which reduce the metabolic impact of larger meals, effectively shift this equilibrium.

DMV Control of Anticipatory Glucose Homeostasis/Cephalic Phase

The vagus nerve (VN) is the cable through which the brain directs cephalic responses and is necessary for the CPIR. The VN's role in mediating cephalic responses has been studied since Pavlov (*58,71)*). Interventions which inhibit vagal communication decrease cephalic responses while activating the VN enhances or recapitulates these responses. Experimentally cutting the VN, a procedure known as a vagotomy, significantly reduces cephalic phase insulin secretion in sheep (*68*) and reduces portal vein insulin levels in dogs (*79*). Conversely, VN stimulation elicits insulin secretion in both dogs and rats (72,73) and significantly improves insulin sensitivity in rats (*74*).

Several other lines of evidence point to the vagus as the locus for anticipatory glucose regulation. Firstly, profound effects on glucose and insulin can be observed via vagal stimulation. Stimulation of both afferent and efferent vagal fibers yields different results then stimulating efferent or afferent projections independently (73). Dual afferent and efferent stimulation resulted in increased blood glucose, increased glucagon secretion, and no change in insulin. Afferent VN stimulation alone resulted in increased blood glucose with no changes to insulin or glucagon (73).Efferent stimulation alone resulted in no increase in blood glucose while eliciting an increase in both insulin and glucagon secretion (*47*). This has implications for VN stimulation therapies as it suggests that stimulation of the afferent VN could suppress insulin secretion caused by efferent stimulation. As the vagus is critical, vagal nuclei are a reasonable place to look for the control of this preemptive glucose control.

The DMV is likely the locus for control of CPIR, since (1) it is the only vagal efferent nucleus which innervates the pancreas and (2) previous studies have shown that manipulating DMV neuron activity affects insulin secretion and glucose tolerance. Early studies showed a prompt rise of both glucagon and insulin with electrical cervical-vagal stimulation which depended on the vagus nerve (29). DMV-specific electrical stimulation has also been observed to cause significant insulin release and was abolished by either pre-treatment of the muscarinic antagonist atropine or vagotomy (77). Chemogenetically activating Chat+ neurons in the hindbrain with hM3Dq led to an increase in IPGTT tolerance while inhibition via hM3Di conversely led to loss of tolerance (78). These results show that the DMV is capable of increasing blood insulin levels and glucose tolerance.

The necessity of cholinergic signaling to cephalic responses can be shown as administration of the muscarinic antagonist atropine blunts or blocks parasympathetic vagal motor activity and reduces gastric tone, motility, and insulin secretion (*15,17*). The gene *Chat* encodes an enzyme necessary for the biosynthesis of the neurotransmitter acetylcholine, and so cholinergic neurons express *Chat*. One important aspect of *Chat*+ DMV neurons is their pace making activity, that is, intrinsic slow and spontaneous activity. This is important as it means small changes in membrane potential within the DMV can have magnified downstream effects (*11*). A neighboring brain region, the NTS, regulates the DMV via both excitatory and inhibitory connections. Chemogenetic activation of inhibitory NTS neurons reduced the tonic firing of DMV neurons, increased blood glucose, and elicited a significant increase in PEPCK1 expression, a rate-limiting enzyme in gluconeogenesis (*78*). In a separate study, optogenetic stimulation of glucose-dependent inhibitory ($Glut2^{+}$) neurons in the NTS led to an increase of vagal activity and an increase in glucagon secretion (*9*). Therefore, DMV neuron activity is necessary for glycemic control and so likely the locus of CPIR.

While parasympathetic fibers originating in the DMV innervate both endocrine and exocrine aspects of the pancreas, it is this innervation of the endocrine pancreas through intrapancreatic ganglia which gives rise to insulin secretion and CPIR (48,80). It is still unclear if parallel or collateral projections from the DMV innervate the islets directly or if all parasympathetic efferents are first relayed through intrapancreatic ganglia (49). Within intrapancreatic ganglia, preganglionic fibers from the DMV primarily release acetylcholine (ACh) onto their postganglionic targets, although they have also shown to release vasoactive intestinal peptide (VIP), gastrin releasing peptide (GRP), pituitary adenylate cyclase activating polypeptide (PACAP) and nitric oxide (NO) (50). These signaling molecules are also released from the intrapancreatic postganglionic target neurons in addition to neuropeptide Y (NPY), noradrenaline (NE), galanin and substance P (SP) (50). Acteylcholine (Ach) signaling in the islets primarily stimulates insulin secretion via beta cell M3 muscarinic receptors. Glucagon secretion can be controlled by ACh, GRP and VIP, norepinephrine (NE), and epinephrine (EPI) signaling. These signals represent a small fraction of the forces that can influence beta and alpha cell secretion.

Hormonal control of glycemia is influenced by the release of ACh, GRP, VIP, NE, and EPI. The DMV may have access to circulating hormones through the nearby circumventricular organ, area postrema, since DMV dendrites extend close to the AP (6). DMV neurons express receptors for pancreatic polypeptide (PP), ghrelin, GLP-1, NO and thyrotrophin-releasing hormone (TRH) (19). The differential release of various hormones would have consequences on blood glucose levels as different aspects of the beta cells respond differently to different transmitters/hormones. Therefore, through the release of a cocktail of certain signals, the DMV can modulate pancreatic islet function. The complex interplay of these signals helping to regulate insulin and glucagon secretion has not been fully explored.

The DMV's role in glycemic regulation appears to be highly specialized and context dependent. It mediates the cephalic phase of digestion (~10-20m) prior to food ingestion to drive an increase in insulin secretion. As previously mentioned, the volume of insulin released through this mechanism accounts for only ~1% of insulin secreted throughout a meal (*50*). Yet when this 1% is lost, dramatic increases in post-prandial glucose levels are observed (80,82)) How can such a small secretory effect have such a large impact on glucose homeostasis, and can these mechanisms be therapeutically manipulated as a means of combating glucose intolerance seen in metabolic conditions such as T2D?

Anticipatory insulin release can act in at least three ways to affect blood glucose levels. The first way is to increase glucose uptake into muscle and adipose tissue. But as previously mentioned, the volume of insulin released during the cephalic phase would not be sufficient to counter glucose levels solely through this mechanism as there simply isn't enough insulin secreted. Cephalic phase insulin must be acting through other mechanisms.

The second effect of cephalic insulin is on the liver. The hepatic portal vein is extremely sensitive to small changes in insulin concentrations, especially when levels are low (79) Indeed, studies have shown very small volumes of insulin in the hepatic portal vein can led to transcriptional effects within the liver that promptly inhibit hepatic gluconeogenesis (*53*). Insulin levels also vary more widely in the portal vein than in peripheral tissues (81) . By inhibiting gluconeogenesis at the onset of feeding, the body can keep blood glucose levels within a healthy range and conserve energy. This is important as it means that the small volume of insulin released during CPIR can have a magnified effect on glucose levels. The DMV also projects to the liver to control hepatic glucose metabolism. The connection between the DMV and the liver could be of vital importance for the DMV's role in glucose regulation and will be mentioned in

the summary. However, the relative contributions of DMV-to-liver and DMV-to-pancreas projections to hepatic regulatory changes is currently unresolved (53, 80, 82, 83).

The third effect of cephalic insulin is on vasculature recruitment. The hemodynamic effect of insulin increases capillary surface area (vascular recruitment), vasodilation and blood flow in muscle tissue (*56*). Approximately 25% of insulin's effect on glucose uptake in muscle tissue is related to these hemodynamic actions (84, 85). This vascular recruitment paired with insulin's dilatory effects increase microcirculation and allow for faster circulation of insulin and faster uptake of glucose (*57*)(*56*)(*58*). Obesity and insulin resistance have been shown to cause impairments in microcirculatory function (*86*). In contrast, functional capillary recruitment was increases in individuals who had received a stimulus designed to elicit cephalic responses (41). Studies also showed that intervention with metformin, a drug which decreases glucose production and increases insulin sensitivity not only increases glucose metabolism by also microcirculatory function/recruitment (87,88).

There is a clear inverse relationship between CPIR and post-prandial glucose levels. Without CPIR, post-prandial blood glucose levels reach a high peak and stay above baseline for a longer period. Post-prandial glucose levels are of significant clinical relevance in diabetes. Elevated levels of blood glucose after a meal are hazardous, as they can cause tissue damage and more insulin to be released which can lead to longer periods of hyperinsulinemia and so contribute to insulin tolerance. High insulin levels sensitize apoptotic pathways, impair electrophysiological function of neurons and is consider toxic to cells as it increases their susceptibility to stress induced damage. Hyperinsulinemia is also associated with increased risk of T2D, obesity, cardiovascular disease and decreases life span (89,90). A longitudinal study carried out with Pima Indians indicates that a defect in acute/early insulin release occurs early in the progression from glucose tolerance to intolerance to diabetes (*91*). A separate study

looked at the effects of supplementing both obese and lean subjects with insulin prior to meal consumption. They found that insulin supplementation during the pre-absorptive state (1st phase) lowered obese subjects' post-prandial glucose levels while having no negative effects on lean subjects (*77*). These results support the link between pre-absorptive insulin secretion and post-prandial glucose levels and reinforce the potential therapeutic value of targeting anticipatory glucose regulation / CPIR.

While DMV-induced insulin secretion is a critical component of glucose tolerance, it is equally important to consider that the DMV may also contribute through other anticipatory mechanisms. As discussed earlier, elements such as glucagon, hepatic glucose metabolism, and incretins like GLP-1 play significant roles in modulating glucose tolerance. Beyond its indirect influence on these organs and molecules through insulin secretion, the DMV exerts direct effects via its projections to the liver, stomach, and pancreas. Understanding which specific cell types coordinate these processes would allow for finer understanding DMV-mediated glucose tolerance and potentially open up new therapeutic possibilities for conditions like Type 2 Diabetes.

Chapter 2. Heart Rate

Summary : [Reproduction of Strain, Conley, Kauffman et al., iScience 27, 109137 March 15, 2024]

Cardiovagal neurons (CVNs) innervate cardiac ganglia through the vagus nerve to control cardiac function. Although the cardioinhibitory role of CVNs in nucleus ambiguous (CVN^{nAMB}) is well established, the nature and functionality of CVNs in dorsal motor nucleus of the vagus (CVN^{DMV}) is less clear. We therefore aimed to characterize CVN^{DMV} anatomically, physiologically, and functionally. Optogenetically activating cholinergic DMV neurons resulted in robust bradycardia through peripheral muscarinic (parasympathetic) and nicotinic (ganglionic) acetylcholine receptors, but not beta-1-adrenergic (sympathetic) receptors. Retrograde tracing from the cardiac fat pad labeled CVN^{nAMB} and CVN^{DMV} through the vagus nerve. Using whole cell patch clamp, CVN^{DMV} demonstrated greater hyperexcitability and spontaneous action potential firing *ex vivo* despite similar resting membrane potentials, compared to CVN^{nAMB}. Chemogenetically activating DMV also caused significant bradycardia with a correlated reduction in anxiety-like behavior. Thus, DMV contains uniquely hyperexcitable CVNs capable of cardioinhibition and robust anxiolysis

Introduction

Cardiovagal neurons (CVNs) send axonal projections from hindbrain to cardiac ganglia through the vagus nerve to elicit cardioinhibitory (i.e., slowing of heart rate; HR) action at rest and during critical cardiorespiratory homeostatic reflexes. Although in mammals most CVNs are found in the nucleus ambiguous (CVN^{nAMB}), 20% of CVNs arise from a second region, the dorsal motor nucleus of the vagus (CVN^{DMV}) (*75*, *82–86*). While the ability of CVN^{nAMB} to control chronotropy (e.g., HR) is well characterized (*67*, *87*, *88*), whether this ability extends to CVN^{DMV} remains controversial, despite their extensive

innervation of cardiac tissue (*89*). CVN^{DMV} innervate cardiac tissue with unmyelinated, C fibers (*90*), the selective activation of which causes a bradycardia (or a decrease in HR) in multiple mammalian species (*91*)(*92*). In addition, studies of CVN ontogenesis implicate DMV, not nAMB, as the primary vagal nucleus in lower-order vertebrates and in early mammalian embryonic development, since CVN^{nAMB} migrate out of DMV (*93*)(*94*), making it possible that CVN^{DMV} retain functional cardioinhibitory activity in mammals. Despite these anatomical studies, functional studies remain conflicting. Some argue that direct electrical stimulation of DMV does not change chronotropy (*67*)(*68*), while others demonstrate local activation (chemical, electrical, optogenetic, or chemogenetic) elicits bradycardias even if only modestly (*95*–*98*)(*70*). However, no activation technique in awake animals used to date rules out incidental stimulation of either neighboring nucleus tractus solitarius (NTS) neurons or inhibitory interneurons within DMV. Stimulation of this latter population could significantly dampen the impact of cholinergic premotor neuron stimulation. Thus, whether cholinergic CVN^{DMV} are capable of controlling chronotropy remains an important but open question. A recent resurgence of interest in understanding of vagal physiology is driven by the growing number of therapeutic applications for vagus nerve stimulation (*69*). Of particular interest, vagus nerve stimulation is a promising treatment for anxiety and post-traumatic stress disorder (*99*, *100*). In rats, stimulating the vagus nerve accelerates extinction of conditioned fear (*72*, *99*) and decreases anxiety-like behavior in the elevated plus maze paradigm (*99*). In humans, vagal nerve stimulation may even reduce treatment-resistant anxiety disorders (*74*). However, the mechanism behind the anxiolytic effect of vagal stimulation is currently unknown. Since the vagus nerve is a bidirectional nerve, carrying sensory information from viscera to brain and motor information from brain to viscera, the extent to which the anxiolytic effect of vagus nerve stimulation depends on sensory or motor signaling is unclear. One possibility is that activating the vagus nerve decreases anxiety by slowing HR, in line with the James-Lange theory of emotions (*101*, *102*). Accordingly, a recent study in mice demonstrated that tachycardia (e.g. increase in HR) is sufficient to induce anxiety-like behavior

(*103*).Controversy over the role of CVN^{DMV} may stem in part from differences in CVN^{nAMB} and CVN^{DMV} electrophysiology and thus their roles in regulating HR. Notably, CVN^{nAMB} are largely quiescent *in vivo* and *ex vivo* (*104*, *105*), responding solely to integrated synaptic signaling. While limited data exist on the electrophysiological properties of CVN^{DMV} specifically, other DMV neuronal populations have unique pace-making properties and maintain a relatively high activity *ex vivo* (*71*), which allows for more complex signal processing. One investigation into their activity also suggests that, unlike CVN^{nAMB}, CVN^{DMV} do not demonstrate robust respiratory burst patterning (*106*). Therefore, it is tempting to speculate that CVN^{DMV} integrate and communicate central information differently from CVN^{nAMB} and represent a functionally unique circuit with respect to CVN^{nAMB}, which is consistent with evidence that CVN^{DMV} and CVN^{nAMB} target different cardiac ganglia (*107*). A more extensive characterization of the electrophysiological properties of CVN^{DMV} will help build a foundation for understanding their cardio-regulatory role, and importantly, for harnessing the therapeutic potential of vagus nerve stimulation. This is critical given that synaptic input to CVN^{DMV} is uniquely sensitive to perturbation of the cardiovascular system, relative to CVN^{NA} (*108*). The aim of the present study was to characterize the ability of DMV neurons to regulate HR functionally, physiologically, and pharmacologically. We hypothesized that activating choline acetyltransferase positive (Chat+) CVN^{DMV} elicits robust bradycardias. Moreover, we sought to characterize the electrophysiological properties of CVN^{DMV} to determine whether they are distinct from the more extensively studied CVN^{nAMB}. Testing of these hypotheses was accomplished using a combination of opto- and chemogenetic stimulation specifically in Chat+ neurons, pharmacology techniques to determine the regulatory role of CVN^{DMV} on chronotropy, and retrograde labeling paired with electrophysiology procedures to examine differences between the two CVN populations. Our results raise the possibility that CVN^{DMV} play a role distinct from CVN^{nAMB} in regulating HR.

Results

Optogenetic stimulation of Chat+ DMV can elicit bradycardia *{Boychuck Lab}*: To determine if CVN^{DMV} activation is capable of cardioinhibition, we used optogenetics to activate cholinergic neurons in DMV. Specifically, we crossed Ai32 mice expressing channelrhodopsin-2/EYFP fusion protein (ChR2) to loxP floxed choline acetyltransferase (Chat-Cre) mice to selectively express ChR2 in Chat+ neurons (Chat-Cre;ChR2). Chat-Cre;ChR2 and Chat-Cre mice were implanted with HR telemetry devices and fiber optic probes above the right DMV. HR was examined before and during photostimulation. A preliminary study found that 20 Hz (-261 ± 32 bpm; n = 4 mice) elicited a significantly larger bradycardia compared to 5 (-58 ± 28 bpm; repeated measure one-way ANOVA with Šídák's post-hoc, $p = 0.0003$), 10 (-126 ± 26 bpm; $p = 0.0064$), and 40 (-43 ± 16 bpm; $p = 0.0002$) Hz stimulation to DMV in Chat-Cre;ChR2mice (data not shown). We further verified that DMV neurons were continuously activated by 20 Hz photostimulation using whole-cell patch-clamp in brain slices from Chat-Cre;ChR2 mice (before: 2.5 ± 1.4 Hz versus during: 13.0 ± 2.7 Hz; repeated measure one-way ANOVA with Tukey's post-hoc, $p = 0.0482$; n = 5 neurons from two mice; DMV neurons from Chat-Cre;ChR2 mice also had lower firing frequencies immediately following stimulation (after: 1.4 ± 1.2 Hz; $p = 0.0321$), and they qualitatively demonstrated a pause immediately following stimulation termination that lasted for 10.3 ± 3.9 s with a range of 0.7 to 18 s.

Photostimulating DMV in awake male and female Chat-Cre;ChR2 mice significantly affected HR compared to Chat-Cre mice. During photostimulation, Chat-Cre;ChR2 decreased HR (271 ± 17 bpm) compared to HR before stimulation (605 ± 18 bpm; repeated measure two-way ANOVA with Šídák's post-hoc, $p < 0.0001$; n = 13 mice). Photostimulation failed to significantly affect HR during stimulation in control, Chat-Cre mice (before: 597 ± 61 bpm vs. during: 606 ± 31 bpm, $p = 0.9633$; n = 4 mice), confirming that photostimulation-induced bradycardia in Chat-Cre;ChR2 was not a consequence of off-

target effects or exposure to a laser (e.g., tissue necrosis, light diffusion, temperature effects). Finally, photostimulation-induced bradycardia in Chat-Cre;ChR2 was significantly different from HR responses to light in Chat-Cre control (comparing both mouse lines during stimulation: $p < 0.0001$). In contrast to photoexcitation of DMV neurons, photoinhibition of cholinergic neurons in DMV of awake mice using Chat-Cre mice crossed to Ai39 mice conditionally expressing halorhodopsin ($NpHR^{EYFP}$), produced no significant HR response to light (before: 629 ± 45 bpm vs. during: 627 ± 38 bpm; two-tailed paired Student's t-test, $p = 0.8950$, n = 3 mice). While these results suggest that under these conditions DMV neurons are sufficient to regulate HR but not necessary for control of resting HR, the decay kinetics of $NpHR^{EYFP}$ expressed by Ai39 mice are sufficiently fast enough that it might not cause a robust neural inhibition (*109*).

Since the axons of CVN^{nAMB} travel dorsally to converge with axons from CVN^{DMV} before turning and exiting the brainstem (e.g., [37]), it was possible that cardioinhibitory actions of DMV resulted from stimulating nearby CVN^{NA} axons. To rule out CVN^{NA} axonal stimulation, we first examined c-Fos expression in ChAT+ neurons two hours post-DMV stimulation. Qualitatively robust c-Fos was seen on the stimulated (right) side of DMV with no c-Fos expression in NA. We also confirmed using immunofluorescence that stimulating nAMB directly causes c-Fos expression. Finally in a subset of anesthetized $Chat^{cre}$;ChR2 mice, photostimulation of the exposed vagus nerve produced no change in HR (before: 422 ± 61 bpm vs. during: 419 ± 60 bmp; two-tailed paired Student's t-test, $p = 0.9723$; n = 3 mice). Taken together, axonal expression of ChR2 in nAMB was not sufficient to activate nAMB and elicit bradycardia.

DMV photostimulation-induced bradycardia works through canonical vagal circuits *{Boychuck Lab}*: To confirm that DMV photostimulation affects HR though autonomic pathways, male Chat-Cre;ChR2 mice

were administered an intraperitoneal (*i.p.)* injection of hexamethonium to block all nicotinic acetylcholine receptor (nAChR) communication between preganglionic and cardiac-projecting postganglionic parasympathetic neurons prior to DMV (n = 4) or nAMB (n = 3) photostimulation. Photostimulation of DMV (-261 ± 32 bpm) produced as similar of a robust bradycardia as photostimulation of nAMB (-255 ± 32 bpm) (repeated measure two-way ANOVA, $p = 0.8157$). As expected, pretreatment with hexamethonium abolished photostimulation-induced bradycardias from both brain regions (HR responses in DMV: 3 ± 3 bpm and HR responses in NA: -2 ± 1, $p < 0.0001$) and HR was also not different between DMV and nAMB during photostimulation after pre-treatment with hexamethonium (p = 0.9931).

To confirm that DMV photostimulation affects HR though muscarinic acetylcholine receptor (mAChR) activation from postganglionic parasympathetic neurons to cardiac tissue, consistent with canonical cardiovagal signaling, $Chat^{cre}$;ChR2 mice received *i.p*. injections of scopolamine methylbromide (to block parasympathetic activity) and atenolol (to block sympathetic activity) in a randomized order prior to photostimulation. In this subset of mice (n = 5), optogenetic activation of DMV neurons again induced robust bradycardia (-405 ± 46 bpm). Although administration of atenolol modestly reduced DMV light-induced bradycardias (-276 ± 39 bpm; repeated measure one-way ANOVA with Tukey's post-hoc, $p = 0.003$; atenolol also significantly decreased resting HR (before: 665 ± 21 vs. atenolol: 527 ± 10, $p = 0.0093$; n = 5). According to a simple linear regression, there was a significant negative relationship between resting HR and DMV light-induced bradycardia ($R^2 = 0.4741$, $p = 0.0277$). Therefore, it is likely that the impact of atenolol on DMV-related bradycardia is through overall reductions in resting HR, and not stimulation of postganglionic sympathetic pathways. Unlike atenolol, however, administering scopolamine methylbromide abolished DMV light-induced bradycardias (14 ± 3 bpm, $p = 0.002$, Thus, both nAChR and mAChR activity is required for photostimulation-induced decreases in HR from DMV,

similar to nAMB. Some reports suggest that DMV-mediated vagal activity on cardiac tissue occurs through non-canonical nAChR communication between postganglionic parasympathetic neurons to cardiac tissue (*110*). However, since mAChR antagonism abolished DMV light-induced bradycardias, this confirms that DMV neurons induce robust bradycardia through the canonical cardiovagal pathway nAChR→mAChR signaling (and not nAChR→nAChR).

DMV innervates cardiac tissue through the vagus nerve *{Boychuck Lab}*: Retrograde tracing with rhodamine and cholera toxin subunit B (CT-B) was done in male C57BL6/J mice to calculate the number of CVN^{DMV} and CVN^{NA} labeled by each tracer (n=6-8 mice per tracer for each CVN group;). Although both tracers identified positive neurons in nAMB and DMV, there were fewer traced neurons in CVN^{DMV} (31 ± 19 neurons) compared to CVN^{NA} regardless of tracer (99 ± 16 neurons; repeated measure two-way ANOVA with Šídák's post-hoc, $p < 0.0001$). In all animals, both right and left DMV contained CT-B labeled cells. In one animal examined for right versus left distribution, the right DMV contained more retrograde labeling (68 neurons) compared to the left DMV (45 neurons). This pattern was similar to previous reports in rats [39]. In addition, CT-B (47 ± 36 neurons) labeled significantly fewer neurons than rhodamine regardless of region (83 ± 33 neurons; $p = 0.0472$). There was not a significant interaction between CVN location and tracer ($p = 0.8294$). To confirm that retrograde labeling of CVN^{DMV} required an intact vagus nerve, a unilateral left vagotomy prior to cardiac injection of rhodamine was performed in a separate group of animals (n = 3 mice,). Unilateral vagotomy eliminated labeling of CVN^{DMV} ipsilateral to vagotomy (2 ± 1 labeled CVN^{DMV}) compared to the contralateral side (32 ± 8 labeled CVN^{DMV}; two-tailed paired Student's t-test, $p = 0.0483$; Taken together, DMV contains neurons that retrogradely label from cardiac tissue in a vagus-dependent manner.

CVN^{DMV} show spontaneous firing and have larger input resistance *ex vivo* compared to CVN^{nAMB}*{Boychuck Lab}*. To characterize the electrophysiological properties of CVN^{DMV} in relation to CVN^{nAMB}, additional studies examined the general excitability of CVNs in male C57BL6/J mice using whole-cell patch-clamp electrophysiology under current clamp configuration. Retrogradely labeled CVNs were identified using visual inspection for rhodamine and anatomical landmarks post-hoc biocytin recovery confirmed location and cholinergic phenotype CVN^{DMV} exhibited more spontaneous firing (8/14 neurons from 10 mice) compared to CVN^{nAMB} (0/10 neurons from 9 mice; Mann Whitney test, p = 0.0064), which were completely devoid of any spontaneous firing activity Of CVN^{DMV} exhibiting spontaneous firing (57%), the average frequency was 1.28 ± 0.31 Hz. No statistical differences in resting membrane potential were found between CVN^{DMV} (-58.60 ± 2.72 mV; n = 14 neurons from 10 mice) and CVN^{nAMB} (-62.18 ± 1.75 mV; n = 10 neurons from 9 mice; two-tailed unpaired Student's t-test, p = 0.3256) However, we found that CVN^{DMV} (492.00 ± 22.02 MΩ; n = 14 neurons from 10 mice) demonstrated significantly larger input resistance (R_{input}) than CVN^{nAMB} (158.20 ± 10.61 MΩ; n = 10 neurons from 9 mice; two-tailed unpaired Student's t-test, $p < 0.0001$;). Additionally, CVN^{DMV} (30.0 ± 1.5 pF) were significantly smaller in size than CVN^{nAMB} (61.1 ± 6.6 pF; two-tailed unpaired Student's t-test, $p<0.0001$) based on their recorded capacitance.

CVN^{DMV} are hyperexcitable compared to CVN^{nAMB} *ex vivo {Boychuck Lab}*: To determine if there were any differences in excitability between CVN^{DMV} and CVN^{nAMB}, CVNs were examined for general excitability through stepped depolarizations of current As expected, regardless of neuronal type, stepped current injections evoked a current dependent increase in action potential frequency (repeated measure two-way ANOVA with Šídák's post-hoc, p <0.0001) Additionally, a significant effect of neuronal type regardless of current injection was found, with CVN^{DMV} exhibiting a significantly greater number of evoked action potentials (5 ± 1 number of action potentials, n = 14 neurons from 10 mice) compared to

CVN^{nAMB} (2 ± 1 number of action potentials, n = 10 neurons from 9 mice; $p < 0.0001$). Finally, we found a significant interaction between current injection and neuronal type ($p < 0.0001$), with significantly more evoked action potentials in CVN^{DMV} compared to the CVN^{nAMB} at 100 (0.30 vs. 3.42 ± 0.5; $p = 0.0001$), 150 (0.80 vs. 5.00 ± 0.5; $p < 0.0001$), 200 (2.10 vs. 5.93 ± 0.5; $p < 0.0001$), and 250 pA (3.80 vs. 6.43 ± 0.6; $p = 0.0017$). Taken together, CVN^{DMV} are more excitable than CVN^{nAMB}.

Chemogenetic activation of DMV suppresses HR for up to 8 hours (Conley, Campbell Lab): Although our optogenetic studies could rule out interneuron activity, they could not exclude the possibility that off target stimulation of nearby Chat+ neurons (e.g., hypoglossal neurons) affected HR. Therefore, to confirm that activating DMV neurons decreases HR, we used an alternative strategy, chemogenetically activating DMV neurons with the excitatory designer receptor, hM3Dq. We specifically targeted hM3Dq expression to DMV neurons using an intersectional genetics approach which leverages the co-expression of *Chat* and *Phox2b* genes by DMV neurons but not by neighboring neurons (i.e., hypoglossal) (*20*, *111*). To validate this intersectional approach, $Chat^{Cre}$;$Phox2b^{Flp}$ mice were crossed with $R26^{ds\text{-}HTB}$ mice, a reporter line which expresses nuclear-localized, green fluorescent protein (GFP)-tagged histone 2b protein (H2b-GFP) upon recombination by both Cre and Flp. In the resulting $Chat^{Cre}$;$Phox2b^{Flp}$;$R26^{ds\text{-}HTB}$ mice, essentially all peripherally-projecting DMV neurons, as labeled by a systemic (*i.p.*) retrograde tracer, Fluoro-Gold, were H2b-GFP immunofluorescent (136/139 DMV neurons from four mice (97.8%) were both Fluoro-Gold+ and H2b-GFP+; representative image in Supplemental Figure 1A). These results confirm that $Chat^{Cre}$ and $Phox2b^{Flp}$ are co-expressed by nearly all DMV vagal efferent neurons and thus validate our intersectional approach. Next, to express hM3Dq specifically in DMV neurons, we injected an adeno-associated virus (AAV) which Cre- and Flp- dependently expresses a hemagglutinin (HA)-tagged hM3Dq (AAV1-CreON/FlpON-hM3Dq-HA; Figure 7A) into the DMV of male and female $Chat^{Cre}$;$Phox2b^{Flp}$;$R26^{ds\text{-}HTB}$ mice. This resulted in hM3Dq-HA expression in the vast majority of H2b-GFP+

DMV neurons ("DMV-hM3Dq" mice; Figures 7A-C). Importantly, we failed to detect any hM3Dq-HA expression in nAMB (Figure 7B-C) or in the DMV of mice lacking Cre and Flp recombinases (Supplemental Figure 1B), confirming the specificity of our injection strategy and AAV expression.

To determine whether chemogenetically activating DMV neurons affects HR, we administered the hM3Dq ligand clozapine N-oxide (CNO; 1 mg/kg; *i.p*.) to DMV-hM3Dq mice while measuring their HR by non-invasive electrocardiography (ECG; n=8 mice per genotype). Administering CNO significantly decreased HR for up to 8 hours compared to baseline (baseline: 718 ± 10 bpm; 20 min: 497 ± 34 bpm, $p = 0.0012$; 40 min: 497 ± 30 bpm, $p = 0.0008$; 60 min: 467 ± 36 bpm, $p = 0.0007$; 2hr: 469 ± 39 bpm, $p = 0.0011$; 6hr: 598 ± 19 bpm, $p = 0.0006$; 8hr: 637 ± 24 bpm, $p = 0.0274$; Figure 7 D). HR returned to baseline by 24 hours post-CNO (24hr: 731 ± 9 bpm, $p = 0.7247$). As expected, the acute bradycardia after CNO administration required peripheral muscarinic signaling, as it was abolished by administering the peripheral muscarinic blocker, methyl-atropine bromide (MA; 1.0 mg/kg; *i.p*.), 20min after CNO (baseline: 747 ± 5 bpm; after CNO: 640 ± 19 bpm *vs*. baseline, $p = 0.0078$; after MA: 801 ± 4 bpm *vs*. baseline, $p = 0.0004$; Figure 7E). On the other hand, administering CNO to hM3Dq-negative control mice failed to significantly alter HR ($p > 0.05$ *vs*. baseline or vehicle; Figure 7E; Supplemental Figure 1C), indicating that CNO alone does not affect HR. These results, together with our optogenetics studies, provide robust evidence that DMV neurons can decrease HR through peripheral muscarinic signaling.

Activating DMV neurons reduces anxiety-like behavior (Conley, Campbell Lab): Tachycardia increases anxiety-like behavior in mice (*103*), consistent with the James-Lange theory that physiological cues can drive emotional states (*101*, *102*). We therefore wondered whether the CNO-induced bradycardia we observed in DMV-hM3Dq mice corresponded to any change in anxiety-like behavior. To investigate, male and female DMV-hM3Dq mice and control mice (n=8 per group) were administered CNO or saline

vehicle and then assessed behaviorally by the open field test, an assay which measures anxiety-like behavior based on time spent in the center of an open arena (Figure 7F) (*112*, *113*). Strikingly compared to vehicle, CNO treatment in DMV-hM3Dq mice significantly increased their time spent in the center of the open field (CNO: 85.31 ± 17.38 s vs. Vehicle: 64.55 ± 13.98 s; two tailed paired Student's t-test, p = 0.0379, Figure 7G). The increased time spent in the center was not due to an increase in overall motility since total time spent moving did not differ significantly between saline and CNO treatments (two tailed paired Student's t-test, p = 0.4643, Figure 7H). In addition, CNO's effects on HR and center time in DMV-hM3Dq mice were moderately correlated (R^2 = 0.7734, p = 0.0414; Figure 7I). Thus, activating DMV neurons caused a correlated decrease in HR and anxiety-like behavior in the open field test.

To confirm the change in anxiety-like behavior, we assessed another cohort of DMV-hM3Dq mice in a different measure of anxiety, the elevated plus maze (*114*). CNO treatment significantly increased the time DMV-hM3Dq mice spent in the open-arms of an elevated plus maze, relative to vehicle treatment, indicating a decrease in anxiety-like behavior (CNO: 16.9 ± 4.83 s vs. Vehicle: 0.23 ± 0.23 s, repeated measure ANOVA with Tukey's post-hoc, p = 0.0235; Figure 7K). CNO treatment also significantly increased other signs of anxiolysis in DMV-hM3Dq mice: time spent moving (CNO: 162.6 ± 14.4 s vs. Saline: 40.7 ± 8.7 s; p = 0.0006; Figure 7L); head dip events (CNO: 4.149 ± 1.022 dips vs. Saline: 0.2414 ± 0.1424 dips; p = 0.0259; Supplemental Figure 1E); and average velocity (CNO: 2.339 ± 0.3068 cm/s vs. Saline, 0.6606 ± 0.2317 s, p = 0.0011; Supplemental Figure 1F). Importantly, however, treating hM3Dq-negative control mice with CNO did not affect their open-arm time, indicating that CNO itself does not decrease anxiety-like behavior (p = 0.3868; Supplemental Figure 1D). In addition, co-administering MA ("CNO+MA") to DMV-hM3Dq mice largely prevented CNO's effects on measures of anxiolysis, indicating that DMV-induced anxiolysis, like DMV-induced bradycardia, requires peripheral mAChR signaling (Figure 7K; Supplemental Figure 1E, F). Specifically, compared to vehicle treatment, CNO+MA failed to

significantly affect open-arm time, time spent moving, velocity or head dip events, relative to treatment with a saline vehicle ($p < 0.05$; Figure 7K, L, Supplemental Figure 1D,E). The decrease in HR trended towards a moderate correlation with the increase in open-arm time ($R^2 = 0.6394$, $p = 0.0878$; Figure 7M). Thus, our results show that activating DMV neurons similarly decreases HR and anxiety-like behavior, and that these effects each depend on peripheral muscarinic signaling.

To identify the muscarinic receptors mediating anxiolysis, we repeated our HR and elevated plus maze studies on DMV-hM3Dq mice but used a selective inhibitor of muscarinic type 2 receptors (M2), AQ-RA 741 ("AQ") (*115*), which does not appear to cross the blood-brain barrier (*116*). Administering AQ after CNO reversed the CNO-induced bradycardia (repeated measure ANOVA with Tukey's post-hoc, $p = 0.0016$; Supplemental Figure 1G). Importantly, in contrast to CNO alone, administering CNO with AQ (CNO+AQ) did not significantly affect time spent in the open-arms relative to saline treatment ($p = 0.2560$; Figure 7N). These results suggest that activating DMV neurons decreases anxiety-like behavior through a M2-dependent mechanism.

FIGURES

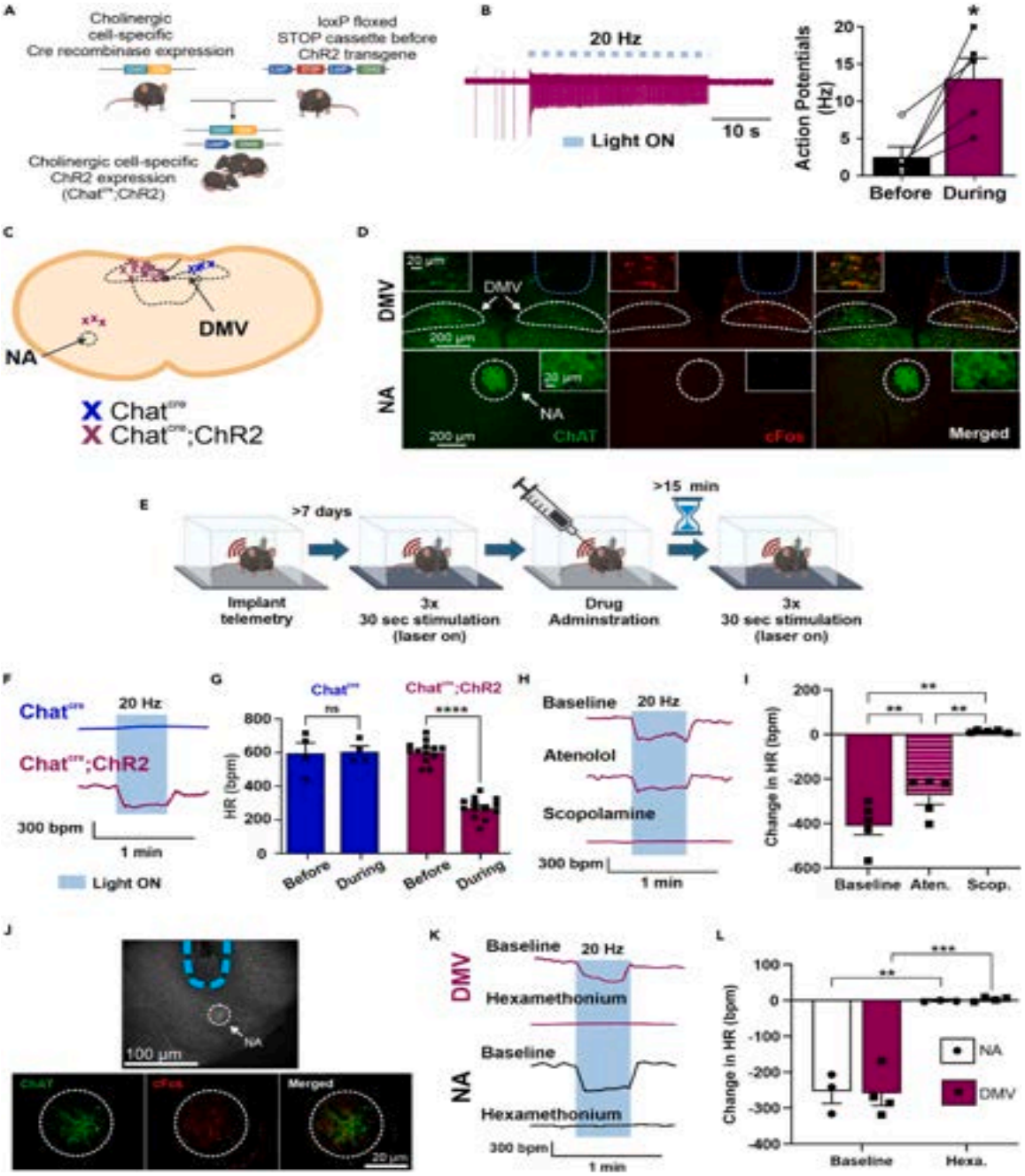

Figure 4: {Boychuck Lab} Optogenetic stimulation of DMV elicits bradycardia in male and female mice

Figure 4. ***{Boychuck Lab}:*** Optogenetic stimulation of DMV elicits bradycardia in male and female mice: Genetic crossbreeding paradigm used to generate transgenic mice harboring loxP-flanked ChR2 in Chat-

positive motor neurons (A). Photostimulation-evoked action potentials from DMV motor neurons to 20 Hz stimulation (B). Representative diagram illustrating confirmed locations of optogenetic probes (C). Representative images of DMV (top) and NA (bottom) stained for the neuronal activation marker, c-Fos (middle panel; red) and GFP (left panel; green) immunoreactivity confirming c-Fos activation in DMV, but not NA, after DMV photostimulation (D). Schematic illustrating time course of optogenetic studies in awake mice (E). Representative trace (F) and mean HR (G) showing optogenetic stimulation of DMV produced a bradycardia in mice expressing $Chat^{cre}$;ChR2 but not in $Chat^{cre}$ mice. Representative trace (H) and mean HR (I) showing i.p. muscarinic parasympathetic blocker, methyl-scopolamine, eliminated the photostimulation-induced bradycardia, while sympathetic blockage with b-1 receptor blocker atenolol mildly reduced this bradycardia. Representative images of probe site (top) and immunohistochemical staining of NA showing c-Fos activation after stimulation of NA (J). Representative trace (K) and mean HR (L) showing the nicotinic antagonist, hexamethonium (i.p.) abolished photostimulation-induced bradycardia in both DMV and NA. Bars represent mean and SEM. Blue bars/shading indicates light stimulation. Data analyzed by a repeated measure one-way ANOVA with Tukey's post hoc (B and I) or repeated measure two-way ANOVA with Sıdak's post hoc when appropriate (G and L). *p= 0.05, **p= 0.01, ***p= 0.001, ****p= 0.0001.

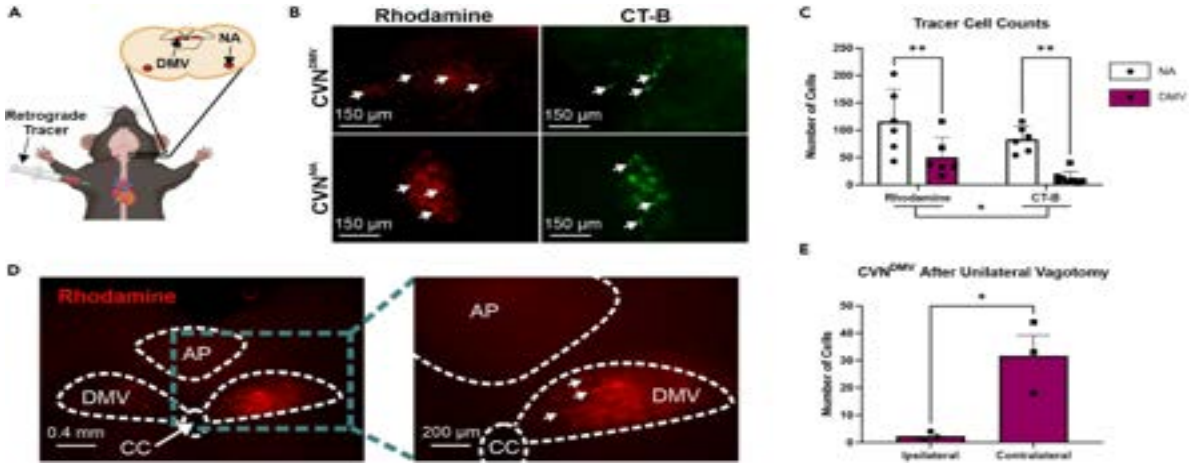

Figure 5: {Boychuck Lab} DMV innervates cardiac tissue through the vagus nerve in male mice

Figure 5. ***{Boychuck Lab}:*** DMV innervates cardiac tissue through the vagus nerve in male mice: Schematic showing injection into the epicardial fat pad and labeling in both CVN brain regions (A). Representative images of DMV and NA after cardiac injection of retrograde tracers, rhodamine (left in red) and cholera toxin subunit B (CT-B; right in green) (B). Both rhodamine and CT-B significantly labeled cardiac projecting neurons in NA and DMV as analyzed by a repeated measure two-way ANOVA with Sí dák's post hoc (C). Representative images of DMV after a right cervical vagotomy (C). Representative image (D) and mean cell count (E) showing a right cervical vagotomy significantly attenuated CVN^{DMV} numbers ipsilateral to vagotomy as analyzed by a two-tailed paired Student's t test. Bars represent mean and SEM. *p= 0.05, **p= 0.01, ***p= 0.001, ****p= 0.0001.

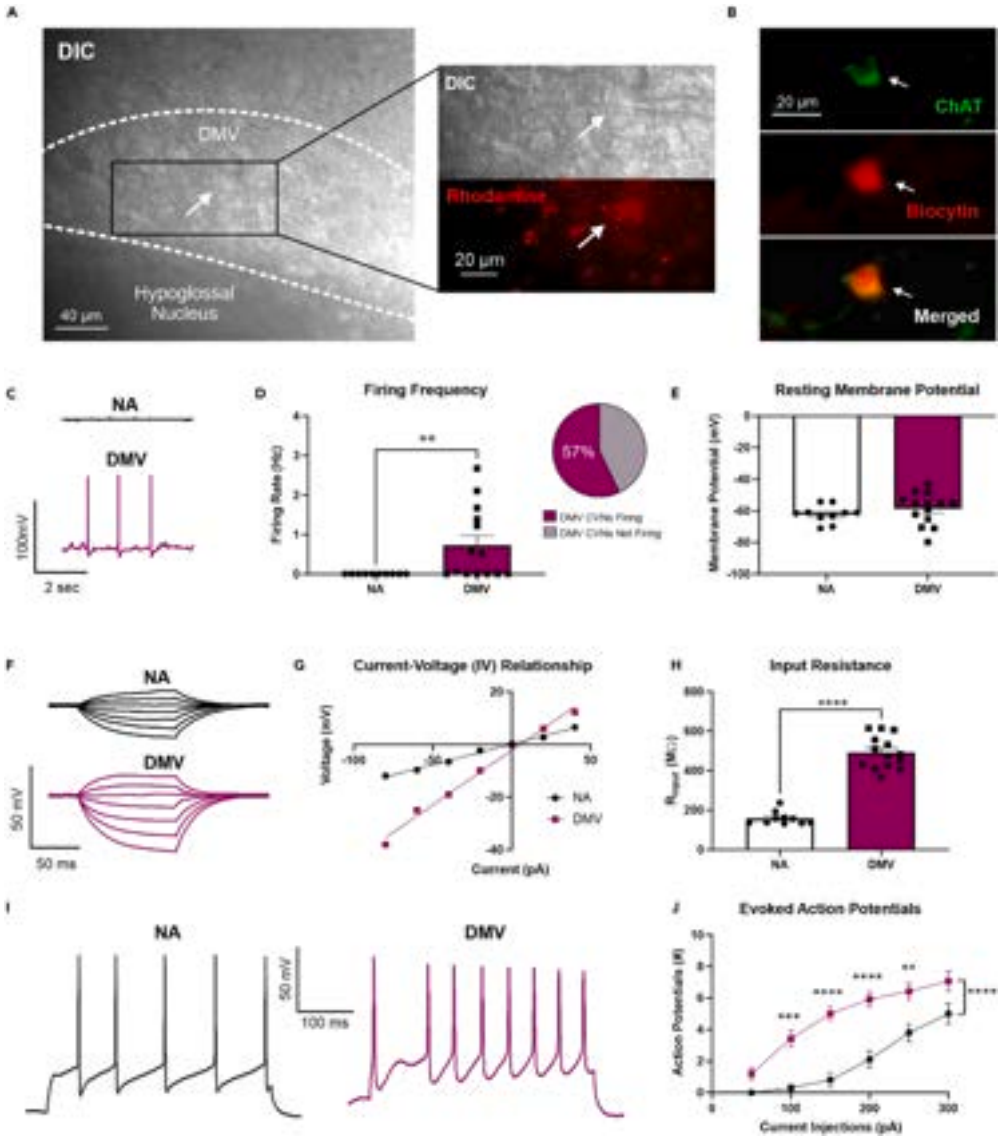

Figure 6: {Boychuck Lab} Differential electrophysiological properties of CVN^{DMV} compared to CVN^{NA}

Figure 6. ***{Boychuck Lab}:*** Differential electrophysiological properties of CVN^{DMV} compared to CVN^{NA} in male mice: Rhodamine-positive DMV neurons showing pipette (top) and rhodamine (bottom; red) (A). Representative immunofluorescence image of CVN^{DMV} showing biocytin recovered patched cardiac-labeled neurons are cholinergic (B). Representative trace (C) and mean firing rate (D) of CVN^{DMV} neurons show significantly higher spontaneous firing rates compared to CVN^{NA}, with the majority of CVN^{DMV} firing as analyzed by a Mann Whitney test. No statistical differences in resting membrane

potential were found between CVN^{DMV} and CVN^{NA} using a two-tailed unpaired Student's t test (E). Representative traces of membrane responses from CVN^{NA} (top) and CVN^{DMV} (bottom) to stepped current injections (F). Current-voltage (I-V) relationship graph obtained from CVN^{NA} and CVN^{DMV} (G). R_{input} was higher in CVN^{DMV} compared to CVN^{NA} as analyzed by a two-tailed unpaired Student's t test (H). Representative action potential responses in CVN^{NA} (top) and CVN^{DMV} (bottom) in response to 300 pA injection of direct depolarizing current (I). Action potential response curves were higher in CVN^{DMV} compared to CVN^{NA} in response to 50 pA-step injections of direct depolarizing current as analyzed by a repeated measure two-way ANOVA with Sídaḱ's post hoc (J). Data represent mean and SEM. *p= 0.05, **p= 0.01, ***p= 0.001, ****p= 0.0001.

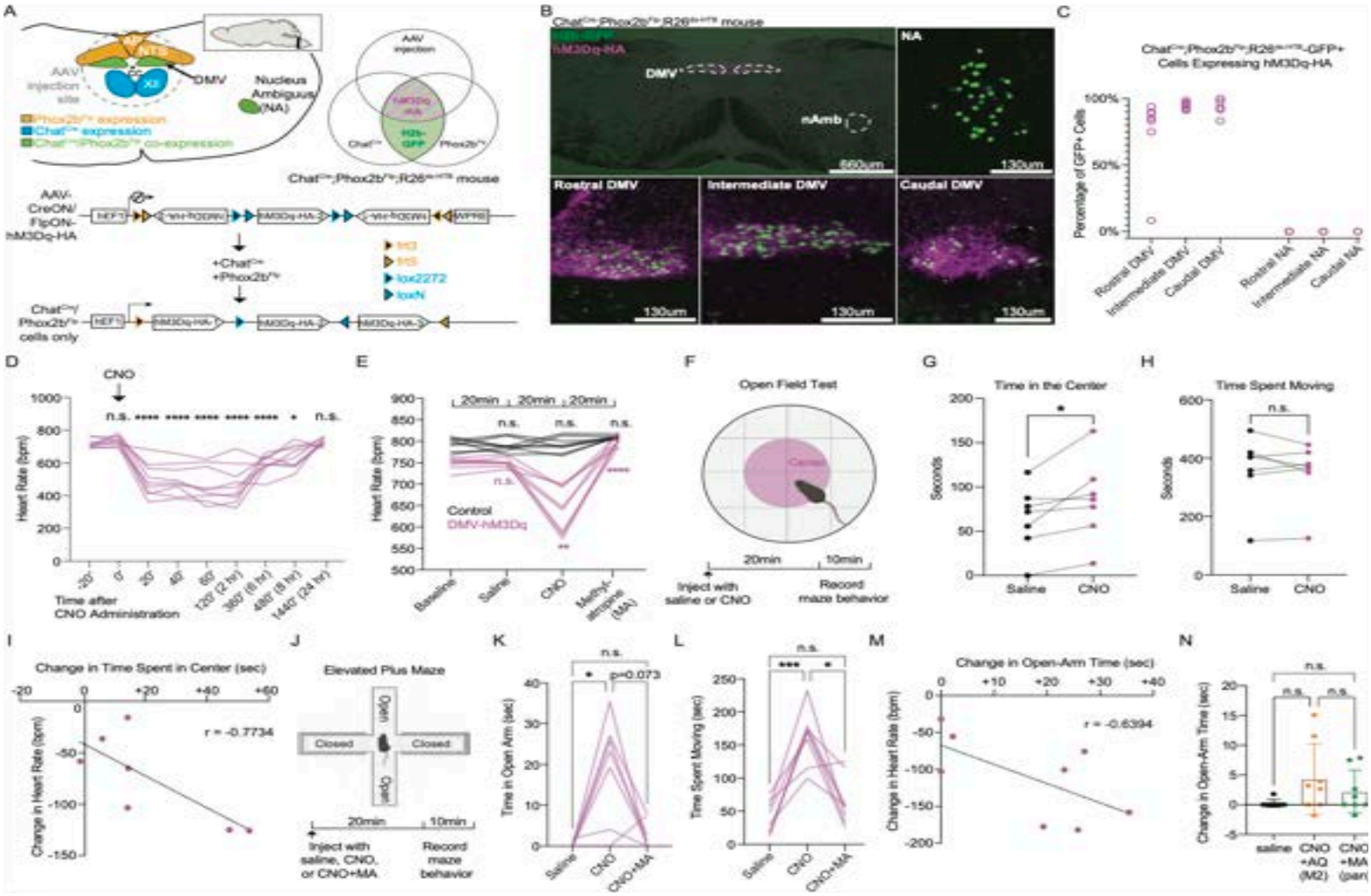

Figure 7: Chemogenetic Stimulation of the DMV produces bradycardia and reduces anxiety in both male and female mice.

Figure 7: Chemogenetic stimulation of DMV produces bradycardia and reduces anxiety in both male and female mice. Illustration of coronal hindbrain section showing injection site and *Chat* and *Phox2b* expression (A, top left); Schematic of AAV1-CreON/FlpON-hM3Dq-HA viral construct (A, bottom); Venn diagram showing expected expression of hM3Dq-HA and H2b-GFP (A, top right). Representative images of rostral, intermediate, caudal DMV and nAMB stained for HA (magenta) and H2b-GFP (green) immunoreactivity in $Chat^{Cre}$;$Phox2b^{Flp}$;$R26^{ds\text{-}HTB}$ mice after DMV injection of AAV1-CreON/FlpON-hM3Dq-HA (B). Percentage of H2b-GFP+ cells immunoreactive for hM3Dq-HA in the rostral, intermediate, and

caudal DMV and nAMB (C). Effect of CNO on HR in DMV-hM3Dq mice over 24-hour period. CNO (1mg/kg, *i.p.)* injected at time = 0 min (D). Effect of *i.p.* saline, CNO and CNO+MA on HR in DMV-hM3Dq (magenta) and control mice (black); comparisons are to baseline (E). Schematic of open field experiment (F). Effects of *i.p.* saline vehicle and CNO on time in the center of the open field, in seconds (G). Correlation between changes in HR and center time between saline and CNO conditions in DMV-hM3Dq mice (H). Schematic of elevated plus maze (EPM) experiment (I). Effects of *i.p.* saline vehicle, CNO and CNO+MA administration on time spent moving in the elevated plus maze, in seconds (J). Effect of *i.p.* saline vehicle, CNO and CNO+MA administration on open-arm time in the elevated plus maze, in seconds (K). Effect of *i.p.* saline vehicle, CNO and CNO+AQ administration on open-arm time in the elevated plus maze, in seconds. (L). Correlation between changes in HR and open-arm time between saline and CNO conditions in DMV-hM3Dq mice (M). Effects of *i.p.* MA and AQ-RA-741 on open-arm time in elevated plus maze, compared to saline; same saline, CNO, and CNO+MA data as in Figure 10K (N). Data represent mean and SEM. *p ≤ 0.05, **p ≤ 0.01, ***p ≤ 0.001, ****p ≤ 0.0001.

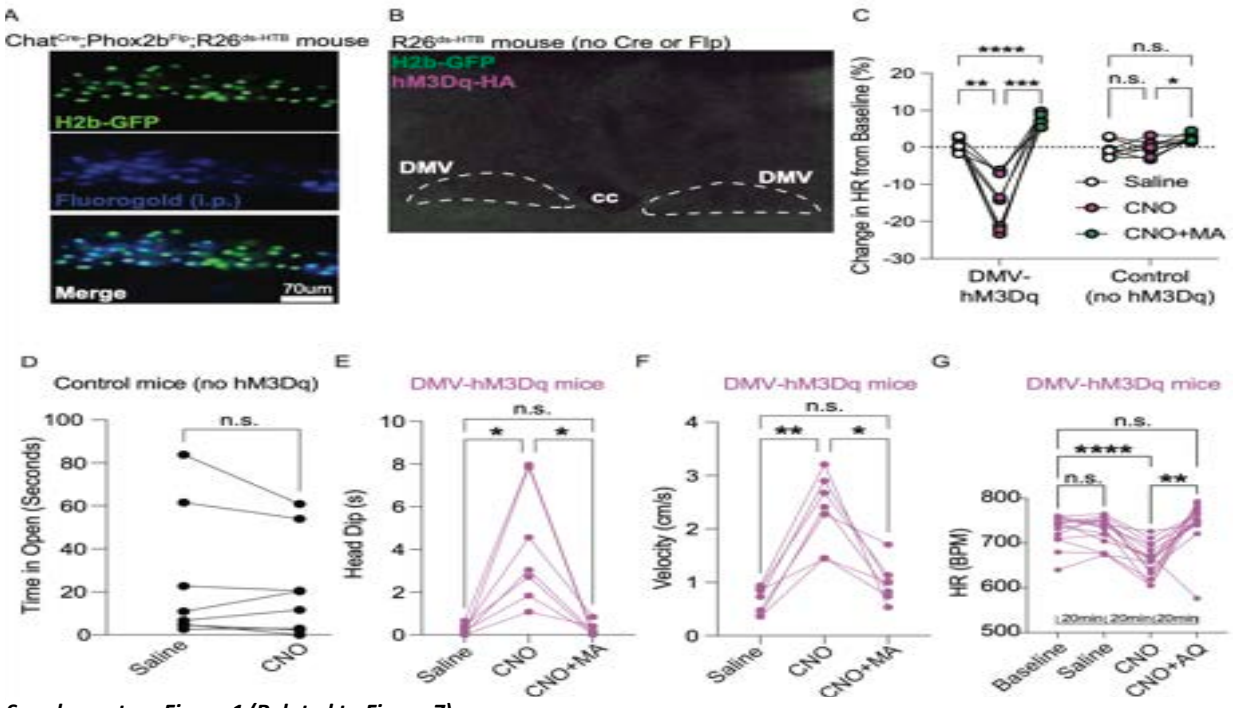

Supplementary Figure 1 (Related to Figure 7)

Supplemental Figure 1, related to Figure 7: Representative images of intermediate DMV hemisphere stained for H2b-GFP (green) and Fluoro-Gold immunoreactivity (blue) in $Chat^{Cre}$;$Phox2b^{Flp}$;$R26^{ds\text{-}HTB}$ mice after *(i.p.)* systemic injection of retrograde tracer Fluorogold (136 of 139, 97.8%, Fluoro-Gold+ DMV neurons were also H2b-GFP+); n=4 mice) (A). Representative images of intermediate DMV stained for HA (magenta) and H2b-GFP (green) immunoreactivity in $R26^{ds\text{-}HTB}$ mice (Cre-/Flp-) after DMV injection of AAV1-CreON/FlpON-hM3Dq-HA (B). Effect of i.p. saline (white), CNO (magenta) and CNO+MA (green) on HR in DMV-hM3Dq and control mice, relative to vehicle (C). Effect of saline or CNO on control mice, which lack hM3Dq expression, open-arm time in the elevated plus maze, n=8 mice (D). Effect of saline, CNO and CNO+MA in DMV-hM3Dq mice on head dip events and velocity in the elevated plus maze (E-F). Effect of saline, CNO and CNO+AQ on HR in DMV-hM3Dq (magenta) mice; same experimental design and baseline, saline, and CNO data as in Figure 7E (G). Data represent mean and SEM. *$p \leq 0.05$, **$p \leq 0.01$, ***$p \leq 0.001$, ****$p \leq 0.0001$.

Discussion

The present study characterized CVN^{DMV} anatomically, physiologically, and functionally. Retrograde tracing from the cardiac fat pad confirmed the presence of CVN in DMV using two different tracers, rhodamine and CT-B, and this labeling required an intact vagus nerve. Electrophysiological comparison of retrogradely-labeled CVN^{DMV} and CVN^{NA} indicate distinct circuits, with CVN^{DMV} being significantly more excitable with higher input resistances and spontaneous activity *ex vivo* whereas CVN^{NA} were not. Optogenetically activating DMV neurons caused bradycardia, which was completely abolished by muscarinic and nicotinic antagonism. Finally, intersectional chemogenetic activation of DMV neurons also caused bradycardia and a correlated decrease in anxiety-like behavior, both of which also required peripheral muscarinic signaling, as they were blocked by muscarinic antagonism. Previous efforts to

characterize *in vivo* electrophysiological properties of DMV neurons are limited, possibly a result of their prominent C-fiber phenotypes and long latency conduction times (*106*) making typical antidromic spike identification challenging. Our retrograde labeling findings are in accordance with previous reports, which suggest that only ~20% of CVN exist within DMV in totality (both sides), making the likelihood of recording from these numbers *in vivo* relatively low (*94*). Importantly, CVNs signal organization is an established example of divergent amplification, meaning that changes in HR arise from modulation (activation or inhibition) of a relatively small number of CVNs (*104*). Therefore, whole-cell patch-clamp recordings paired with retrograde labeling in adult animals—albeit confounded by the absence of relevant synaptic inputs *in vivo*—is a powerful technique that future studies should continue to use to aid in the investigation of this population of neurons both in health and disease. Our *ex vivo* results are consistent with electrophysiological recording in other DMV populations. DMV neurons demonstrate an on-going activity phenotype (71, *117*, *118*). This was true in the present study as ~57% of CVN^{DMV} demonstrated a spontaneously active firing pattern during the recording period. With regards to CVNs, this on-going firing activity is unique to CVN^{DMV} since no CVN^{NA} recorded exhibited any spontaneous activity in our slice preparation, which is also consistent with previous results from CVN^{NA} [31]. While future studies will need to demonstrate how this spontaneous activity is generated, it is consistent with the intrinsic pace-making properties of other DMV neurons. However, it also suggests that CVN^{DMV} may represent a functionally discrete circuit for cardiac-related vagal motor output. Previous studies suggest that CVN^{DMV} have little respiratory-related burst activity, despite robust lung-related afferent activity (*106*), which is in contrast to the CVN^{NA}, which show robust respiratory-related burst activity both *in vivo* and *ex vivo* (*104*). While we are only beginning to elucidate the complexity of vagal circuits as it relates to any vagal motor output, there is increasing evidence for distinct circuits related to vagal sensory afferents. Similar distinct circuits also likely exist in vagal motor nuclei (*20*, *21*, *57*). While some parallel circuits have converging anatomy and function, they may be distinct in terms of their physiological roles

(*57*). Finally, CVN^{DMV} demonstrated a significantly higher input resistance, higher number of spiking activity to current injections, and smaller size compared to CVN^{NA}. During optogenetic stimulation, CVN^{DMV} were also silenced for several seconds after stimulation implicating additional electrophysiological properties (i.e., unique ion channel contributions or stimulation-induced plasticity in neurotransmitter contributions) that could be investigated. Therefore, CVN^{DMV} are more excitable than CVN^{NA}. In other brain regions, this type of behavior confers a coincidence detection phenotype over a simple integrator (*119*). Therefore, future work should continue to investigate how CVNs in nAMB and DMV differ in their microcircuit construction in relation to the basic circuit building blocks of critical homeostatic regulating networks. Despite historical controversy about the capacity of CVN^{DMV} to impact HR, our results demonstrate that optogenetic and chemogenetic activation of Chat+ DMV neurons each caused robust bradycardia (~56% and ~65.5% of resting HR, respectively) in awake, behaving mice. Cardioinhibitory responses using optogenetic techniques in urethane-anesthetized rats and ketamine/xylazine-anesthetized mice demonstrated variable strength of the response (*95*, *98*), implicating differences in anesthesia for differences in effect size. Alternatively, previous species used (namely cats and rats) may exhibit less DMV-driven bradycardia than mice because of differences in vagal tonus. Since mice have a lower vagal tone than rats for example (*120–122*), CVN^{DMV} activation in mice may recruit a larger number of CVN^{DMV} which were not previously active. Although it is possible that fast decay kinetics of $NpHR^{EYFP}$ in the Ai39 mouse line limited the ability to significantly inhibit DMV neurons (*109*), the lack of an effect on HR of optogenetic inhibition of DMV in mice is similar to previous reports using inhibitory chemogenetic receptors (*70*). Therefore, while the present study introduced a significant refinement of techniques using $Chat^{cre}$ mice to eliminate the impact of known interneurons within DMV, it may suggest that CVN^{DMV} activity is not necessary for generation of resting HR, similar to a previous report (*70*).

While our Chat-targeted approach avoids influence of interneurons within DMV, the anatomical proximity of vagal axons from nAMB and the optical fiber in DMV (*94*) raises the possibility that DMV stimulation resulted in axonal stimulation of CVN^{NA} neurons. However, we failed to detect c-Fos expression in nAMB and DMV contralateral to the optical fiber, despite robust c-Fos immunoreactivity in the ipsilateral DMV. In addition, direct photostimulation of the vagus nerve in $Chat^{cre}$;ChR2 animals did not produce bradycardia. Finally, the more specifically targeted chemogenetic receptor hM3Dq expressed in DMV, but not other nearby cholinergic regions such as nAMB or hypoglossal neurons, caused a similar cardioinhibition to DMV stimulation in $Chat^{cre}$;ChR2. Taken together, these data provide robust evidence that solely activating DMV is sufficient for cardioinhibition. As expected, pharmacological testing confirmed that DMV stimulation-induced bradycardia requires mACh receptor activation in mice, since scopolamine (but not atenolol) and MA abolished optogenetically- and chemogenetically induced bradycardia, respectively. Notably, while the traditional concept of vagal motor signaling to cardiac tissue requires nicotinic receptor-dependent communication between preganglionic and postganglionic parasympathetic neurons, some studies report that intracardiac ganglia harvested from SA node also show mACh receptor-dependent neurotransmitter and calcium mobilization (*123*). Additional studies have attributed pharmacological differences in vagal fiber activation to C-fiber (presumably from DMV) versus B-fiber bradycardia (presumably from NA) since hexamethonium did not block the HR responses to non-myelinated fiber activation in these studies (*124*). Still, it is important to note that these studies did not comment on whether postganglionic neurons were isolated from cardiac nodal cells, nor did they directly address the effect of neurotransmitter release on the observed HR responses. Our findings are in accordance with the canonical signaling pathway between preganglionic and postganglionic parasympathetic neurons, as pre-treatment with the mACh receptor antagonist, scopolamine, completely abolished light-induced bradycardia in $ChAT^{cre}$;ChR2 mice. Recent research suggests that HR can influence emotional states,

supporting a theory of emotion separately proposed by the physiologist Carl Lange and psychologist William James over a century ago. As explained by James: "*My thesis […] is that the bodily changes follow directly the Perception of the exciting fact, and that our feeling of the same changes as they occur IS the emotion.*" (*102*). In other words, the James-Lange theory holds that HR does not increase because of anxiety; rather, the perception of HR increase is the anxiety. Consistent with this theory, a recent study in mice demonstrated that optogenetically increasing HR is sufficient to drive anxiety-like behaviors in the elevated plus maze (*103*). Inversely, beta-blockers such as propranolol, which robustly decrease HR (*125*), also reduce anxiety-like behaviors in mice (*126*, *127*). Beta-blockers and other drugs which decrease HR have shown promise for treating anxiety and related disorders (*128*), though the mechanism is not yet known. Studies of brain activity in humans and mice suggest the insular cortex may play a key role in sensing HR and other interoceptive cues (*103*)(*129–131*) and so could couple the perception of HR to emotional state.

Importantly, however, while our study is the first to our knowledge to demonstrate a correlation between vagally-mediated bradycardia and anxiolysis, more research is needed to establish a causal relationship. Our results with the cardio-selective M2 receptor antagonist AQ-RA 741 (*115*), which does not appear to cross the blood-brain barrier (*116*), suggests a cardiogenic mechanism for the anxiolysis we observed when activating DMV neurons. For instance, one possibility is that DMV decreases anxiety-like behavior by decreasing HR. This would agree with recent studies showing that optogenetically increasing HR is anxiogenic (*103*), whereas pharmacologically decreasing HR is anxiolytic (*132*). Indeed, the M2 receptors blocked by AQ-RA 741 are enriched in the heart relative to other organs innervated by the DMV (115,133) and are necessary for vagally-mediated bradycardia (*134*). However, M2 receptors are also present in the gastrointestinal tract where they interact with M3 receptors to modulate smooth muscle contraction (*135*). Therefore, our results do not rule out the possibility that DMV decreases

anxiety-like behavior through its projections to the gut (*135*)(*136*). Further research, e.g., targeting organ-specific DMV circuits, is needed to establish the mechanism by which DMV neurons can decrease anxiety. Whether other physiological functions of DMV, such as gut motility, glucose metabolism, and suppressing inflammation (*125*), are involved remains unknown.

In summary, this study demonstrates the existence of CVN^{DMV} neurons and their ability to suppress HR and anxiety-like behavior. The cardioinhibitory and behavioral effects both require mACh receptor activity, and our results also suggest that nACh receptors are involved in the signaling between CVN^{DMV} and cardiac parasympathetic neurons, implicating canonical vagal pathways in DMV's facilitation of cardioinhibitory activity. CVN^{DMV} also has distinct electrophysiological properties, namely spontaneous firing activity and higher R_{input}, compared to CVN^{NA} *in slice*. Therefore, we further speculate that CVN^{DMV} represents a unique population of CVNs, distinct from the more thoroughly characterized CVN^{NA}. Further research is needed to identify the molecular profile of CVN^{DMV}, the mechanisms underlying their distinct electrophysiological properties, and their physiological role.

Methods

EXPERIMENTAL MODEL AND SUBJECT DETAILS Mice: All animal procedures were approved by the Institutional Animal Care and Use Committee (IACUC) at the University of Texas Health San Antonio (UTHSA) or University of Virginia (UVA). Procedures were in accordance with the National Institutes of Health Guide for the Care and Use of Laboratory Animals (*137*). All mice were maintained under standard conditions with access to food and water *ad libitum* on a 14:10 light cycle in a temperature regulated room (23.9 ± 1.7 °C) at the University of Texas Health San Antonio (UTHSA) or a 12:12 light cycle in a temperature regulated room (20.6 ± 1.9 °C) at the University of Virginia (UVA). Mice were randomly assigned to experimental groups and age-matched (9-52 weeks old). Animals were group

housed unless stated otherwise. Sex is stated in the figure legends. All mice are maintained on a C57BL6/J background unless otherwise specified, and genotyping was performed according to guidelines from Jackson Laboratory or by Transnetyx. C57BL6/J adult mice (JAX #000664) were used for all experiments if not otherwise defined.

Optogenetic activation and HR: To generate a colony of transgenic mice with a constitutive knock-in of channelrhodopsin (ChR2) or halorhodopsin ($NpHR^{EYFP}$) in cholinergic neurons ($Chat^{cre}$;ChR2 and $Chat^{cre}$;NpHR, respectively), mice harboring a Cre-dependent cation channel channelrhodopsin (ChR2; Ai32(RCL-ChR2(H134R)/EYFP; JAX#024109) or halorhodopsin ($NpHR^{EYFP}$; Ai39(RCL-eNpHR3.0/EYFP; JAX#014539) were crossed with a $ChAT^{IRES\text{-}cre}$ ("$Chat^{cre}$") mouse lines (B6.129S-$Chat^{tm1(cre)Lowl}$/MwarJ; JAX#031661). This breeding strategy generates mice expressing ChR2 or $NpHR^{EYFP}$ in Chat neurons ("$Chat^{cre}$;ChR2" and "$Chat^{cre}$;NpHR" mice, respectively).

For brain region-specific optogenetic stimulation, $Chat^{cre}$;ChR2, $Chat^{cre}$;NpHR, or control ($Chat^{cre}$) mice were implanted with an optical fiber over the DMV or NA. First, mice were anesthetized with isoflurane to effect on a heating pad. Surgical sites were shaved and aseptically prepared with betadine and alcohol. Mice were first implanted with a HR telemetry (HRT) device (DSI, ETA-F10 implants, catalog # 270-0160-001) (*138*). Briefly, a vertical midline abdominal incision was made through the skin and peritoneal cavity. The telemetry device was placed in the peritoneal cavity with the leads tunneled to protrude from the peritoneal space. HR leads were then sutured in place in Lead II configuration and the peritoneal cavity closed with 4-0 silk suture. Wound clips were used to close the abdominal incision. Following HRT implantation, mice were fixed in a stereotaxic frame (Kopf Instruments, Model 962) and an optical fiber cannula (Thorlabs, 0.50 NA, Ø200 µm Core Multimode Fiber, FP200URT) was inserted through a hole drilled through the skull just dorsal to the DMV (from bregma; anterior/posterior: -7.43

mm, medial/lateral: 0.25 mm, dorsal/ventral: -2.65 mm) or nAMB (anterior/posterior: -7.31 mm, medial/lateral: 1.25 mm, dorsal/ventral: -3.95 mm). Optical fibers were secured using dental cement (A-M Systems, catalog # 525000 and 526000) and skull screws (Plastics One, 0-80- X 1/16). Subcutaneous administration of analgesics (buprenorphine 0.1 mg/kg and carprofen 10 mg/kg) were administered on the day of surgery and as needed for pain relief. Mice were monitored post-operatively for three days and allowed a week for recovery and acclimation to recording chambers.

During optogenetic stimulation trials, awake, behaving mice were temporarily singly housed with water available *ad libitum.* Photostimulation was performed using a diode-pumped solid-state blue (for $Chat^{cre}$;ChR2; 470 nm, Opto Engine LLC, MDL-III-470-300mW) or green laser (for $Chat^{cre}$;NpHR; 532 nm; Opto EngineLLC, MGL-III-532-300mW). Optical matching gel (Zeiss, Immersol 518F) was applied at the ferrule junction to reduce light loss. Transmission efficiency of all implanted lasers was confirmed prior to implantation (≥14 mW, 26.2 ± 6.8 mW) with a light meter (ThorLabs, PM100D). Phototrials consisted of 30 s of 20 Hz stimulation at 25mW pulsed laser output for DMV and 8mW for NA. All recordings occurred between 12:00 and 18:00 hour. Signals from HRT probes were acquired at a sampling frequency of 1 kHz using the DSITalker interface (Cambridge Electronic Design Limited) connected to the MX2 PhysioTel telemetry hardware (Data Sciences Inc.). HR was acquired 30 s before photostimulation and during a 30 s photostimulation period using Spike 2 (version 9) software (Cambridge Electronic Design Limited). All probe placements were confirmed postmortem.

For assessment of autonomic contributions to optogenetic stimulation, scopolamine methylbromide (1 mg/kg, Sigma Aldrich, catalog # S8502), a muscarinic acetylcholine receptor antagonist; atenolol (10 mg/kg, Sigma Aldrich, catalog # A7655), a β1 adrenergic receptor antagonist; and autonomic ganglionic blocker hexamethonium (30 mg/kg, Sigma Aldrich, catalog # H2138), a nicotinic ACh receptor (nAChR)

antagonist, were injected intraperitoneally (*i.p.*). A minimum of 15 minutes was allotted after drug injection before optogenetic stimulation.

Optogenetic stimulation of the vagus nerve: Chat^{cre};ChR2 mice (10-20 weeks old; body weight, 31 ± 6g) were anesthetized with ketamine/xylazine (100 mg/kg; 10 mg/kg) and placed on a heating pad before the surgical site was shaved and aseptically prepared with betadine and alcohol. A five mm cervical incision was made at midline. Blunt dissection was used to isolate the right cervical vagus nerve from the carotid sheath. Mineral oil was applied to the exposed nerve to keep it moist. An optogenetic probe was placed one mm from the exposed vagus nerve. After a 15-minute acclimation period, the vagus nerve was stimulated for 20 s at 20 Hz at an intensity of 25 mW. Three simulations were done with a 5-minute inter-stimulation interval.

Retrograde Tracing: Mice were anesthetized with ketamine/xylazine (100 mg/kg; 10 mg/kg) and ventilated (CWE SAR-830/AP with mouse attachment 12-01020) in the supine position on a heating pad (37 ˚C). The surgical site was shaved and aseptically prepared with betadine and alcohol. A small (~5 mm) incision was made to access the thoracic cavity and the pericardial sac was incised. Cholera toxin subunit-b (recombinant) conjugated with Alexa Fluor 488 (CT-B; 0.1 % v/v, 100 mM, Invitrogen, catalog # C34776) or tetramethylrhodamine-5-(and-6)-isothiocyanate conjugated with 5(6)-TRITC (rhodamine; 100 mL, Invitrogen T490) was then injected into the pericardial fat pad near the posterior right atrioventricular junction where cardiovagal nerve endings terminate. Surgical incisions were closed with 4-0 silk suture. Mice were monitored post-operatively for 3-6 days and allowed a week for recovery before experiments. Subcutaneous administration of analgesics (buprenorphine 0.1 mg/kg and carprofen 10 mg/kg) were administered on the day of surgery and as needed for pain relief.

Vagotomy: A subset of mice were anesthetized with ketamine/xylazine (100 mg/kg; 10 mg/kg) and ventilated (CWE SAR-830/AP, with mouse attachment 12-01020) in the supine position on a heating pad (37 ˚C). The surgical site was shaved and aseptically prepared with betadine and alcohol before a 5 mm cervical incision was made at midline. Blunt dissection was used to isolate the right cervical vagus nerve from the carotid sheath. A ~ 2 mm section was transected from the left cervical vagal nerve—sparing the aortic depressor nerve—to prevent regrowth/reattachment of the nerve. The superficial muscle and the cutaneous layer of the neck were sutured close with 4-0 silk suture. Mice then underwent retrograde tracing procedures as detailed above. Brains were harvested for immunohistochemistry procedures six days after retrograde tracing.

Electrophysiology: Mice (9-11 weeks old; 24.17 ± 0.86 g) were deeply anesthetized with isoflurane (3-4% in O_2) to effect (*i.e.*, lack of tail-pinch response) and decapitated while anesthetized. Brainstems were rapidly removed and immediately submerged in ice-cold (0–4°C) artificial cerebrospinal fluid (aCSF) equilibrated with carbogen gas (95% O_2, 5% CO_2). The aCSF composition (in mM) was: 124 NaCl, 3 KCl, 26 $NaHCO_3$, 1.4 NaH_2PO_4, 11 glucose, 1.3-2 $CaCl_2$, and 1.3 $MgCl_2$ (*139*). Osmolarity of all solutions was 290–305 mOSM; pH = 7.3–7.4. Brainstems were mounted and 300 µm coronal slices containing DMV and nAMB were cut using a vibratome (Leica Biosystems). Slices were transferred to a holding chamber and incubated in warmed (32–34 °C) oxygenated aCSF containing 1mM kynurenic acid (kyn-aCSF) for 20 min. Slices were then transferred to an oxygenated holding chamber at room temperature where they were maintained before being placed in a recording chamber mounted on a fixed stage of an upright microscope (BX51WI; Olympus), where they were continuously super fused again with warmed (32–34 °C), oxygenated aCSF (not containing kyn).

Whole-cell patch-clamp recordings under current clamp configuration were performed using infrared illumination and differential interference contrast optics (IR-DIC) under visual control. For recordings, glass pipettes (2–5 MΩ; King Precision Glass) were filled with a solution containing the following (in mM): 130 K+-gluconate, 1 NaCl, 5 EGTA, 10 HEPES, 1 $MgCl_2$, 1 $CaCl_2$, and Mg-ATP, pH titrated to 7.33-7.39 with KOH. Biocytin (Sigma Aldrich, catalog # B4261) was added to the internal solution to identify patched neuron identity and location post-recording. Action potential (AP) frequency, resting membrane potential (RMP), and input resistance (R_{input}) were measured. RMP was corrected for liquid junction potential post hoc (−7 mV). R_{input} was measured by injecting 400 ms current pulse of -80 to +40 pA in 20 pA increments. To measure AP response to depolarizing current pulses (400 ms) of increasing amplitude (50 to 300 pA), background current was injected to maintain the membrane potential of patched neurons at approximately −60 mV to ensure a consistent starting voltage between current injection sweeps. Number of APs during each depolarizing current step were counted.

Recordings were discarded if series resistance was >25 MΩ or changed by >20% throughout the course of the experiment. Average series resistance was 9.64 ± 1.01 MΩ in the DMV and 11.71 ± 1.55 MΩ in the NA. Electrophysiological signals were acquired at 10 kHz and recorded using an Axoclamp 700B amplifier (Molecular Devices), low-pass filtered at 2 kHz, and stored to a computer using a Digidata 1440A digitizer and pClamp 10.2 software (Molecular Devices). For all electrophysiological experiments, data from only one cell per slice was included for data analysis. No more than three cells were used from one animal per region. A minimum of 8-10 min following establishment of whole-cell configuration was used to allow equilibration of the intracellular recording pipette contents. Two min of continuous recording of steady-state activity was analyzed offline with Clampex 10.6 (Molecular Devices).

Chemogenetic activation: For chemogenetic studies, $Chat^{Cre}$;$Phox2b^{Flp}$;$R26^{ds\text{-}HTB}$ mice (13-52 weeks old; body weight, 25 ± 5g) were generated by first breeding Chat-Cre mice ($Chat^{tm1(cre)Lowl}$; JAX #028861) to Phox2b-Flp mice (Tg(Phox2b-flpo)3276Grds; JAX #022407), and then crossing the $Chat^{Cre}$;$Phox2b^{Flp}$ offspring to $R26^{ds\text{-}HTB}$ mice (gift of Martyn Goulding, Salk Institute for Biological Studies). The $R26^{ds\text{-}HTB}$ mouse line expresses a nuclear-localized, green fluorescent protein (GFP)-tagged histone 2b protein from the Rosa26 locus upon recombination by both Cre and Flp. Adult $Chat^{Cre}$;$Phox2b^{Flp}$;$R26^{ds\text{-}HTB}$ mice and $R26^{ds\text{-}HTB}$-only control mice were anesthetized with ketamine (80 mg/kg) and xylazine (10 mg/kg) then placed in a stereotaxic frame and on a servo-controlled heating pad to maintain a 37.0 ± 0.2 °C body temperature (RightTemp Jr.; Kent Scientific). Surgical sites were shaved and cleaned with betadine and isopropyl alcohol and injected with Nocita (long-lasting bupivacaine, 5.3 mg/kg, subcutaneously) for pre-operative analgesia. The dorsal surface of the medulla was then exposed by gently retracting the overlaying neck muscles and incising the meninges. A NanoJect III (Drummond Scientific, catalog # 3-000-207) was used to inject 40nL of adeno-associated virus (AAV) Cre/Flp-dependently expressing hemagglutinin (HA)-tagged hM3Dq (ssAAV-1/2-hEF1a/hTLV1-CreON/FlpON(HA_hM3D(Gq))-WPRE-hGHp(A), Viral Vector Facility, University of Zurich and ETH Zurich, catalog # vhW34-1) at each of 8 injection sites (320nL total volume) to ensure infection throughout the DMV (from calamus scriptorius; anterior/posterior: ±0.3 mm, medial/lateral ±0.15 mm, dorsal/ventral: -0.25 and -0.5 mm). Injections were made at 25nL/sec and the injection pipette was left in place for 5 minutes to minimize viral spread up the pipette track. After the final injection, the retracted muscles were sutured together over the injection site using absorbable sutures, and the skin was closed with Vetbond surgical glue. Mice were provided with Meloxicam Sustained-Release (ZooPharm; 5mg/kg; IP) for post-operative analgesia, 1 mL of lactated Ringers solution in 5% dextrose to support hydration and returned to the vivarium when ambulatory. These AAV-injected $Chat^{Cre}$;$Phox2b^{Flp}$;$R26^{ds\text{-}HTB}$ mice are referred to as “DMV-hM3Dq” mice.

Mice were monitored post-operatively for five days and allowed to fully recover for three weeks before acclimation to experimental environments and procedures.

Non-Invasive Electrocardiography: For 24-hour HR monitoring, mice were placed individually in portable electrocardiography (ECG) towers (ECGenie, Mouse Specifics Inc.) according to the manufacturer's instructions. ECG data were analyzed with EzCG software (Mouse Specifics, Inc.). After a 30 min acclimation period, baseline HR measurements (-20 min timepoint) were obtained by averaging at least three 10 sec epochs, which were manually reviewed to exclude those containing motion artifacts. Mice were then intraperitoneally injected with CNO (1.0mg/kg) at time 0. HR measurements from at least three 10 sec epochs were averaged per mouse per time point: 0 min; 20 min; 40 min; 60 min; 120 min; 6 hr; 8 hr; and 24 hr. Mice were kept in the towers from the -20 min time point until the 60 min time point, after which they were returned to their cages with access to food and water. For the 120 min, 6 hr, and 8 hr time points, mice were placed back into the towers for ECG recording and then returned to their cages. After the 8 hr time point, mice were returned to the vivarium. For the 24 hr time point, mice were re-acclimated for 30 min in the towers before collecting ECG data. Male and female mice were run on separate days.

For acute HR monitoring, mice were housed individually in ECGenie towers. As controls, we used CaTCh mice, a Cre/Flp reporter strain (Gt(ROSA)26Sor$^{tm80.1(CAG-COP4*L132C/EYFP)Hze}$, JAX#025109, (*140*) on a (129S6/SvEvTac x C57BL/6NCrl) genetic background. Mice were acclimated to the towers for 30 min before recording baseline HR measurements. At 20 min intervals, mice were temporarily removed from the towers and administered each of the following injections (i.p) in the order listed, in equal volumes per mouse: saline vehicle, CNO (1.0 mg/kg, Tocris Bioscience, catalog # 6329) and either CNO plus MA (CNO+MA) (CNO, 1.0 mg/kg; MA, 1.0 mg/kg, Sigma Aldrich, catalog # 2870-71-5) or CNO plus AQ-RA 741

(CNO+AQ) (CNO, 1.0 mg/kg; AQ, 1.0 mg/kg, Tocris Bioscience, catalog # 2292). HR measurements were recorded 15 min after each injection and averaged as described above. Other than temporary removal for injections, mice remained in the ECG towers for the duration of the experiment (approximately 1.5 hr).

Open Field: The open field (OF) maze is made of composite plastics and consists of a single circular arena 100 cm in diameter, enclosed by a wall 40 cm in height (Figure 7F). The maze arena consists of a center and outer ring, with the center ring extending to a radius of 29.4 cm, representing ¼ of the total area (*141*, *142*). The maze occupies a dedicated procedural room which is kept at constant temperature (19.0 °C) and illumination (100-120 lumens). Barriers are used so that the experimenter cannot be seen while the mouse is in the maze. All mice were acclimated to the experimenter and handled at least 5 days before testing. Additionally, mice were acclimated to the behavioral room and maze for 3 training sessions prior to testing. DMV-hM3Dq mice (n=7) were randomly assigned to two groups and the order of the two treatments – saline vehicle and CNO 1.0mg/kg - was randomized. The experimenter running the OF test was blinded to drug treatment until after all treatments were complete. Just prior to testing, mice were acclimated to the behavior room for 30 min. Each mouse received one *i.p*. injection, either saline vehicle or CNO, 20 min prior to testing and was then gently placed into the center of the open field test. Mice are allowed free exploration of the maze for 10 mins. Mouse movement was tracked over this 10 min period using a video camera and automated tracking software (EthoVision, Noldus). The time in the center and total time spent moving was calculated for the 10 min period using Noldus EthoVision software (Figure 7G,H). The maze was wiped clean with 70% ethanol spray before each use.

Elevated Plus Maze: The elevated plus maze (EPM) is made of plexiglass and consists of four arms (two open without walls and two closed with walls) (Figure 7J). The maze sits approximately 0.6 meters above

the floor, on a columnar platform, and underneath a video camera. The maze occupies a dedicated procedural room (see open field above) which is kept at constant temperature (66 °C) and illumination (100-120 lumens). Barriers are used so that the experimenter cannot be seen while the mouse is in the maze. All mice were acclimated to the experimenter and handled at least 5 days before testing. Additionally, mice were acclimated to the behavioral room and maze for 3 training sessions prior to testing. DMV-hM3Dq mice (see above; n=8) and their controls (n=8) were randomly assigned to four groups and the order of these four treatments was randomized: saline vehicle, CNO 1.0mg/kg, CNO+MA (CNO, 1.0 mg/kg; MA, 1.0mg/kg) and CNO+AQ (CNO, 1.0mg/kg; AQ-RA 741, "AQ", 1.0mg/kg). The experimenter running the EPM test was blinded to treatment until after all treatments were complete. Just prior to testing, mice were acclimated to the behavior room for 30 min. Each mouse received one *i.p*. injection, either saline vehicle, CNO, CNO+MA, or CNO+AQ, 20 min prior to testing and was then gently placed into the closed arm of the maze. Mice are allowed free exploration of the maze for each 10 min session. Mouse movement was tracked over this 10 min period using a video camera and automated tracking software (EthoVision, Noldus). The time spent in open-arms, time spent moving, velocity and head dip events are each calculated for the 10 min period using Noldus EthoVision software. Mice underwent each treatment condition twice, and results were averaged between the two trials. Mice were allowed at least 24 hours recovery between testing days. The maze was wiped clean with 70% ethanol spray before each use.

Immunohistochemistry: At the termination of optogenetic experiments, mice were deeply anesthetized with isoflurane then transcardially perfused with 0.1 M phosphate buffered saline (PBS) followed by 4% paraformaldehyde (PFA). Brains were cryoprotected in 30% sucrose before being sectioned (40 µm) on a cryostat at -19 ˚C (Leica Biosystems; CM 1860). Immunohistochemistry was performed on free floating sections for the immediate early gene product, cFos protein, as a marker of neuronal activation (rabbit

anti-cFos, 1:1000, Synaptic Systems, catalog # 226 003), and ChAT (goat anti-ChAT, 1:250, Sigma Aldrich, catalog # AB144P) to identify ChAT-positive motor neurons in DMV and NA. The following secondary antibodies were used: donkey-anti-rabbit (Alexa Fluor 488, 1:200, Invitrogen, catalog # A32790) and donkey-anti-goat (Alexa Fluor 568, 1:200, Invitrogen, catalog # A-11057). Negative controls were run without primary antibody.

At the termination of electrophysiology experiments, brain slices were post-fixed with 4% PFA and then cryoprotected in 30% sucrose for at least two days before being sectioned (40 µm) on a cryostat at -19 ˚C. Biocytin-filled neurons were processed via avidin, Texas Red staining (TX Red Avidin D; 1:400; Vector Laboratories, catalog # A-2206). Free floating sections were also immuno-labeled for ChAT (goat anti-ChAT, 1:250, Sigma Aldrich, catalog # AB144P) to detect ChAT-positive motor neurons as detailed above. At the termination of chemogenetic HR and behavioral studies, mice were transcardially perfused as described above. Brains were then cryoprotected in 25% sucrose solution before being sectioned (35 µm) on a freezing microtome (SM2010R, Leica Biosystems). Next, brain sections were washed 3 times for 5 minutes each in phosphate buffered saline (PBS) on a shaker. After washing, brain sections were incubated in blocking solution (PBS with 0.1% Triton X, PBT, plus 2% donkey serum) overnight at 4°C. Next, immunohistochemistry was performed on free floating sections for hemagglutinin (HA; reporter for hM3Dq expression) (chicken-anti-HA 1:200, Aves Labs, catalog # ET-HA100) and ChAT (goat anti-ChAT, 1:250, Sigma Aldrich, catalog # AB144P) on brain sections representing the rostral, mid, and caudal DMV. Primary antibodies were diluted in blocking solution and added to brain sections for 2 hours at room temperature. A second wash cycle (3 rounds of 5 min) with PBS is performed before transferring the brain sections to secondary antibody solution. The following secondary antibodies were used: donkey-anti-chicken (Alexa Fluor 647, 1:2000, Thermo Scientific, catalog # A78952) and donkey-anti-goat (Alexa Fluor 568, 1:200, Invitrogen, catalog # A-11057). All secondaries were diluted in

blocking solution and left to incubate overnight at room temperature. Following secondary incubation, brain sections underwent a third wash cycle (3 rounds of 5 min) in PBS before brain tissue was then mounted on glass slides, cover-slipped with a DAPI-containing mounting medium (Vectashield, Vector Labs, catalog # H-1000), and imaged on a fluorescence microscope (Revolve, Echo) using filters suitable for the appropriate fluorescent dyes and the following objectives: Olympus 2x Apochromat PLAN APO 2X objective, numerical aperture (NA) 0.08, working distance (WD), 6.2mm; Olympus 10x Fluorite U PLAN PHASE FLUORITE 10X objective, Ph1 Phase,nAMB0.30, WD 10mm; Olympus 20x Apochromat U PLAN S-APO 20X objective,nAMB0.75, WD 0.6mm. Images were processed using Revolve Pro software and Image J (*143*).

QUANTIFICATION AND STATISTICAL ANALYSIS

Results are reported as mean ± standard error of the mean (S.E.M.). For *in vivo* experiments, 'n' is the number of animals. For *ex vivo* experiments, 'n' is reported as number of recorded cells and the number of animals. These values are stated when appropriate throughout the Results and Figure Legends. Graph creation and statistical analysis was conducted in GraphPad Prism 9 (GraphPad Software). Specific statistical tests are noted in the Results. In general, two-tailed Student's t-test was conducted with parametric data containing two groups (paired or unpaired when appropriate). A Mann Whitney test was conducted with non-parametric data containing two groups. A one-way ANOVA followed by Tukey's multiple comparisons was used when there was one independent variable and more than two groups. A two-way ANOVA followed by Šídák's Multiple Comparison Test was used when there were two independent variables. Repeated-measures ANOVA was used when comparing multiple timepoints within subjects. The Geisser-Greenhouse correction was used if the sphericity assumption for ANOVA was not met. Simple linear regression was used to examine the relationship between two continuous

variables. Pearson correlation was used to examine the strength of the relationship between two variables. Differences were considered statistically significant if $p \leq 0.05$. Graphs indicate individual mouse data or mean and SEM.

Acknowledgements

We gratefully acknowledge Martyn Goulding (Salk Institute) for the $R26^{ds\text{-}HTB}$ mouse line. Funding was provided by a Pathway to Stop Diabetes Initiator Award 1-18-INI-14 and an NIH R01 HL153916 to J.N.C., an NIH R01 HL157366 to C.R.B. and an NIH T32 HL007446 for M.M.S

Author Contributions.

M.M.S., N.J.C., L.S.K., M.J., S.B.G.A., J.N.C., and C.R.B. designed experiments. M.M.S, L.E., and S.F. performed optogenetic and cardiac tracing studies, including HR analysis, and all histology/immunofluorescence. L.E. and C.R.B. performed electrophysiological studies. A question from G.E.H. inspired the study of anxiety-like behavior. N.J.C., L.S.K., M.E.C., and P.C.M. performed chemogenetic study of HR and anxiety-like behavior. N.J.C. and L.S.K. performed histology and immunofluorescence experiments related to chemogenetic studies. M.M.S., N.J.C., J.N.C., L.E., and C.R.B. prepared figures. M.M.S., N.J.C., L.S.K., C.R.B., and J.N.C. wrote the manuscript with input from all authors.

Chapter 3: Glucose Tolerance

Summary

The DMV is a region of the medulla which is the primary source of parasympathetic output to the digestive tract and controls glucose metabolism. Different subtypes of DMV neurons are thought to have distinct physiological roles, but their specific functions, gene expression, and synaptic circuitry are not well-defined. To address these knowledge gaps, we used an intersectional genetics approach to identify DMV neurons which can control glucose metabolism. Our results identified a molecularly and anatomically distinct subtype of DMV neurons marked by expression of the gene *Calb2*. We compared Calb2 DMV neurons with another DMV neuron subtype, Grp DMV neurons, in terms of anatomy and organ innervation. Calb2 DMV neurons were found in different subregions of the DMV and, unlike Grp DMV neurons, selectively innervated the pancreas and not the stomach. Chemogenetic activation of DMV neurons in general improved glucose tolerance during an intraperitoneal glucose tolerance test but did not alter baseline blood glucose levels. Surprisingly, activation of Calb2+ DMV neurons had no significant effect on glucose tolerance or insulin secretion. Our findings suggest that a molecularly distinct subtype of Calb2- DMV neurons control DMV-mediated insulin secretion. Identifying and understanding the specific DMV neurons involved opens potential avenues for targeted therapies for metabolic disorders such as diabetes.

Introduction

The regulation of glucose levels in the blood is crucial for an organism's well-being and survival. Both hyperglycemia (high blood sugar) and hypoglycemia (low blood sugar) can be toxic and life-threatening. Due to these dangers and its importance as an essential fuel, circulating glucose levels are tightly

maintained within a homeostatic window of 4-6 mM (39). A critical component in maintaining blood glucose levels is the parasympathetic nervous system, which provides anticipatory control over pancreas endocrine functions and the generation, storage, and release of glucose in the liver. These anticipatory mechanisms function to prime the body to handle incoming glucose challenges more effectively and work in conjunction with glucose-induced reactive mechanisms. For instance, before and at the onset of a meal, the parasympathetic nervous system works through the vagus nerve to decrease glucose release from the liver and increase insulin secretion from the pancreas. These physiological changes help the body shift from internal to dietary sourcing of glucose and reduce postprandial hyperglycemia. Parasympathetic neurons which innervate the pancreas and liver are found exclusively in one region of the medulla, the dorsal motor nucleus of the vagus (DMV). Previous studies have found that electrically stimulating or genetically disinhibiting DMV neurons increases blood insulin levels (29, 15, 154). Other studies have shown that chemogenetically activating or inhibiting cholinergic neurons within the dorsal medulla, including the DMV neurons, increases and decreases glucose tolerance, respectively (76). However, the DMV also contains neurons which control gut motility, gastric acid secretion, and other digestive functions, and the specific identity and functional organization of DMV neurons which control glucose metabolism remain unknown.

A recent single-cell genomic study identified molecular subtypes of DMV neurons which form distinct circuits to the digestive tract, raising the possibility that these molecular subtypes are functional units of the DMV (24, 25) Among these were cholinergic DMV neurons which express the gene encoding melanocortin 4 receptor (Mc4r), previously shown to control blood insulin and glucose levels and project to the pancreas (55, 154, 155, 156). We therefore investigated whether these neurons innervate the pancreas and can control glucose metabolism. Our results reveal a molecularly and anatomically distinct subtype of DMV neurons which selectively innervate the pancreas and surprisingly do not

secreted insulin when activated and, unlike DMV neurons more generally, do not improve glucose tolerance when activated during an IPGTT.

Results

Calb2 expression marks an anatomically and molecularly distinct population of DMV neurons. Since previous research showed that *Mc4r*+ DMV neurons control blood insulin levels, we used an existing single-cell genomics dataset to identify a genetic marker for targeting *Mc4r*+ DMV neurons. Our analysis showed that the gene *Calb2* [Figure 8D], which encodes the calcium-binding protein Calbindin 2, was highly co-localized with *Mc4r* expression among DMV neurons. To validate *Calb2* as a marker for DMV neurons and characterize their anatomy, we performed RNA fluorescent in situ hybridization (RNA FISH) and imaged DMV expression of *Chat* (a marker for cholinergic neurons*), Calb2* and *Grp*, a marker for a different (*Calb2*-negative) DMV neuron subtype. Our results show that *Calb2* and *Grp* mark distinct DMV neurons found in different DMV subregions [Figure 8C]. Specifically, Grp*+* DMV neurons are found more medially and caudally, while *Calb2*+ DMV neurons largely reside at the lateral poles of the intermediate DMV [Figure 8C,E]. This location is significant because previous studies have shown that electrically stimulating the lateral poles of DMV elicits the most insulin and most glucagon secretion (*68*).

Calb2+ DMV neurons innervate the pancreas but not the stomach. To determine whether Calb2 DMV neurons innervate the pancreas, we performed anterograde tracing from Calb2 DMV neurons using a Calb2-Cre mouse line (JaxID 010774) and an adeno-associated virus (AAV) which Cre-dependently expresses placental alkaline phosphatase (157) Transgenic PLAP expression enables chromogenic staining of neural processes so that they can be visualized in optically cleared organs (157) [Figure 9A]. After transducing DMV neurons with AAV-DIO-PLAP in adult Calb2-Cre and Grp-Cre mice, we harvested and optically cleared stomach and pancreas samples, chromogenically stained PLAP+ axons, and imaged

the stained axons in cleared tissue samples by stereoscope microscopy. As a positive control, we repeated these studies in Chat-Cre mice, which express Cre in all DMV neurons (22) Our results show that, while DMV neurons in general ($Chat^{DMV}$ neurons) innervate both the pancreas and the stomach [Figure 9B, Supplemental Figure 2A], $Calb2^{DMV}$ neurons innervate the pancreas but not the stomach [Figure 9C.E], whereas the opposite was true for Grp^{DMV} neurons [Figure 9D, Supplemental Figure 2C]. These results indicate that, unlike Grp^{DMV} neurons, $Calb2^{DMV}$ neurons selectively target the pancreas, consistent with previous studies of *Mc4r*+ DMV neurons (156).

To further characterize the pancreas projections of *Calb2*+ DMV neurons, we performed anterograde tracing from Calb2-Cre DMV neurons using a AAV which Cre-dependently expresses the cytosolic fluorescent protein, tdTomato (AAV-FLEX-tdTomato) [Figure 9A]. Imaging cleared tissue samples of the pancreas showed tdTomato-immunofluorescent fibers (blue) co-localized with pan-neuronal marker PGP9.5 immunofluorescence (orange), confirming the tdTomato+ fibers as neural processes [Figure 9F-H]. Consistent with our PLAP tracing results, we observed $Calb2^{DMV}$;tdTomato+ fibers entering the pancreas [Figure 9F,G] and branching off deeper within the pancreas [Figure 9H]. Our PLAP and tdTomato anterograde tracing results show that $Calb2^{DMV}$ neurons innervate the pancreas.

Optogenetically Activating DMV Vagal Efferent Neurons Significantly Improves Glucose Tolerance

To confirm that activating DMV neurons can improve glucose tolerance, as previously reported (76), we performed an intraperitoneal glucose tolerance test (IPGTT) while using optogenetics to stimulate DMV neurons in awake, behaving mice. IPGTT's were performed to bypass any oral phase of digestion. To specifically activate DMV neurons, we used intersectional genetics to target expression of a calcium-conducting channelrhodopsin2 variant (CaTCh) to cells co-expressing Chat-Cre and Phox2b-Flp, which is specific to DMV vagal efferent neurons within the dorsal medulla [Figure 8F]. We then surgically placed

an optical fiber over the DMV to selectively stimulate CaTCh+ DMV neurons. We measured fasting glucose levels in tail blood samples collected at regular intervals before and after an intraperitoneal administration of glucose to fasted mice, with or without ("sham stimulation") optogenetic stimulation. Comparing the same mice between stimulation and sham conditions showed that photo-stimulating DMV neurons significantly decreased blood glucose levels during IPGTT [Figure 10B]. This effect persisted after normalizing blood glucose measurements to baseline [Figure 10C]. In addition, analyzing the area under the curve revealed significant decreases in glucose at both 15 min and 120 min [Figure 10D]. These results indicate that activating DMV vagal efferent neurons increases glucose tolerance, consistent with previous reports (76).

Chemogenetically Activating DMV Vagal Efferent Neurons Significantly Improves Glucose Tolerance

To confirm our intersectional optogenetic results, we used another approach, intersectional chemogenetics, to activate DMV neurons while measuring glucose tolerance. To target the excitatory chemogenetic receptor, hM3Dq, to DMV vagal efferent neurons ($Chat^{DMV}$ neurons), we injected a Cre- and Flp-dependent AAV-hM3Dq-HA into the DMV of adult Chat-Cre;Phox2b-Flp mice, an approach we previously validated for specifically activating DMV neurons (148 Figure 4) We then injected the mice with the hM3Dq ligand, clozapine-n-oxide (CNO; 1 mg/kg), to activate hM3Dq+ DMV neurons, or saline vehicle, while measuring tail blood glucose levels during an IPGTT. Baseline pre-IPGTT blood glucose levels did not differ significantly 20min after CNO treatment relative to vehicle [Figure 10F], suggesting that activating $Chat^{DMV}$ neurons does not alter basal blood glucose levels in fasted mice. However, CNO treatment significantly improved glucose tolerance at both the 5 min and 15 min IPGTT timepoints, relative to vehicle treatment [Figure 12F]. These effects were present even after normalizing to pre-IPGTT baseline blood glucose levels [Figure 10G], consistent with an increase in glucose tolerance. In addition, similar to our results with optogenetic stimulation of $Chat^{DMV}$ neurons, we observed a

significant decrease in the glucose AUC at the 15 min IPGTT timepoint [Figure 12H]. Unlike optogenetic stimulation, however, AUC did not differ significantly between CNO and vehicle treatments at the 120 min IPGTT timepoint. Together, our results indicate that activating DMV vagal efferent neurons, whether optogenetically or chemogenetically, increases glucose tolerance.

Calb2+ DMV Chemogenetic Activation Insufficient for Glucose Tolerance

Since Calb2^{DMV} neurons innervate the pancres, we investigated whether they can control glucose tolerance by activating them with intersectional chemogenetics [Figure 8A,B] while measuring glucose tolerance [Figure 10I-K]. Surprisingly, unlike what we observed when activating Chat^{DMV} neurons, administering CNO (1.0mg/kg) to activate Calb2^{DMV} neurons did not result in an improvement in glucose tolerance [Figure 10I-k]. These results indicate that Calb2^{DMV} neurons are not sufficient for improving IP glucose tolerance.

To determine whether Calb2 neurons were sufficient for controlling insulin release we looked at blood insulin levels after baseline, saline and CNO treatments [Figure 10L]. No significant change in insulin levels was observed between the treatment conditions indicating that Calb2^{DMV} neurons are also insufficient for insulin secretion. While insignificant, we also observed a biphasic trend in glucose tolerance during Calb2^{DMV} activation, where glucose tolerance is slightly perturbed 0-15min and slightly improved 15-120min [Figure 10I,J, Supplementary Figure 2D]. This effect appears to be sexually dimorphic with male Calb2^{DMV} animals exhibiting a larger 0-15min increase in glucose and females exhibiting a larger 15-120min decrease in glucose.

Figures

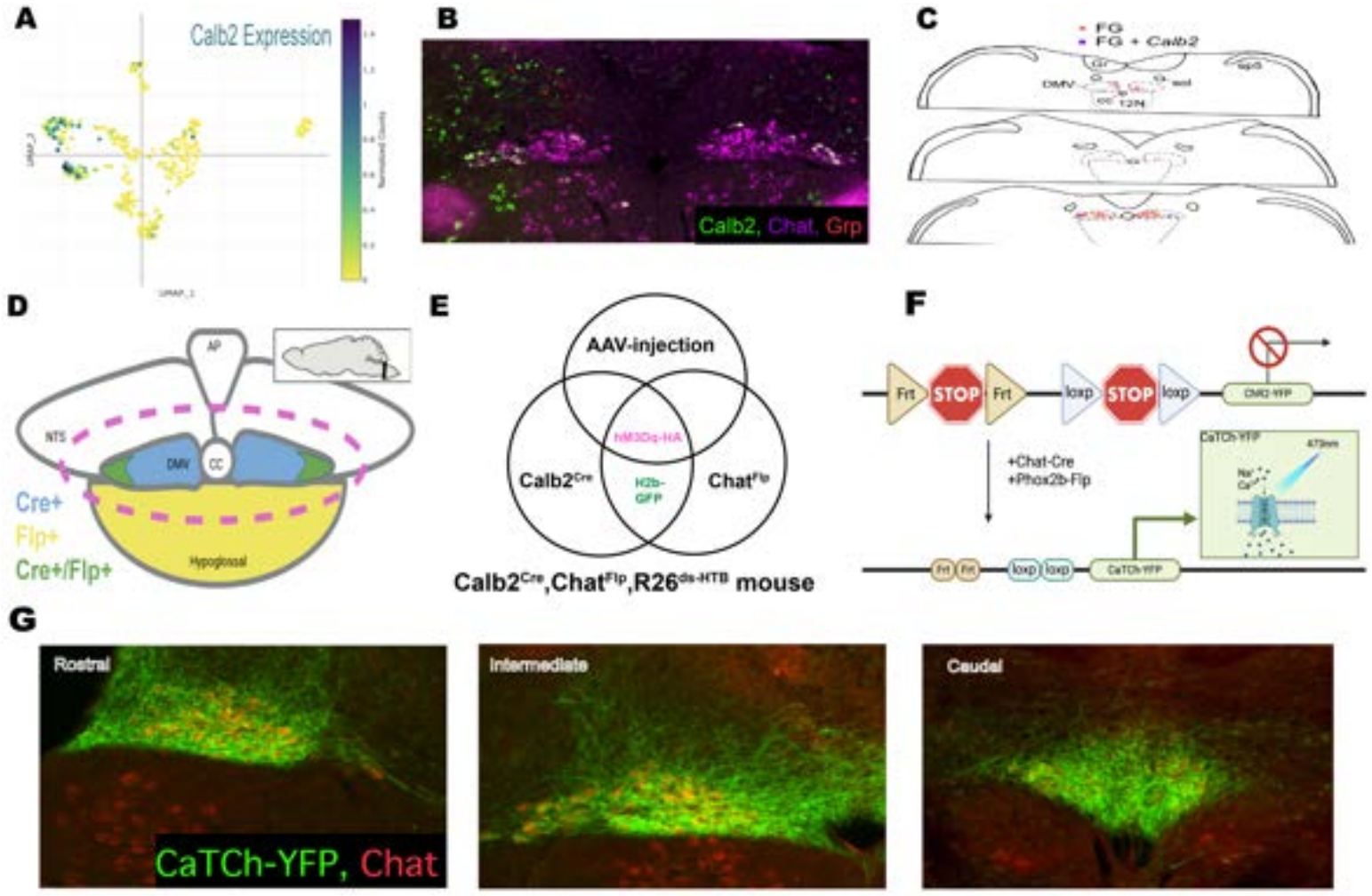

***Figure 8: Calb2* is a discrete population of DMV neurons with unique spatial localization**

Figure 8. Calb2 is a discrete population of DMV neurons with unique spatial localization

(A) Calb2 expression heatmap (modified 22). B) Representative images of Calb2, Grp and Chat RNA FISH in the intermediate DMV. (C) anatomical map of Calb2+ DMV neurons, prepared by Stephen B. G. Abbott from our RNA FISH data (Fluorogold+, Flurogold+Calb2+). (D) Schematic of DMV, Intersectional approach for Calb2+Chat+. (E) Calb2-Cre;Chat-Flp;dsHTB. (F) Cre-On Flp-On Schematic, Chat-Cre:Phox2b-

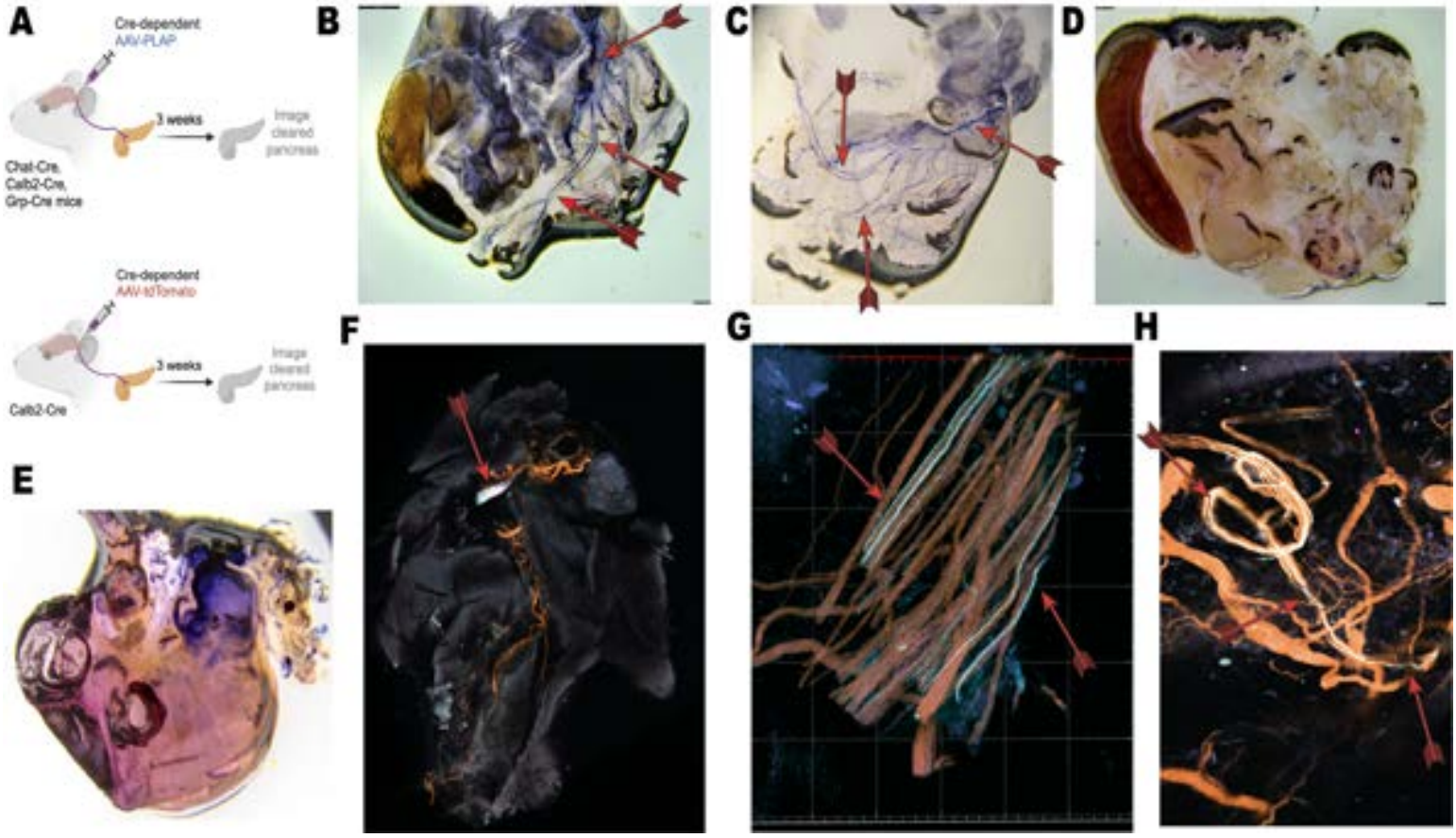

Figure 9: Calb2 DMV Neurons Innervate the Pancreas

Figure 9: Calb2+ DMV neurons project to the pancreas (A top) Schematic of PLAP anterograde tracing method used for (B-E). (A bottom) Schematic of tdTomato anterograde tracing method used for (F-H). (B) PLAP anterograde tracing in pancreas from Chat-Cre DMV neurons. (C) PLAP anterograde tracing in pancreas from Calb2-Cre DMV neurons. (D) PLAP anterograde tracing in pancreas from Grp-Cre DMV neurons. (E) PLAP anterograde tracing in stomach from Calb2-Cre DMV neurons. (F-I) tdTomato anterograde tracing cleared pancreas from Calb2-Cre DMV neurons. PGP9.5, tdTOM

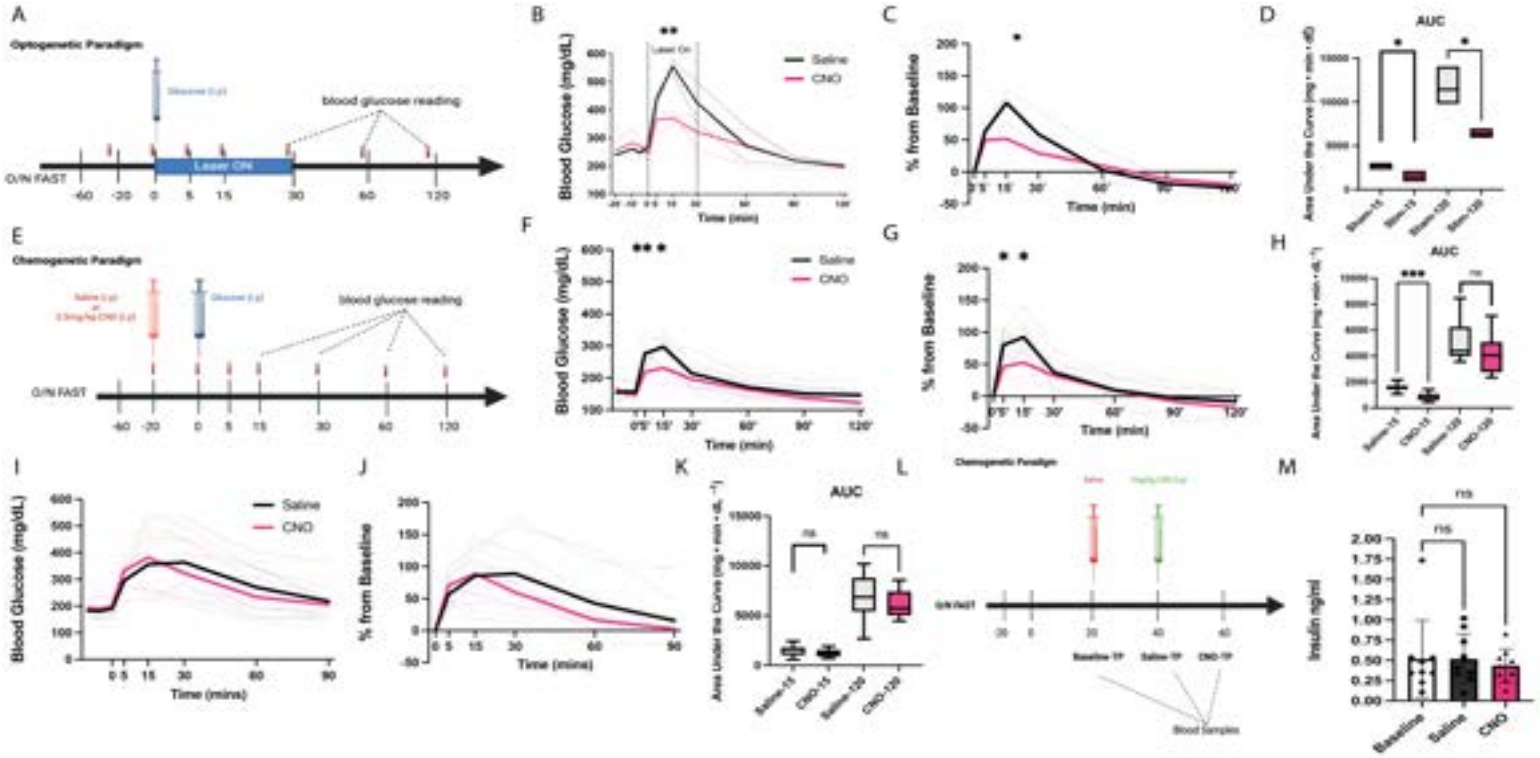

Figure 10: Effects of optogenetic and chemogenetic activation on glucose tolerance in Calb2^{DMV} and Chat^{DMV}

Figure 10: Chemogenetic and Optogenetic IPGTT for Chat-Cre;Phox2b-Flp and Calb2-Cre;Chat-Flp: (A) Schematic of optogenetic-IPGTT paradigm. (B) Chat-Cre;Phox2b-Flp;CaTCh IPGTT absolute values; two-way ANOVA, Šidák's multiple comparison test, p=0.0006, n=3. (C) % baseline change; two-way ANOVA, Šidák's multiple comparison test, p=0.0051, n=3. (D) area under the curve; welch's t-test, p=0.0.134(120mins), p=0.0448(15mins), n=3. (E) Schematic of chemogenetic-IPGTT paradigm. (F) Chat-Cre;Phox2b-Flp;dsHTB IPGTT absolute values; two-way ANOVA, Šidák's multiple comparison test, p=0.0052(5min), p=0.0363(15min), n=8. (G) baseline change; two-way ANOVA, Šidák's multiple comparison test, p=0.0146(5min), p=0.0174(15min), n=8. (H) area under the curve; Welch's t-test, p=0.0008(15mins), n=8. (I) Calb2-Cre;Chat-Flp;dsHTB IPGTT absolute values; two-way ANOVA, Šidák's multiple comparison test p=ns, n=8. (J) % baseline change; two-way ANOVA, Šidák's multiple comparison test p=ns, n=8. (K) area under the curve; Welch's t-test, p=ns, n=8. (L) Insulin ELISA performed on fasted Calb2-Cre;Chat-Flp;dsHTB; two-way ANOVA, Šidák's multiple comparison test p=ns, n=9. *p ≤ 0.05, **p ≤ 0.01, ***p ≤ 0.001, ****p ≤ 0.0001

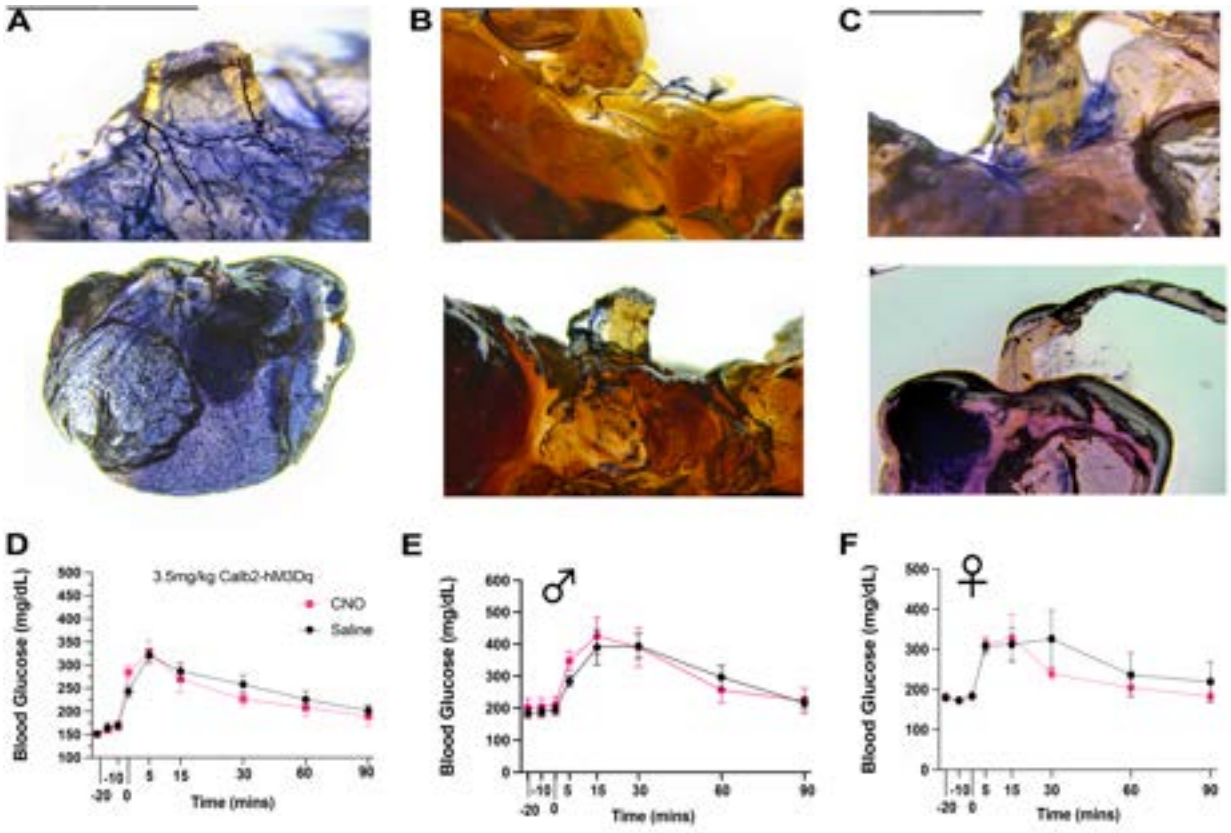

Supplementary Figure 2 (Related to Figures 9,10)

Supplementary Figure 2., Related to Figure 9,10: (A) PLAP anterograde tracing in Chat-Cre stomach (B) PLAP anterograde tracing in Chat-Cre Liver (C) PLAP anterograde tracing in Grp-Cre stomach/lower esophageal sphincter (D) Calb2-hM3Dq IPGTT performed with 3.5mg/kg. (E) Male Calb-hM3Dq IPGTT 3.5mg/kg CNO vs saline (F) Female Calb2-hM3Dq IPGTT 3.5mg/kg CNO vs saline.

Discussion

Whole DMV stimulation via chemogenetic activation of Chat+Phox2b+ neurons was sufficient to increase glucose tolerance. This result supports previous literature in which Chat+ DVC chemogenetic stimulation improved glucose tolerance at t=30min (*76*). The relevant impact of simultaneous DMV and

hypoglossal stimulation may account for the difference seen in how long glucose tolerance modulation took to manifest between studies.

Unexpectedly, chemogenetic activation of Calb2^{DMV} neurons did not significantly affect glucose tolerance or insulin secretion. One possible explanation is that Calb2^{DMV} neurons primarily innervate the pancreas to control exocrine functions, such as amylase and lipase secretion, rather than endocrine functions.

Alternatively, Calb2^{DMV} neurons may regulate pancreatic endocrine function by promoting glucagon secretion instead of insulin. Glucagon is known to modulate glucose-induced insulin secretion through beta-cell glucagon receptors (GCGR) (159). When beta cells are active, glucagon can act on beta-cells' GLP-1 receptors (GLP-1Rs), enhancing insulin secretion and lowering glucose levels (42) . Moreover, ablation of alpha cells or their secretory products has been shown to impair insulin secretion (43). Cephalic glucagon responses have been observed (160), and recent studies suggest that alpha cells are crucial for the cephalic insulin response and glucose tolerance (161) This highlights glucagon as a potentially critical potentiation mechanism for beta-cell insulin secretion. Optogenetic stimulation of ARC-POMC to DMV-ACh neurons has been shown to promote hepatic glucose output and gluconeogenesis (55) emphasizing the DMV's role in regulating hepatic function and maintaining glucose levels and tolerance. Recently, a pre-meal rise in GLP-1 has been observed within a restricted feeding paradigm, likely affecting glucose levels directly through canonical GLP-1 pathways and indirectly by enhancing sweet taste (162). Additionally, optogenetic stimulation of glucose-sensing GLP-1R+ neurons in the DMH project through the DMV to regulate insulin and basal glucose levels (163).

The absence of DMV-mediated signaling to the stomach and liver in the Calb2^{DMV} stimulation, as opposed to Chat^{DMV} stimulation, could clarify our findings. The potential role of glucagon as the primary cephalic phase glucose-regulating secretory product might be crucial here. Given that glucagon and

alpha cells are essential for cephalic phase insulin release (CPIR) in mice, we propose that DMV-mediated glucagon release, which enhances beta cells' sensitivity to glucose-induced insulin secretion (GIIS), is a critical early endocrine event in the cephalic cascade. However, this mechanism alone may not be sufficient to improve glucose tolerance.

We speculate that without proper DMV-mediated inhibition of hepatic gluconeogenesis and signaling to the stomach for GLP-1 secretion, the DMV-pancreas endocrine response is unable to adequately compensate for prandial glucose flux. The DMV's orchestration of these mechanisms likely primes maximal insulin secretion and optimal glucose tolerance. This hypothesis aligns with previous suggestions that subtypes of pancreas-projecting DMV neurons are distinct, responding either to GLP-1 or PP but not both (164) We further speculate that separate Calb2-DMV+ populations may exist to control these cephalic endocrine responses. If so, it could imply that various subtypes work together to orchestrate distinct functions, rather than one subtype controlling a single function. It appears to be a modular system where subtypes perform specific elements of a function via their target organ, and the timing and overlap of these mechanisms maintain optimal tolerance. If DMV subtypes responsible for these discrete elements of glucose tolerance are genetically distinct, it will allow for their selective molecular targeting for therapeutic manipulation and further understanding.

Our RNA scope results confirm and support previous models of the DMV that spatial regions of the DMV are genetically distinct from one another (*24*) and form longitudinal columns (*12,29*) [Figure 8C,E]. Interestingly the DMV subtype marked by Calb2 localized to the lateral poles, where the most insulin and glucagon secretion was observed during an electrical stimulation study (*29*). Anterograde tracing results support previous research showing that genetically distinct DMV subtypes innervate separate target organs with Calb2 projecting to the pancreas and Grp projecting to the stomach/lower esophageal sphincter (*24,25,92*). One key limitation of our anterograde tracing studies is that they don’t

allow for the differentiation between left and right vagal innervation, so it is impossible to determine the relative contributions of each hemisphere to these pancreas projecting neurons.

Methods

Experimental Model Details: All animal care and experimental procedures were approved in advance by the University of Virginia Institutional Animal Care and Use Committee and in accordance with the National Institutes of Health Guide for the Care and Use of Laboratory Animals (*137*). All mice were maintained under standard conditions with access to food and water *ad libitum* on a 12:12 light cycle in a temperature regulated room (20.6 ± 1.9 °C) at the University of Virginia (UVA). Mice were randomly assigned to experimental groups and age-matched (9-72 weeks old). Animals were group housed unless stated otherwise. Sex is stated in the figure legends when data is seperated. All mice are maintained on a C57BL6/J background unless otherwise specified, and genotyping was performed according to guidelines from Jackson Laboratory or by Transnetyx.

The fluorescent *in situ* hybridization experiments used C57BL/6J mice from the Jackson Laboratory (JAX, 000664). The following mouse lines were used for optogenetic studies: Chat-Cre;Phox2b-Flp;CaTCh (Chat-Cre Rossi et al., 2011; JAX, 028861)(Phox2b-Flp Hirsch et al., 2013; JAX, 22407)(CaTCh Daigle et al., 2018; JAX, 025109). The chemogenetic experiments used Calb2-Cre;Chat-Flp (Calb2-Cre Huang Jax, 013730)(Chat-Flp Jax, 033850) Chat-Cre;Phox2b-Flp (Chat-Cre Rossi et al., 2011; JAX, 028861)(Phox2b-Flp Hirsch et al., 2013; JAX, 22407). The anterograde tracing experiments used Chat-Cre, Grp-Cre and Calb2-Cre. Unless otherwise specified, all experiments used adult mice with approximately equal

numbers of male and female mice (+/-1). Mice were housed at 22–24 C with a 12-h light:12-h dark cycle and *ad libitum* access to standard mouse chow and water unless otherwise stated for experimental purposes.

RNA fluorescence in situ hybridization (FISH): FISH experiments were performed on brain tissue from mice that received intraperitoneal injections of 2% Fluorogold (Fluorochrome) a minimum of 5-days prior to euthanasia. Mice were terminally anesthetized with ketamine (20 mg/kg) and xylazine (2 mg/kg) in PBS, followed by transcardial perfusion with 0.9% saline plus heparin and 4% paraformaldehyde. Brains were extracted and post-fixed for 24 h at 4 C. Following fixation, brains were sectioned coronally at 30–35 um thick sections. The day before FISH, the sections were rinsed in PBS and then mounted on slides (Fisher) and left to dry overnight. An ImmEdge Hydrophobic Barrier Pen was used to draw a barrier around the sections. The slides were then incubated in Protease IV in a HybEZ II Oven for 30 min at 40 C, followed by incubation with target probes (*Chat*, *Calb2, Grp*) for 2 h at 40 C. Slides were then treated with AMP 1–3, HRP-C1, HRP-C2, HRP-C3, and HRP Blocker for 15–30 min at 40 C, as previously described (Wang et al., 2012). FITC, Cy3, and Cy5 (Perkin Elmer) were used for probe visualization. Fluorogold was either imaged in its native state or visualized using immunofluorescence with a rabbit anti-Fluorogold primary antibody (Fluorochrome, 1:5000) overnight and a donkey anti-rabbit 647 secondary antibody (Thermo Scientific Cat# A31573, Lot# 2083195, 1:1000) for 2–4 h. Images were taken using a confocal microscope (Zeiss). Cell distributions were mapped in Neurolucida software (version 11, MBF Bioscience) using an AxioImager M2 (Carl Zeiss)(Dr. Stephen Abbot).

Intersectional Genetic Targeting Approach: We used intersectional chemogenetics to specifically activate either all DMV vagal neurons or just the *Calb2+* subtype of DMV neurons. *Chat* is present throughout the DMV and the hypoglossal nucleus, *Phox2b* is present throughout the DMV and NTS,

while *Calb2 is* present in only a subset of DMV neurons. Therefore, to intersectionally define the Phox2b/Chat or Calb2/Chat co-expressing neuron populations, we crossed the corresponding Cre- and Flp-expressing mouse lines to generate Cre;Flp mice. We injected the Cre;Flp mice with a Cre/Flp-dependent AAV-hM3Dq (AAV1-CreOn/FlpOn-hM3dq-HA) into the DMV (8 injection sites within the DMV, 40nL/site) and later intraperitoneally administered the hM3Dq ligand, clozapine-N-oxide (CNO) to activate the hM3Dq+ neurons.

Intracranial AAV Injections: Mice were anesthetized with ketamine (20 mg/kg) and xylazine (2 mg/kg) diluted in PBS and positioned into a stereotaxic apparatus (Kopf). A pulled glass micropipette was used for stereotaxic injections of an adeno-associated virus vector, AAV-DIO-tdTomato, AAV-CON-FON-hM3Dq, or AAV9-CAG-FLEX-PLAP (157), a gift of Dr. Stephen Liberles (Harvard Medical School, Howard Hughes Medical Institute), using the following stereotaxic coordinates for the DMV: anterior/posterior +/- 3mm, lateral/medial +/- 0.15 mm, and dorsal/ventral -2.5mm -4mm, from the calamus scriptorius. Following local anesthetization with bupivacaine, virus was injected (80nl nL/injection, 4 injections/side) using a Nanoject III system. This injection strategy was designed to fully cover the DMV. The pipette was removed 3–5 min after injections, followed by wound closure using sutures or surgical wound glue (Vetbond). Meloxicam SR (5 mg/kg; sustained release, SR) was injected subcutaneously for post-operative analgesia.

PLAP Anterograde Tracing: Following 3-4wk after AAV9-CAG-FLEX-PLAP injection, mice were terminally anesthetized with ketamine (20 mg/kg) and xylazine (2 mg/kg) diluted in PBS, followed by transcardial perfusion with 0.9% saline plus heparin then 4% paraformaldehyde (Thomas Scientific). The brains, esophagus, trachea, larynx, and lungs were collected and post-fixed for 24 h at 4 C. Following fixation, brains **w**ere sectioned coronally at 30 or 35 um thickness on a vibratome (Leica). A single series of sections per animal was used in histological studies to confirm injection site and PLAP expression. All

subjects determined to be surgical "misses'' based on little or absent reporter expression were excluded from analyses. The liver, brain, stomach, pancreas and spleen were washed three times for 1 h at room temperature in PBS, followed by incubation in alkaline phosphatase (AP) buffer (0.1 M Tris HCl pH 9.5, 0.1 M NaCl, 50 mM MgCl2, 0.1% Tween 20, 5 mM tetramisole-HCl) for two hours at 70 C. Afterward, the samples were equilibrated to room temperature and then washed twice in AP buffer. AP activity was visualized with NCT/BCIP solution (ThermoFisher Scientific 34042) and stained samples were rinsed in AP buffer for 15 min, post-fixed in 4% PFA for 1 h, and washed in PBS. Samples were then dehydrated through a series of ethanol washes (15%–100%) and cleared using a 1:2 mixture of benzyl alcohol (Sigma-Aldrich 402834-500 ML) and benzyl benzoate (Sigma-Aldrich B6630-1L). Whole mount images were taken using a brightfield stereomicroscope (Leica M205 FCA Stereomicroscope with color camera) and fluorescence microscope (Echo Revolve).

Fluorescent Anterograde tracing: Following 3-4wk after AAV-DIO-tdTomato injection we transcardially perfused the mice with saline and 4% PFA (paraformaldehyde). We then removed and fixed the brain and pancreas. After fixation the brains were cut into ~35um sections on a freezing microtome and mounted to slides to allow for target validation. Organs underwent IHC to boost the tdTomato signal, along with counterstaining for Chat, and neuronal markers such as PGP9.5. We used the clearing method iDISCO to optically clear organs and image tdtomato+ fluorescence. After organs are optically cleared, they are cut and mounted on slides and the projections are visualized on a confocal microscope.

Optogenetic Implant Surgery: To optogenetically stimulate the DMV and optogenetic ferrule was implanted over the DMV to allow for delivery of 473nm blue light. Mice were prepared for surgery as described above. Under the guidance of a stereotaxic alignment system, a ferrule-embedded optical fiber stub was lowered into the brain through a small hole in the skull, at a depth just dorsal to the DMV (AP:-3.0, ML:-0.15, DV: -3; from lambda) The fiber stub will be anchored to the skull using dental acrylic,

covering the external end with a protective cap or coupled to a patch cord during experimental stimulation. The scalp will be glued around the dried dental acrylic, and the mouse will undergo the post- operative procedures and monitoring as described (see above and below). This procedure was identical for optogenetic and fiber photometry methods.

Optogenetic Activation: Optogenetic activation was carried out with a blue light laser controlled via an Arduino board and 473nm blue laser. Our stimulation parameters (5hz, 10ms, 1 sec on, 3 sec off) are informed by a recent study of vagal stimulation in rats which saw variable effects on blood glucose between different frequencies (5-20hz) and stimulation types (intermittent vs continuous), with 5hz intermittent stimulation producing the largest decreases in blood glucose (74).

Chemogenetic Activation: Adult Chat-Cre;Phox2b-Flp;R26-dsHTB mice and Calb2-Cre;Chat-Flp;R26-dsHTB mice were anesthetized with ketamine (80 mg/kg) and xylazine (10 mg/kg) then placed in a stereotaxic frame and on a servo-controlled heating pad to maintain a 37.0 G 0.2 C body temperature (RightTemp Jr.; Kent Scientific). Surgical sites were shaved and cleaned with betadine and isopropyl alcohol and injected with Nocita (long-lasting bupivacaine, 5.3 mg/kg, subcutaneously) for pre-operative analgesia. The dorsal surface of the medulla was then exposed by gently retracting the overlaying neck muscles and incising the meninges. A NanoJect III (Drummond Scientific, catalog # 3-000-207) was used to inject 40nL of adeno-associated virus (AAV) Cre/Flp-dependently expressing hemagglutinin (HA)-tagged hM3Dq (ssAAV-1/2-hEF1a/hTLV1-Con/ Fon(HA_hM3D(Gq))-WPRE-hGHp(A), Viral Vector Facility, University of Zurich and ETH Zurich, catalog # vhW34-1) at each of 8 injection sites (320nL total volume) to ensure infection throughout the DMV (from calamus scriptorius; anterior/posterior: 0.3 mm, medial/ lateral 0.15 mm, dorsal/ventral: -0.25 and -0.5 mm). Injections were made at 25nL/sec and the injection pipette was left in place for 5 minutes to minimize viral spread up the pipette track. After the final

injection, the retracted muscles were sutured together over the injection site using absorbable sutures, and the skin was closed with Vetbond surgical glue. Mice were provided with Meloxicam Sustained-Release (ZooPharm; 5mg/kg; IP) for post-operative analgesia, 1 mL of lactated Ringers solution in 5% dextrose to support hydration and returned to the vivarium when ambulatory. These AAV-injected Chat-Cre;Phox2b-Flp;R26-dsHTB mice are referred to as ‘‘DMV-hM3Dq’’ mice. Mice were monitored post-operatively for five days and allowed to fully recover for three weeks before acclimation to experimental environments and procedures.

Glucose Tolerance: All mice were acclimated to the experimenters, handling, tail vein clips, and sham intraperitoneal (*i.p.*) injections in the week prior to testing. Following an overnight fast in same-sex cages with access to water *ad libitum*, the mice were temporarily single-housed for the experiment. 30min prior to experiment start tails were clipped to ensure flow of venous blood throughout the experiment and to ensure stress would dissipate before sampling. All blood glucose measurements were performed by wiping the tail cut site with moist ethanol cloth, letting dry and applying a glucometer test strip to the flowing venous blood. The mice were then injected *i.p.* with either the ligand of the hM3Dq receptor clozapine-N-oxide (CNO, 1.0 mg/kg) or saline (1.0 mg/kg) control at t=(-20min). Two baseline blood glucose measurements were taken 10 and 20 min after the CNO/saline injections. A 20% D(+)Glucose solution (10uL/g)(sigma Aldrich 16301) is injected *i.p* into all animals at (t=0min). Immediately following *i.p* glucose injection we record tail blood glucose as mentioned above at t=0,5,15,30,60,120mins. The order of experimental injections was randomized with half of the mice mouse receiving saline or CNO first. We waited 48 hours before retesting the same animal. Paired data was analyzed in prism using AUC & two-way anova.

Blood Sampling: For blood glucose measurements we used a hand-held glucometer (OneTouch Ultra Milpitas, CA) that required one drop of blood. We would cut the distil 1mm of tail with scissors 60min prior to testing. To obtain repeated samples, we wiped the tail tip with a moist towel to reinitiate blood flow. To obtain enough blood for plasma insulin measurements we used the same tail-bleed method, placing the mouse on a wire hopper we would gently stroke the tail over the side (using gravity) to collect 30uL of blood. The blood samples were collected in 30µl EDTA-coated capillary tubes (Innovative Medical Technologies, Inc.; Shawnee Mission, KS). They were initially stored on ice. After centrifugation (7 min at 7000 rpm), the decanted plasma was stored at −80 °C until analysis with the Ultra-Sensitive Mouse Insulin ELISA (Crystal Chem; Downers Grover, IL).

QUANTIFICATION AND STATISTICAL ANALYSIS

Results are reported as mean standard error of the mean (S.E.M.). For in vivo experiments, 'n' is the number of animals. For ex vivo experiments, 'n' is reported as number of recorded cells and the number of animals. These values are stated when appropriate throughout the Results and Figure Legends. Graph creation and statistical analysis was conducted in GraphPad Prism 9 (GraphPad statistical tests are noted in the Results. In general, two-tailed Student's t-test was conducted with parametric data containing two groups (paired or unpaired when appropriate). A Mann Whitney test was conducted with non-parametric data containing two groups. A one-way ANOVA followed by Tukey's multiple comparisons was used when there was one independent variable and more than two groups. A two-way ANOVA followed by Sıdak's Multiple Comparison Test was used when there were two independent variables. Repeated-measures ANOVA was used when comparing multiple timepoints within subjects. The Geisser-Greenhouse correction was used if the sphericity assumption for ANOVA was not met. Simple linear regression was used to examine the relationship between two continuous variables. Pearson correlation

was used to examine the strength of the relationship between two variables. Differences were considered statistically significant if p % 0.05. Graphs indicate individual mouse data or mean and SEM.

Acknowledgements

We gratefully acknowledge Bradford Lowell for the Chat-p2a-Flp mouse; Sara Prescott and Stephen Liberles for the AAV-FLEX-PLAP and histology method; Martyn Goulding (Salk Institute) for the $R26^{ds\text{-}HTB}$ mouse line. Patrice G. Guyenet and Hui Zong for co-acquisition of pilot funding; Ruth Stornetta and Stephen Abbot for training in microscopy. Neurolucida imaging was done by Stephen Abbot and Chelsea Li; Daniel Stornetta for training in the RNAscope method; and Lane Vandervoort, Lily Kauffman, Cate Bundon, Pati Castro, Ian Irushalmi, Chelsea Li, and Maisie Crook for technical support. Funding for this study was provided by a University of Virginia 3 Cavaliers award to J.N.C a Pathway to Stop Diabetes Initiator Award 1-18-INI-14, NIH R01 HL153916, pilot grant funding, and transgenic core service from the Boston Nutrition Obesity Research Center (NIH grant no. P30 DK046200) and the Boston Area Diabetes Endocrinology Research Center (BADERC; NIH, grant no. P30 DK057521) to J.N.C.

Author Contributions

N.J.C., L.S.K., L.AV., P.M.C., J.N.C designed experiments. N.J.C., R.A.F performed anterograde tracing and tissue clearing experiments. N.J.C., L.S.K., L.A.V., C.B.B., I.A.I and P.C.M performed chemogenetic studies N.J.C and L.S.K performed optogenetic studies, N.J.C., L.S.K., P.C.M and C.L performed histology, immunofluorescence, and in-situ experiments. N.J.C., and P.C.M imaged. N.J..,C and L.A.V., C.B.B and D.S.L performed insulin experiments., N.J.C., and I.A.I performed stats. N.J.C., I.A.I and J.N.C prepared figures

Summary/Conclusion

DMV-Mediated Cardiac Function

Unlike the nucleus ambiguous, the traditional vagal cardiac regulator, the DMV contains uniquely hyperexcitable cardiovagal neurons (CVNs) capable of strong cardioinhibition. This DMV-mediated cardioinhibition may be linked to cognitive appraisal mechanisms, resulting in reduced anxiety measures in behavioral tests. Our results support a model in which activating the vagus nerve decreases anxiety by slowing heart rate aligning with the James-Lange theory of emotion. The James-Lange theory, expanded upon by Cannon-Bard and later Schachter-Singer, ultimately culminating in modern cognitive appraisal theory, states that our physiological states precede emotional states, and that our brain's attempt to interrupt these physiological biomarkers (such as heart rate, blood pressure, temperature etc) is identical to our emotional state (111,112) Supporting this notion, a recent study in mice demonstrated that inducing tachycardia is sufficient to evoke anxiety-like behavior (38,113), This finding has significant implications for mood disorders such as anxiety and post-traumatic stress disorder, where altered heart rate variability and vagal tone are often observed.

DMV-Mediated Glucose Regulation

The DMV plays a crucial role in autonomic anticipatory regulation of glucose metabolism. Calb2+ DMV neurons, located at the lateral poles of the DMV, project to the pancreas but do not influence insulin secretion. Alone these neurons are not sufficient to improve glucose tolerance during a glucose challenge. In contrast, broader stimulation of the entire DMV does enhance glucose tolerance, potentially due to differential and combined effects on glucagon, GLP-1, and hepatic glucose output.

These results suggest a model of DMV is which the concerted action of multiple DMV subtypes including Calb2, control insulin, glucagon, liver, and stomach responses to facilitate post-prandial glucose clearance. Despite the necessity of insulin for glucose regulation, there is a paradoxical necessity of alpha cells for optimal prandial glucose tolerance. As mentioned previously glucagon can, under certain physiological parameters, act to enhance insulin secretion indirectly by hepatic gluconeogenesis, by increasing glucose levels and directly acting on beta cells to sensitize them to glucose induced insulin secretion (*155*). This combined with the fact that ablation of alpha cells inhibits cephalic insulin secretion (*161*) makes a strong case for glucagon's critical role in the optimization of glycemic consequences. In addition, the DMV projects to the liver and stomach and has effects on gluconeogenesis, glycolysis, and GLP-1 secretion. The signals between the DMV and these organs are likely of vital importance for the DMV's role in glucose regulation.

In this model [Figure 11] two or more populations of DMV neurons go to IPG's to result in insulin and glucagon release respectively. Our results suggest that Calb2+ DMV neurons could communicate to the pancreas to release glucagon to potentiate insulin secretion, although it is also possible that they don't

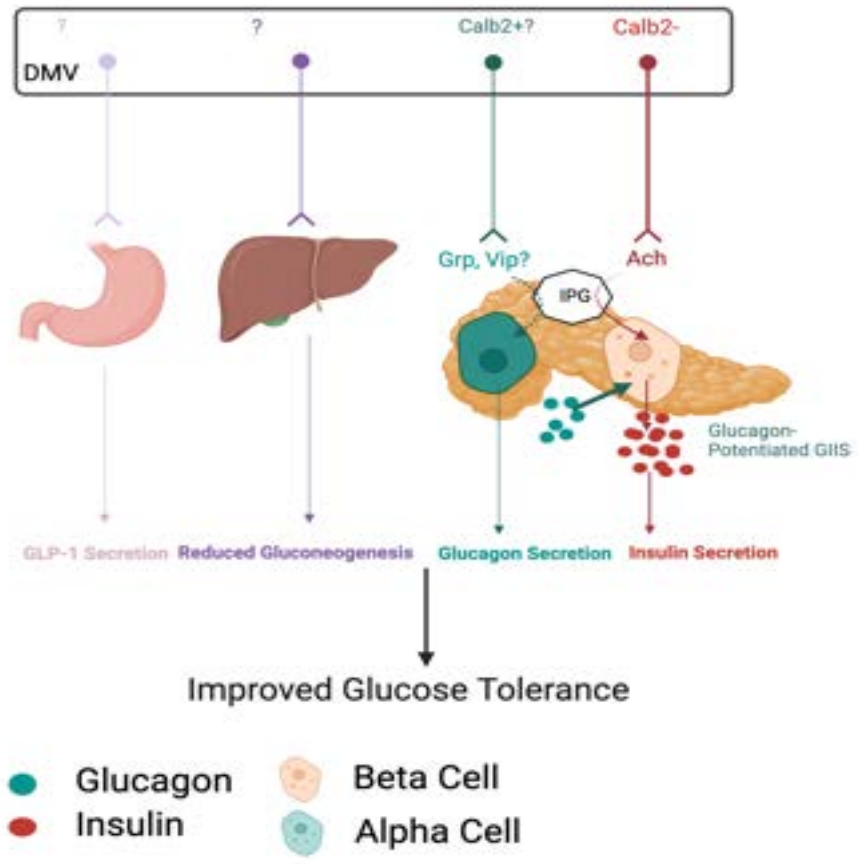

Figure 11: *Hypothesized model of DMV mediated glucose tolerance. DMV-Stomach elicits GLP-1, DMV-Liver decreases gluconeogenesis, Calb2$^-$ DMV-Pancreas secretes insulin, Calb2$^+$ DMV-Pancreas secretes glucagon to potentiate glucose induced insulin secretion?*

control endocrine but rather exocrine function. Additional Calb2- population(s) likely signal to the stomach to increase GLP-1 and the liver to inhibit gluconeogenesis. By these mechanisms, the combined effect of glucagon and subsequent insulin and GLP-1 secretion coupled with reduced gluconeogenesis could lead to a maximized glucose tolerance in response to meal consumption. If this is true, then this could mean these DMV populations have unique genetic markers and would allow for the selective manipulation of one but not the other, as a tool to learn more about how the CNS coordinates glucose regulation and to combat metabolic hormonal conditions such as T2D. Given the insufficiency of insulin alone, essential role of glucagon, and the likely involvement of GLP-1 and liver signaling, I propose that the term 'Cephalic Phase Endocrine Response' (CPER) should be used to describe the anticipatory mechanisms regulating glycemia. This is because multiple hormones and target organs are crucial for achieving optimal cephalic glucose tolerance.

Future Directions

DMV-Mediated Cardiac Function

Our research on DMV control of the heart, summarized in Figure 12, raises several intriguing questions. Key areas for further investigation include the molecular identity of CVN-DMV neurons, the mechanisms

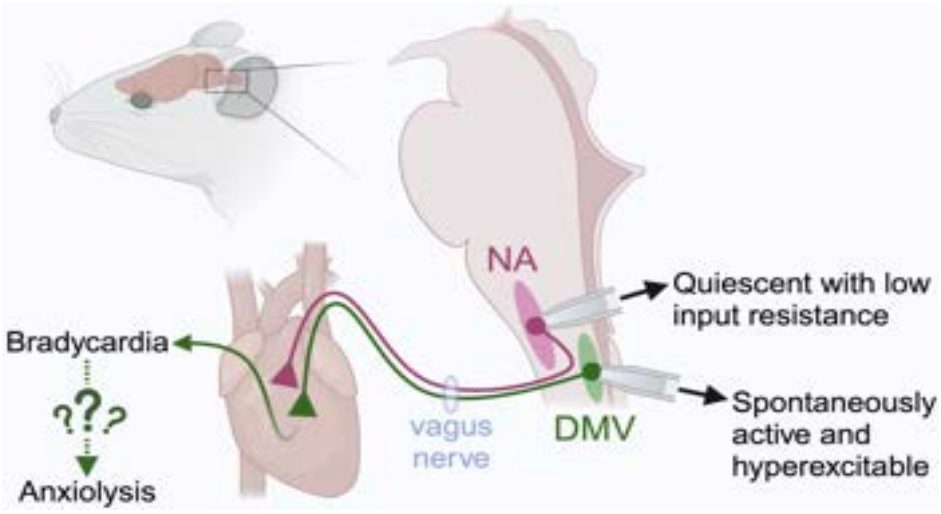

***Figure 12**: Schematic of DMV-mediated cardioinhibition and anxiolysis, differences between CVN-DMV and CVN-NA electrophysiological properties (148 Intro Figure)*

behind their distinct electrophysiological properties, and their physiological roles. Identifying the DMV molecular subtypes that project to the heart could provide a deeper understanding of the signals influencing CVN-DMV neurons and facilitate the search for novel therapeutic targets for conditions like tachycardia and anxiety.

Pharmacological testing confirmed that DMV stimulation-induced bradycardia requires mACh receptor activation. Scopolamine, but not atenolol, abolished optogenetically- and chemogenetically induced bradycardia, while MA and AQ-RA-741 ameliorated chemogenetic-mediated anxiolysis. However, a limitation is that AQ-RA-741 antagonizes both peripheral and central M2 receptors. Further studies are needed to elucidate the roles of cardiac receptors at both the DMV and heart levels in mediating bradycardia and anxiolysis. Future electrophysiological studies on CVN-DMV neurons are essential to elucidate the mechanisms underlying their increased spontaneous activity, higher input resistance, and distinct spiking activity in response to current injections. These neurons also exhibit smaller sizes compared to CVN-NA neurons. Understanding why the electrophysiological properties of CVN-DMV and CVN-NA neurons differ so significantly and the functional implication for parasympathetic cardiac regulation is crucial.

Given the DMV's role in feed-forward metabolic regulation, it is worth exploring why certain DMV neurons would exert significant cardioinhibitory and anxiolytic effects in the first place. Fear is a potent inhibitor of foraging behavior. I hypothesize that DMV-mediated anxiolysis reduces the perception of fear to encourage foraging in risky environments. A starving and a sated mouse must assess the risk of an owl above a foraging patch differently to survive. Reduced heart rate and anxiety might temporarily allow behaviors that would otherwise be too risky, whether they involve intra- or interspecies conflicts. This mechanism is illustrated in Figure 13. When a mouse is sated, its energy needs are low, and the

sight or smell of an owl inhibits foraging through fear. As energy levels drop and the need for food increases, the sight and smell food increasing reduces heart rate, decreasing fear and enabling action. If this hypothesis is correct, the DMV's effect on heart rate and anxiety might also represent a cephalic response. Understanding this connection could reveal new insights into the autonomic regulation of mood and anxiety disorders.

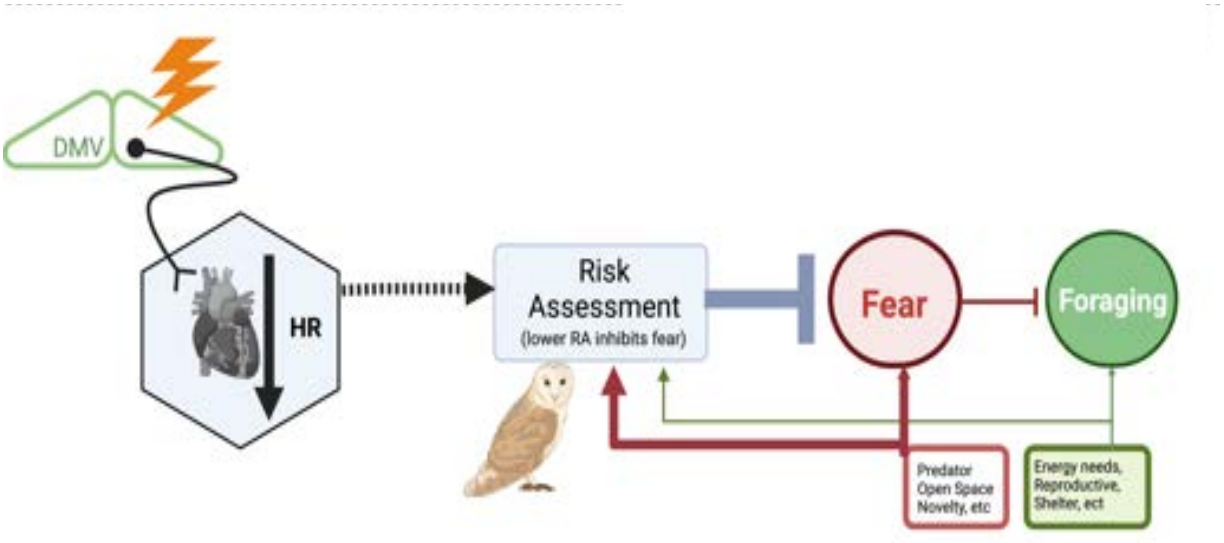

***Figure 13**: Hypothesized model of DMV-mediated pro-foraging.*

As many diverse sex differences in cardiovagal function have been observed, a logical avenue for research would be to examine the sex difference in CVN-DMV electrophysiological properties, cardiac innervation, and function. Our unpublished analyses suggest that females have a more pronounced HR reduction and increase in open arm time.

Our results raise the possibility that bradycardias might be sufficient to produce anxiolysis, aligning with the James-Lange theory of emotions. I'm particularly fascinated by the brain regions that interpret these signals and the mechanisms of this interpretation. It seems likely that our brain uses both the current biomarker state and past interpretations of similar biomarker states to form these interpretations. It's not just "my heart rate is low, so I'm calm," but rather "my heart rate is low, and I've previously

interpreted a low heart rate as calm, so I feel calm." If this is true, could a large percentage of our waking emotional state be conditioned emotional responses?

DMV-Mediated Glucose Regulation

Our research has raised new questions about the DMV's role in glucose regulation and insulin secretion. One limitation is the use of the transcriptional profile of only 306 cells to define molecular subtypes. As more transcriptional data becomes available, it will allow for finer subtype resolution and probing of this 2000-cell nucleus, especially concerning subtype anatomy, target-projection profile, and function. Further research is needed to colocalize Calb2+ DMV fibers with their pancreatic targets to determine whether efferent vagal innervation synapses onto IPGs, islets, or both and which signaling molecules they release. Additionally, developing a working genetic mechanism to inhibit DMV neurons will be crucial for testing the necessity of Calb2+Chat+ DMV neurons for endocrine hormone secretion. To better understand the dynamic changes in glucose and hormone levels during the pre- and post-mealtimes, we propose using wireless glucose probes for continuous monitoring and catheterizing mice for frequent blood-hormone assays while minimizing stress.

Fiber photometry experiments are underway to examine endogenous Chat+ and Calb2+ DMV activity. Understanding the endogenous activity patterns of DMV neurons during the dynamic period prior to and during initial meal consumption is crucial. By characterizing these temporal patterns, we can enhance our knowledge of the DMV-mediated anticipatory glucose regulation. This improved temporal characterization will enable us to design precisely timed experimental manipulations and therapeutic interventions aimed at inhibiting or rescuing this regulation and enhancing cephalic-mediated glucose tolerance. While the role of sweet taste in the cephalic insulin response has been characterized how other sensory inputs are integrated and associated with taste to predict future metabolic outcomes is

currently unknown. To begin to understand the relative contributions of the sensory modalities on DMV neuronal activity fiber photometry experiments could be performed in parallel on mice with impaired taste, smell, or sight. Understanding the food-related signals that the brain uses to predict metabolic consequences is essential.

Additionally, investigating DMV function in obesity, and various diabetic models will shed light on DMV-mediated glucose tolerance under pathological conditions. Because of the influence palatability has on cephalic phase responses, we hypothesize that Calb2+ DMV neuron activity correlates with the palatability of food, with more palatable foods eliciting higher calcium release and neuronal activation.

A key area of interest is determining the extent to which DMV activity is learned or conditioned and identifying the sensory elements that influence this process. To investigate this, we could habituate mice to anticipate specific metabolic consequences from distinct sensory cues, such as a specific tone or smell (e.g., cherry smell associated with low palatability chow and lemon smell associated with high palatability peanut butter). Once the mice are habituated, we would test their insulin secretion and glucose tolerance by either gastric infusion or gavaging with food-1 while providing cue-1. Subsequently, we would test insulin secretion and glucose tolerance for food-1 when paired with cue-2 and vice versa. I hypothesize that when the cue is switched, the magnitude of the metabolic response would more closely resemble the metabolic outcome associated with the previously associated food. This approach would help elucidate how prior food experiences are integrated to predict future metabolic outcomes. Furthermore, the influence of cephalically mediated insulin secretion on food intake should be examined. Although unconfirmed, pilot experiments to this end show no effect with standard chow, but a sex-dependent effect on high fat diet with females eating more and males eating less than their control counterparts. This may make sense as the cephalic responses correlate with palatability and

exist in part to allow for greater consumption of a food within a sitting. While speculative, it's possible that the metabolic needs of pregnancy alter DMV activity in such a way as to facilitate increased consumption. Sex differences in DMV architecture, innervation and function have been observed and the relative differences in Calb2 function is a logical area for experimentation.

The critical questions that emerge are (1) what role does premeal glucagon secretion, GLP-1 secretion, and hepatic glucose regulation play in optimizing both insulin levels and glucose levels in the post-meal environment and (2) do Calb2+ DMV neurons influence glucagon secretion. Additional hormonal assays, transcriptional profiling, in-situ hybridization, projection profiling and functional tests are needed to determine the DMV's role in these processes. Understanding the molecular subtypes of DMV neurons that regulate glucagon, GLP-1, and hepatic glucose output is essential for identifying druggable targets for metabolic disorders of perturbed glucose regulation.

Conclusion

This dissertation deepens our understanding of the DMV's role in glucose regulation and cardiac function, uncovering an unexpected role for the DMV in controlling heart rate and anxiety. It also identifies a novel subtype of DMV neurons that innervates the pancreas. These insights not only expand our knowledge of DMV-mediated homeostasis but also underscore the DMV's critical significance in metabolic and cardiovascular health, paving the way for future research.

References (Chapter 1,3)

1. Berthoud, H. R. & Neuhuber, W. L. Functional and chemical anatomy of the afferent vagal system. *Auton. Neurosci.* **85**, 1–17 (2000).

2. Berthoud, H.-R. & Neuhuber, W. L. Vagal mechanisms as neuromodulatory targets for the treatment of metabolic disease. *Ann. N. Y. Acad. Sci.* **1454**, 42–55 (2019).

3. Benedict, S. *Über die Medulla Oblongata*. (1843).

4. Baker, Lui, E. F. Vagal Nerve Nuclei. in *Neuroanatomy* (StatPearls Publishing, 2021).

5. Neuhuber, W. L. & Berthoud, H.-R. Functional anatomy of the vagus system – Emphasis on the somato-visceral interface. in *Autonomic Neuroscience* vol. Volume 236, 2021 (2021).

6. Hong Gao, Nicholas R, R. Glatzer, Bret N. Smith & Dan Liu. *Morphological and electrophysiological features of motor neurons and putative interneurons in the dorsal vagal complex of rats and mice,*. vol. Volume 1291, (2009).

7. Ludwig, M. Q. *et al.* A genetic map of the mouse dorsal vagal complex and its role in obesity. *Nat. Metab.* **3**, 530–545 (2021).

8. Altschuler, S. M., Bao, X. M., Bieger, D., Hopkins, D. A. & Miselis, R. R. Viscerotopic representation of the upper alimentary tract in the rat: sensory ganglia and nuclei of the solitary and spinal trigeminal tracts. *J. Comp. Neurol.* **283**, 248–268 (1989).

9. Lamy, C. M. *et al.* Hypoglycemia-activated GLUT2 neurons of the nucleus tractus solitarius stimulate vagal activity and glucagon secretion. *Cell Metab.* **19**, 527–538 (2014).

10. Teff, K. Nutritional implications of the cephalic-phase reflexes: endocrine responses. *Appetite* **34**, 206–213 (2000).

11. Travagli, R. A. & Anselmi, L. Vagal neurocircuitry and its influence on gastric motility. *Nat. Rev. Gastroenterol. Hepatol.* **13**, 389–401 (2016).

12. Fox, E. A. & Powley, T. L. Longitudinal columnar organization within the dorsal motor nucleus represents separate branches of the abdominal vagus. *Brain Res.* **341**, 269–282 (1985).

13. Zhou, S.-Y., Lu, Y.-X., Yao, H. & Owyang, C. Spatial organization of neurons in the dorsal motor nucleus of the vagus synapsing with intragastric cholinergic and nitric oxide/VIP neurons in the rat. *Am. J. Physiol. Gastrointest. Liver Physiol.* **294**, G1201-9 (2008).

14. Travagli, R. A., Hermann, G. E., Browning, K. N. & Rogers, R. C. Brainstem circuits regulating gastric function. *Annu. Rev. Physiol.* **68**, 279–305 (2006).

15. Loewy, A. D. & Spyer, K. M. *Vagal preganglionic neurons. In CentralRegulation of Autonomic Functions*. 66–67 (1990).

16. Zafra, M. A., Molina, F. & Puerto, A. The neural/cephalic phase reflexes in the physiology of nutrition. *Neurosci. Biobehav. Rev.* **30**, 1032–1044 (2006).

17. Verberne, A. J. M., Sabetghadam, A. & Korim, W. S. Neural pathways that control the glucose counterregulatory response. *Front. Neurosci.* **8**, 38 (2014).

18. Babic, T., Browning, K. N. & Travagli, R. A. Differential organization of excitatory and inhibitory synapses within the rat dorsal vagal complex. *Am. J. Physiol. Gastrointest. Liver Physiol.* **300**, G21-32 (2011).

19. Capilupi, M. J., Kerath, S. M. & Becker, L. B. Vagus nerve stimulation and the cardiovascular system. *Cold Spring Harb. Perspect. Med.* **10**, (2020).

20. Mussa, B. M. & Verberne, A. J. M. The dorsal motor nucleus of the vagus and regulation of pancreatic secretory function. *Exp. Physiol.* **98**, 25–37 (2013).

21. Li, Y., Wu, X., Zhao, Y., Chen, S. & Owyang, C. Ghrelin acts on the dorsal vagal complex to stimulate pancreatic protein secretion. *Am. J. Physiol. Gastrointest. Liver Physiol.* **290**, G1350-8 (2006).

22. Huang, X. F., Törk, I. & Paxinos, G. Dorsal motor nucleus of the vagus nerve: a cyto- and chemoarchitectonic study in the human. *J. Comp. Neurol.* **330**, 158–182 (1993).

23. Browning, K. N., Renehan, W. E. & Travagli, R. A. Electrophysiological and morphological heterogeneity of rat dorsal vagal neurones which project to specific areas of the gastrointestinal tract. *J Physiol (Lond)* **517 (Pt 2)**, 521–532 (1999).

24. Tao, J. *et al.* Highly selective brain-to-gut communication via genetically defined vagus neurons. *Neuron* **109**, 2106-2115.e4 (2021).

25. Coverdell, T. C., Abraham-Fan, R.-J., Wu, C., Abbott, S. B. G. & Campbell, J. N. Genetic encoding of an esophageal motor circuit. *Cell Rep.* **39**, 110962 (2022).

26. Veerakumar, A., Yung, A. R., Liu, Y. & Krasnow, M. A. Molecularly defined circuits for cardiovascular and cardiopulmonary control. *Nature* **606**, 739–746 (2022).

27. Coverdell, T. C., Abbott, S. B. G. & Campbell, J. N. Molecular cell types as functional units of the efferent vagus nerve. *Semin. Cell Dev. Biol.* **156**, 210–218 (2024).

28. Geis, G. S. & Wurster, R. D. Cardiac responses during stimulation of the dorsal motor nucleus and nucleus ambiguus in the cat. *Circ. Res.* **46**, 606–611 (1980).

29. Laughton, W. B. & Powley, T. L. Localization of efferent function in the dorsal motor nucleus of the vagus. *Am. J. Physiol.* **252**, R13-25 (1987).

30. Machhada, A. *et al.* Origins of the vagal drive controlling left ventricular contractility. *J Physiol (Lond)* **594**, 4017–4030 (2016).

31. Sun, P. *et al.* Improved outcomes of cardiopulmonary resuscitation in rats treated with vagus nerve stimulation and its potential mechanism. *Shock* **49**, 698–703 (2018).

32. Ottaviani, M. M., Vallone, F., Micera, S. & Recchia, F. A. Closed-Loop Vagus Nerve Stimulation for the Treatment of Cardiovascular Diseases: State of the Art and Future Directions. *Front. Cardiovasc. Med.* **9**, 866957 (2022).

33. Han, W. *et al.* A Neural Circuit for Gut-Induced Reward. *Cell* **175**, 665-678.e23 (2018).

34. Peña, D. F., Engineer, N. D. & McIntyre, C. K. Rapid remission of conditioned fear expression with extinction training paired with vagus nerve stimulation. *Biol. Psychiatry* **73**, 1071–1077 (2013).

35. Souza, R. R. *et al.* Timing of vagus nerve stimulation during fear extinction determines efficacy in a rat model of PTSD. *Sci. Rep.* **12**, 16526 (2022).

36. George, M. S. *et al.* A pilot study of vagus nerve stimulation (VNS) for treatment-resistant anxiety disorders. *Brain Stimulat.* **1**, 112–121 (2008).

37. Hsieh, J. H., Chen, R. F., Wu, J. J., Yen, C. T. & Chai, C. Y. Vagal innervation of the gastrointestinal tract arises from dorsal motor nucleus while that of the heart largely from nucleus ambiguus in the cat. *J. Auton. Nerv. Syst.* **70**, 38–50 (1998).

38. Bach, J. *Principles of synthetic intelligence PSI: an architecture of motivated cognition*. (Oxford University Press, 2009). doi:10.1093/acprof:oso/9780195370676.001.0001.

39. Röder, P. V., Wu, B., Liu, Y. & Han, W. Pancreatic regulation of glucose homeostasis. *Exp. Mol. Med.* **48**, e219 (2016).

40. Yoshizane, C. *et al.* Glycemic, insulinemic and incretin responses after oral trehalose ingestion in healthy subjects. *Nutr. J.* **16**, 9 (2017).

41. Daenen, S. *et al.* Peak-time determination of post-meal glucose excursions in insulin-treated diabetic patients. *Diabetes Metab.* **36**, 165–169 (2010).

42. Capozzi, M. E. *et al.* Glucagon lowers glycemia when β-cells are active. *JCI Insight* **5**, (2019).

43. Traub, S. *et al.* Pancreatic α Cell-Derived Glucagon-Related Peptides Are Required for β Cell Adaptation and Glucose Homeostasis. *Cell Rep.* **18**, 3192–3203 (2017).

44. Nadkarni, P., Chepurny, O. G. & Holz, G. G. Regulation of glucose homeostasis by GLP-1. *Prog. Mol. Biol. Transl. Sci.* **121**, 23–65 (2014).

45. Burcelin, R. The gut-brain axis: a major glucoregulatory player. *Diabetes Metab.* **36 Suppl 3**, S54-8 (2010).

46. Noguchi, G. M. & Huising, M. O. Integrating the inputs that shape pancreatic islet hormone release. *Nat. Metab.* **1**, 1189–1201 (2019).

47. Dolenšek, J., Rupnik, M. S. & Stožer, A. Structural similarities and differences between the human and the mouse pancreas. *Islets* **7**, e1024405 (2015).

48. Li, W.-H. Functional analysis of islet cells in vitro, in situ, and in vivo. *Semin. Cell Dev. Biol.* **103**, 14–19 (2020).

49. Lin, E. E., Scott-Solomon, E. & Kuruvilla, R. Peripheral innervation in the regulation of glucose homeostasis. *Trends Neurosci.* **44**, 189–202 (2021).

50. Li, W., Yu, G., Liu, Y. & Sha, L. Intrapancreatic ganglia and neural regulation of pancreatic endocrine secretion. *Front. Neurosci.* **13**, 21 (2019).

51. Olmsted, J. M. D. Claude Bernard, 1813-1878: A Pioneer in the Study of Carbohydrate Metabolism. *Diabetes* **2**, 162–164 (1953).

52. Bernard, C. *Leçons sur les propriétés physiologiques et les altérations pathologiques des liquides de l'organisme / par Claude Bernard.* (Bailleère, 1859). doi:10.5962/bhl.title.1814.

53. Pocai, A., Obici, S., Schwartz, G. J. & Rossetti, L. A brain-liver circuit regulates glucose homeostasis. *Cell Metab.* **1**, 53–61 (2005).

54. Bernard, C. *Leçons de physiologie expérimentale appliquée à la médecine, faites au Collège de France,*. (J.B. Baillière et fils; [etc., etc.], 1855). doi:10.5962/bhl.title.1818.

55. Kwon, E. *et al.* Optogenetic stimulation of the liver-projecting melanocortinergic pathway promotes hepatic glucose production. *Nat. Commun.* **11**, 6295 (2020).

56. Song, W.-J. *et al.* Activation of ChAT+ neuron in dorsal motor vagus (DMV) increases blood glucose through the regulation of hepatic gene expression in mice. *Brain Res.* **1829**, 148770 (2024).

57. Woods, S. C. The eating paradox: how we tolerate food. *Psychol. Rev.* **98**, 488–505 (1991).

58. Pavlov, I. P. *The work of the digestive glands*. (Griffin, 1897).

59. Smeets, P. A. M., Erkner, A. & de Graaf, C. Cephalic phase responses and appetite. *Nutr. Rev.* **68**, 643–655 (2010).

60. Teff, K. L. How neural mediation of anticipatory and compensatory insulin release helps us tolerate food. *Physiol. Behav.* **103**, 44–50 (2011).

61. Pullicin, A. J., Glendinning, J. I. & Lim, J. Cephalic phase insulin release: A review of its mechanistic basis and variability in humans. *Physiol. Behav.* **239**, 113514 (2021).

62. Langhans, W., Watts, A. G. & Spector, A. C. The elusive cephalic phase insulin response: triggers, mechanisms, and functions. *Physiol. Rev.* **103**, 1423–1485 (2023).

63. Gerich, J. E. Is reduced first-phase insulin release the earliest detectable abnormality in individuals destined to develop type 2 diabetes? *Diabetes* **51 Suppl 1**, S117-21 (2002).

64. Del Prato, S. & Tiengo, A. The importance of first-phase insulin secretion: implications for the therapy of type 2 diabetes mellitus. *Diabetes Metab. Res. Rev.* **17**, 164–174 (2001).

65. Trimble, E. R., Siegel, E. G., Berthoud, H. R. & Renold, A. E. Intraportal islet transplantation: functional assessment in conscious unrestrained rats. *Endocrinology* **106**, 791–797 (1980).

66. Louis-Sylvestre, J. Feeding and metabolic patterns in rats with truncular vagotomy or with transplanted beta-cells. *Am. J. Physiol.* **235**, E119-25 (1978).

67. Snowdon, C. T. & Epstein, A. N. Oral and intragastric feeding in vagotomized rats. *J. Comp. Physiol. Psychol.* **71**, 59–67 (1970).

68. Herath, C. B., Reynolds, G. W., MacKenzie, D. D., Davis, S. R. & Harris, P. M. Vagotomy suppresses cephalic phase insulin release in sheep. *Exp. Physiol.* **84**, 559–569 (1999).

69. Snowdon, C. T. Gastrointestinal sensory and motor control of food intake. *J. Comp. Physiol. Psychol.* **71**, 68–76 (1970).

70. Kraft, T. S. *et al.* The energetics of uniquely human subsistence strategies. *Science* **374**, eabf0130 (2021).

71. Pavlov, I. P. *Conditioned Reflexes: An Investigation of thePhysiological Activity of the Cerebral Cortex*. (Oxfod University Press, 1927).

72. Frohman, L. A., Ezdinli, E. Z. & Javid, R. Effect of vagotomy and vagal stimulation on insulin secretion. *Diabetes* **16**, 443–448 (1967).

73. Meyers, E. E., Kronemberger, A., Lira, V., Rahmouni, K. & Stauss, H. M. Contrasting effects of afferent and efferent vagal nerve stimulation on insulin secretion and blood glucose regulation. *Physiol. Rep.* **4**, (2016).

74. Yin, J., Ji, F., Gharibani, P. & Chen, J. D. Vagal nerve stimulation for glycemic control in a rodent model of type 2 diabetes. *Obes. Surg.* **29**, 2869–2877 (2019).

75. Ionescu, E., Rohner-Jeanrenaud, F., Berthoud, H. R. & Jeanrenaud, B. Increases in plasma insulin levels in response to electrical stimulation of the dorsal motor nucleus of the vagus nerve. *Endocrinology* **112**, 904–910 (1983).

76. NamKoong, C. *et al.* Chemogenetic manipulation of parasympathetic neurons (DMV) regulates feeding behavior and energy metabolism. *Neurosci. Lett.* **712**, 134356 (2019).

77. Teff, K. L. & Townsend, R. R. Early phase insulin infusion and muscarinic blockade in obese and lean subjects. *Am. J. Physiol.* **277**, R198-208 (1999).

78. Boychuk, C. R. *et al.* A hindbrain inhibitory microcircuit mediates vagally-coordinated glucose regulation. *Sci. Rep.* **9**, 2722 (2019).

79. Ishida, T. *et al.* Effects of portal and peripheral venous insulin infusion on glucose production and utilization in depancreatized, conscious dogs. *Diabetes* **33**, 984–990 (1984).

80. Güemes, A., Herrero, P., Bondia, J. & Georgiou, P. Modeling the effect of the cephalic phase of insulin secretion on glucose metabolism. *Med. Biol. Eng. Comput.* **57**, 1173–1186 (2019).

81. Meier, J. J., Veldhuis, J. D. & Butler, P. C. Pulsatile insulin secretion dictates systemic insulin delivery by regulating hepatic insulin extraction in humans. *Diabetes* **54**, 1649–1656 (2005).

82. Luzi, L. & DeFronzo, R. A. Effect of loss of first-phase insulin secretion on hepatic glucose production and tissue glucose disposal in humans. *Am. J. Physiol.* **257**, E241-6 (1989).

83. Edgerton, D. S. *et al.* Insulin's direct hepatic effect explains the inhibition of glucose production caused by insulin secretion. *JCI Insight* **2**, e91863 (2017).

84. Vincent, M. A. *et al.* Microvascular recruitment is an early insulin effect that regulates skeletal muscle glucose uptake in vivo. *Diabetes* **53**, 1418–1423 (2004).

85. Baron, A. D. *et al.* Insulin-mediated skeletal muscle vasodilation contributes to both insulin sensitivity and responsiveness in lean humans. *J. Clin. Invest.* **96**, 786–792 (1995).

86. Buss, C., Maranhão, P. A., de Souza, M. das G. C., Bouskela, E. & Kraemer-Aguiar, L. G. Obesity blunts cephalic-phase microvascular responses to food. *Physiol. Behav.* **225**, 113087 (2020).

87. de Aguiar, L. G. K. *et al.* Metformin improves endothelial vascular reactivity in first-degree relatives of type 2 diabetic patients with metabolic syndrome and normal glucose tolerance. *Diabetes Care* **29**, 1083–1089 (2006).

88. Kraemer de Aguiar, L. G. *et al.* Metformin improves skin capillary reactivity in normoglycaemic subjects with the metabolic syndrome. *Diabet. Med.* **24**, 272–279 (2007).

89. Kolb, H., Kempf, K., Röhling, M. & Martin, S. Insulin: too much of a good thing is bad. *BMC Med.* **18**, 224 (2020).

90. Weyer, C., Bogardus, C., Mott, D. M. & Pratley, R. E. The natural history of insulin secretory dysfunction and insulin resistance in the pathogenesis of type 2 diabetes mellitus. *J. Clin. Invest.* **104**, 787–794 (1999).

91. Baier, L. J. & Hanson, R. L. Genetic studies of the etiology of type 2 diabetes in Pima Indians: hunting for pieces to a complicated puzzle. *Diabetes* **53**, 1181–1186 (2004).

92. Corbett, E. K., Batten, T. F., Kaye, J. C., Deuchars, J. & McWilliam, P. N. Labelling of rat vagal preganglionic neurones by carbocyanine dye DiI applied to the heart. *Neuroreport* **10**, 1177–1181 (1999).

93. Izzo, P. N., Deuchars, J. & Spyer, K. M. Localization of cardiac vagal preganglionic motoneurones in the rat: immunocytochemical evidence of synaptic inputs containing 5-hydroxytryptamine. *J. Comp. Neurol.* **327**, 572–583 (1993).

94. Massari, V. J., Johnson, T. A. & Gatti, P. J. Cardiotopic organization of the nucleus ambiguus? An anatomical and physiological analysis of neurons regulating atrioventricular conduction. *Brain Res.* **679**, 227–240 (1995).

95. Standish, A., Enquist, L. W. & Schwaber, J. S. Innervation of the heart and its central medullary origin defined by viral tracing. *Science* **263**, 232–234 (1994).

96. Ter Horst, G. J., Hautvast, R. W., De Jongste, M. J. & Korf, J. Neuroanatomy of cardiac activity-regulating circuitry: a transneuronal retrograde viral labelling study in the rat. *Eur. J. Neurosci.* **8**, 2029–2041 (1996).

97. Gilbey, M. P., Jordan, D., Richter, D. W. & Spyer, K. M. Synaptic mechanisms involved in the inspiratory modulation of vagal cardio-inhibitory neurones in the cat. *J Physiol (Lond)* **356**, 65–78 (1984).

98. McAllen, R. M. & Spyer, K. M. Bradycardia produced by iontophoretic activation of preganglionic vagal motoneurones [proceedings]. *J Physiol (Lond)* **269**, 49P (1977).

99. Cheng, Z., Powley, T. L., Schwaber, J. S. & Doyle, F. J. Projections of the dorsal motor nucleus of the vagus to cardiac ganglia of rat atria: an anterograde tracing study. *J. Comp. Neurol.* **410**, 320–341 (1999).

100. Ford, T. W., Bennett, J. A., Kidd, C. & McWilliam, P. N. Neurones in the dorsal motor vagal nucleus of the cat with non-myelinated axons projecting to the heart and lungs. *Exp. Physiol.* **75**, 459–473 (1990).

101. Jones, J. F., Wang, Y. & Jordan, D. Heart rate responses to selective stimulation of cardiac vagal C fibres in anaesthetized cats, rats and rabbits. *J Physiol (Lond)* **489 (Pt 1)**, 203–214 (1995).

102. Nosaka, S., Yamamoto, T. & Yasunaga, K. Localization of vagal cardioinhibitory preganglionic neurons with rat brain stem. *J. Comp. Neurol.* **186**, 79–92 (1979).

103. Taylor, E. W., Wang, T. & Leite, C. A. C. An overview of the phylogeny of cardiorespiratory control in vertebrates with some reflections on the “Polyvagal Theory”. *Biol. Psychol.* **172**, 108382 (2022).

104. Taylor, E. W. *et al.* The phylogeny and ontogeny of autonomic control of the heart and cardiorespiratory interactions in vertebrates. *J. Exp. Biol.* **217**, 690–703 (2014).

105. Machhada, A. *et al.* Optogenetic stimulation of vagal efferent activity preserves left ventricular function in experimental heart failure. *JACC Basic Transl. Sci.* **5**, 799–810 (2020).

106. Falvey, A. *et al.* Electrical stimulation of the dorsal motor nucleus of the vagus regulates inflammation without affecting the heart rate. *BioRxiv* (2023) doi:10.1101/2023.05.17.541191.

107. Sporton, S. C., Shepheard, S. L., Jordan, D. & Ramage, A. G. Microinjections of 5-HT1A agonists into the dorsal motor vagal nucleus produce a bradycardia in the atenolol-pretreated anaesthetized rat. *Br. J. Pharmacol.* **104**, 466–470 (1991).

108. Thompson, D. A. *et al.* Optogenetic stimulation of the brainstem dorsal motor nucleus ameliorates acute pancreatitis. *Front. Immunol.* **14**, 1166212 (2023).

109. Shivaswamy, T., Souza, R. R., Engineer, C. T. & McIntyre, C. K. Vagus Nerve Stimulation as a Treatment for Fear and Anxiety in Individuals with Autism Spectrum Disorder. *J. Psychiatr. Brain Sci.* **7**, (2022).

110. Groves, D. A. & Brown, V. J. Vagal nerve stimulation: a review of its applications and potential mechanisms that mediate its clinical effects. *Neurosci. Biobehav. Rev.* **29**, 493–500 (2005).

111. Lange, C. G. The emotions. in *The emotions, Vol. 1.* (eds. Lange, C. G. & James, W.) 33–90 (Williams & Wilkins Co, 1922). doi:10.1037/10735-002.

112. James, W. The emotions. in *The emotions, Vol. 1.* (eds. Lange, C. G. & James, W.) 93–135 (Williams & Wilkins Co, 1922). doi:10.1037/10735-003.

113. Hsueh, B. *et al.* Cardiogenic control of affective behavioural state. *Nature* **615**, 292–299 (2023).

114. McAllen, R. M. & Spyer, K. M. Two types of vagal preganglionic motoneurones projecting to the heart and lungs. *J Physiol (Lond)* **282**, 353–364 (1978).

115. Mendelowitz, D. Firing properties of identified parasympathetic cardiac neurons in nucleus ambiguus. *Am. J. Physiol.* **271**, H2609-14 (1996).

116. Jones, J. F., Wang, Y. & Jordan, D. Activity of C fibre cardiac vagal efferents in anaesthetized cats and rats. *J Physiol (Lond)* **507 (Pt 3)**, 869–880 (1998).

117. Cheng, Z., Zhang, H., Guo, S. Z., Wurster, R. & Gozal, D. Differential control over postganglionic neurons in rat cardiac ganglia by NA and DmnX neurons: anatomical evidence. *Am. J. Physiol. Regul. Integr. Comp. Physiol.* **286**, R625-33 (2004).

118. Cauley, E. *et al.* Neurotransmission to parasympathetic cardiac vagal neurons in the brain stem is altered with left ventricular hypertrophy-induced heart failure. *Am. J. Physiol. Heart Circ. Physiol.* **309**, H1281-7 (2015).

119. Madisen, L. *et al.* A toolbox of Cre-dependent optogenetic transgenic mice for light-induced activation and silencing. *Nat. Neurosci.* **15**, 793–802 (2012).

120. Gee, M. M. *et al.* Unpacking the multimodal, multi-scale data of the fast and slow lanes of the cardiac vagus through computational modelling. *Exp. Physiol.* (2023) doi:10.1113/EP090865.

121. Kang, B. J. *et al.* Central nervous system distribution of the transcription factor Phox2b in the adult rat. *J. Comp. Neurol.* **503**, 627–641 (2007).

122. Christmas, A. J. & Maxwell, D. R. A comparison of the effects of some benzodiazepines and other drugs on aggressive and exploratory behaviour in mice and rats. *Neuropharmacology* **9**, 17–29 (1970).

123. Crawley, J. N. Exploratory behavior models of anxiety in mice. *Neurosci. Biobehav. Rev.* **9**, 37–44 (1985).

124. Lister, R. G. The use of a plus-maze to measure anxiety in the mouse. *Psychopharmacology (Berl)* **92**, 180–185 (1987).

125. Doods, H., Entzeroth, M. & Mayer, N. Cardioselectivity of AQ-RA 741, a novel tricyclic antimuscarinic drug. *Eur. J. Pharmacol.* **192**, 147–152 (1991).

126. Cohen, V. I. *et al.* Novel potent and m2-selective antimuscarinic compounds which penetrate the blood-brain barrier. *Eur. J. Med. Chem.* **30**, 61–69 (1995).

127. Travagli, R. A., Gillis, R. A., Rossiter, C. D. & Vicini, S. Glutamate and GABA-mediated synaptic currents in neurons of the rat dorsal motor nucleus of the vagus. *Am. J. Physiol.* **260**, G531-6 (1991).

128. Travagli, R. A. & Gillis, R. A. Hyperpolarization-activated currents, IH and IKIR, in rat dorsal motor nucleus of the vagus neurons in vitro. *J. Neurophysiol.* **71**, 1308–1317 (1994).

129. König, P., Engel, A. K. & Singer, W. Integrator or coincidence detector? The role of the cortical neuron revisited. *Trends Neurosci.* **19**, 130–137 (1996).

130. Swoap, S. J., Overton, J. M. & Garber, G. Effect of ambient temperature on cardiovascular parameters in rats and mice: a comparative approach. *Am. J. Physiol. Regul. Integr. Comp. Physiol.* **287**, R391-6 (2004).

131. Carnevali, L. & Sgoifo, A. Vagal modulation of resting heart rate in rats: the role of stress, psychosocial factors, and physical exercise. *Front. Physiol.* **5**, 118 (2014).

132. Marmerstein, J. T., McCallum, G. A. & Durand, D. M. Direct measurement of vagal tone in rats does not show correlation to HRV. *Sci. Rep.* **11**, 1210 (2021).

133. Beker, F., Weber, M., Fink, R. H. A. & Adams, D. J. Muscarinic and nicotinic ACh receptor activation differentially mobilize Ca2+ in rat intracardiac ganglion neurons. *J. Neurophysiol.* **90**, 1956–1964 (2003).

134. Ford, T. W. & McWilliam, P. N. The effects of electrical stimulation of myelinated and non-myelinated vagal fibres on heart rate in the rabbit. *J Physiol (Lond)* **380**, 341–347 (1986).

135. Black, J. W., Crowther, A. F., Shanks, R. G., Smith, L. H. & Dornhorst, A. C. A NEW ADRENERGIC BETARECEPTOR ANTAGONIST. *Lancet* **1**, 1080–1081 (1964).

136. Gorman, A. L. & Dunn, A. J. Beta-adrenergic receptors are involved in stress-related behavioral changes. *Pharmacol. Biochem. Behav.* **45**, 1–7 (1993).

137. Wohleb, E. S. *et al.* β-Adrenergic receptor antagonism prevents anxiety-like behavior and microglial reactivity induced by repeated social defeat. *J. Neurosci.* **31**, 6277–6288 (2011).

138. Repova, K., Aziriova, S., Krajcirovicova, K. & Simko, F. Cardiovascular therapeutics: A new potential for anxiety treatment? *Med. Res. Rev.* **42**, 1202–1245 (2022).

139. Critchley, H. D., Wiens, S., Rotshtein, P., Ohman, A. & Dolan, R. J. Neural systems supporting interoceptive awareness. *Nat. Neurosci.* **7**, 189–195 (2004).

140. Khalsa, S. S., Rudrauf, D., Feinstein, J. S. & Tranel, D. The pathways of interoceptive awareness. *Nat. Neurosci.* **12**, 1494–1496 (2009).

141. Hassanpour, M. S. *et al.* The insular cortex dynamically maps changes in cardiorespiratory interoception. *Neuropsychopharmacology* **43**, 426–434 (2018).

142. Woodman, R., Student, J., Miller, C. & Lockette, W. Ivabradine-Induced Bradycardia is Accompanied by Reduced Stress-Related Anxiety. *Am. J. Hypertens.* **36**, 316–323 (2023).

143. Saternos, H. C. *et al.* Distribution and function of the muscarinic receptor subtypes in the cardiovascular system. *Physiol. Genomics* **50**, 1–9 (2018).

144. Fisher, J. T., Vincent, S. G., Gomeza, J., Yamada, M. & Wess, J. Loss of vagally mediated bradycardia and bronchoconstriction in mice lacking M2 or M3 muscarinic acetylcholine receptors. *FASEB J.* **18**, 711–713 (2004).

145. Arsen'eva, M. G., Savchenko, O. N., Stepanov, G. S. & Ryzhova, R. K. [Hormonal function of the ovaries in women with breast hyperplasia]. *Vopr. Onkol.* **22**, 13–19 (1976).

146. Jiang, Y., Greenwood-Van Meerveld, B., Johnson, A. C. & Travagli, R. A. Role of estrogen and stress on the brain-gut axis. *Am. J. Physiol. Gastrointest. Liver Physiol.* **317**, G203–G209 (2019).

147. National Research Council (US) Committee for the Update of the Guide for the Care and Use of Laboratory Animals. *Guide for the care and use of laboratory animals*. (National Academies Press (US), 2011). doi:10.17226/12910.

148. Strain, M. M. *et al.* Early central cardiovagal dysfunction after high fat diet in a murine model. *Sci. Rep.* **13**, 6550 (2023).

149. Littlejohn, E. L., Espinoza, L., Lopez, M. M., Smith, B. N. & Boychuk, C. R. GABAA receptor currents in the dorsal motor nucleus of the vagus in females: influence of ovarian cycle and 5α-reductase inhibition. *J. Neurophysiol.* **122**, 2130–2141 (2019).

150. Daigle, T. L. *et al.* A Suite of Transgenic Driver and Reporter Mouse Lines with Enhanced Brain-Cell-Type Targeting and Functionality. *Cell* **174**, 465-480.e22 (2018).

151. Golden, S. A., Covington, H. E., Berton, O. & Russo, S. J. A standardized protocol for repeated social defeat stress in mice. *Nat. Protoc.* **6**, 1183–1191 (2011).

152. La-Vu, M., Tobias, B. C., Schuette, P. J. & Adhikari, A. To approach or avoid: an introductory overview of the study of anxiety using rodent assays. *Front. Behav. Neurosci.* **14**, 145 (2020).

153. Schneider, C. A., Rasband, W. S. & Eliceiri, K. W. NIH Image to ImageJ: 25 years of image analysis. *Nat. Methods* **9**, 671–675 (2012).

154. Rossi, J. *et al.* Melanocortin-4 receptors expressed by cholinergic neurons regulate energy balance and glucose homeostasis. *Cell Metab.* **13**, 195–204 (2011).

155. Berglund, E. D. *et al.* Melanocortin 4 receptors in autonomic neurons regulate thermogenesis and glycemia. *Nat. Neurosci.* **17**, 911–913 (2014).

156. Tsumori, T., Oka, T., Yokota, S., Niu, J.-G. & Yasui, Y. Intrapancreatic ganglia neurons receive projection fibers from melanocortin-4 receptor-expressing neurons in the dorsal motor nucleus of the vagus nerve of the mouse. *Brain Res.* **1537**, 132–142 (2013).

157. Prescott, S. L., Umans, B. D., Williams, E. K., Brust, R. D. & Liberles, S. D. An airway protection program revealed by sweeping genetic control of vagal afferents. *Cell* **181**, 574-589.e14 (2020).

158. Strain, M. M. *et al.* Dorsal motor vagal neurons can elicit bradycardia and reduce anxiety-like behavior. *iScience* **27**, 109137 (2024).

159. Holter, M. M., Saikia, M. & Cummings, B. P. Alpha-cell paracrine signaling in the regulation of beta-cell insulin secretion. *Front Endocrinol (Lausanne)* **13**, 934775 (2022).

160. Papatryphon, E. Early insulin and glucagon response associated with food intake in a teleost, the striped bass (Morone saxatilis). *Fish Physiology and Biochemistry 24, 31–39 (2001* (2001).

161. Trimigliozzi, K. A. *et al.* 1526-P: Cephalic Phase Insulin Release Requires Alpha Cells. *Diabetes* **72**, (2023).

162. Williams, D. L. Expecting to eat: glucagon-like peptide-1 and the anticipation of meals. *Endocrinology* **151**, 445–447 (2010).

163. Huang, Z. *et al.* Glucose-sensing glucagon-like peptide-1 receptor neurons in the dorsomedial hypothalamus regulate glucose metabolism. *Sci. Adv.* **8**, eabn5345 (2022).

164. Wan, S., Coleman, F. H. & Travagli, R. A. Glucagon-like peptide-1 excites pancreas-projecting preganglionic vagal motoneurons. *Am. J. Physiol. Gastrointest. Liver Physiol.* **292**, G1474-82 (2007).

165. Breit, S., Kupferberg, A., Rogler, G. & Hasler, G. Vagus Nerve as Modulator of the Brain-Gut Axis in Psychiatric and Inflammatory Disorders. *Front. Psychiatry* **9**, 44 (2018).

166. Woo-Jin Song, Deok-Hyeon Cheon, HeeIn Song, Daeun Jung, Hae Chan Park, Ju Yeong Hwang, Hyung-Jin Choi, Cherl NamKoong, Activation of ChAT+ neuron in dorsal motor vagus (DMV) increases blood glucose through the regulation of hepatic gene expression in mice, Brain Research, Volume 1829,2024, 148770, ISSN 0006-8993,

REFERENCES- (Chapter 2) Strain, Coney, Kauffman et al 2024

1. Corbett, E.K., Batten, T.F., Kaye, J.C., Deuchars, J., and McWilliam, P.N. (1999). Labelling of rat vagal preganglionic neurones by carbocyanine dye DiI applied to the heart. Neuroreport 10, 1177–1181. https://doi.org/ 10.1097/00001756-199904260-00004.

2. Hsieh, J.H., Chen, R.F., Wu, J.J., Yen, C.T., and Chai, C.Y. (1998). Vagal innervation of the gastrointestinal tract arises from dorsal motor nucleus while that of the heart largely from nucleus ambiguus in the cat. J. Auton. Nerv. Syst. 70, 38–50. https://doi.org/10.1016/ s0165-1838(98)00027-7.

3. Izzo, P.N., Deuchars, J., and Spyer, K.M. (1993). Localization of cardiac vagal preganglionic motoneurones in the rat: immunocytochemical evidence of synaptic inputs containing 5-hydroxytryptamine. J. Comp. Neurol. 327, 572–583. https://doi. org/10.1002/cne.903270408.

4. Massari, V.J., Johnson, T.A., and Gatti, P.J. (1995). Cardiotopic organization of the nucleus ambiguus? An anatomical and physiological analysis of neurons regulating atrioventricular conduction. Brain Res. 679, 227–240. https://doi.org/10.1016/0006- 8993(95)00227-h.

5. Standish, A., Enquist, L.W., and Schwaber, J.S. (1994). Innervation of the heart and its central medullary origin defined by viral tracing. Science 263, 232–234. https://doi. org/10.1126/science.8284675.

6. Ter Horst, G.J., Hautvast, R.W., De Jongste, M.J., and Korf, J. (1996). Neuroanatomy of cardiac activity-regulating circuitry: a transneuronal retrograde viral labelling study in the rat. Eur. J. Neurosci. 8, 2029–2041. https://doi.org/10.1111/j.1460-9568.1996. tb00723.x.

7. Geis, G.S., and Wurster, R.D. (1980). Cardiac responses during stimulation of the dorsal motor nucleus and nucleus ambiguus in the cat. Circ. Res. 46, 606–611. https://doi.org/10. 1161/01.res.46.5.606.

8. Gilbey, M.P., Jordan, D., Richter, D.W., and Spyer, K.M. (1984). Synaptic mechanisms involved in the inspiratory modulation of vagal cardio-inhibitory neurones in the cat. J. Physiol. 356, 65–78. https://doi.org/10. 1113/jphysiol.1984.sp015453.

9. McAllen, R.M., and Spyer, K.M. (1977). Bradycardia produced by iontophoretic activation of preganglionic vagal motoneurones [proceedings]. J. Physiol. 269, 49P.

10. Cheng, Z., Powley, T.L., Schwaber, J.S., and Doyle, F.J., 3rd (1999). Projections of the dorsal motor nucleus of the vagus to cardiac ganglia of rat atria: an anterograde tracing study. J. Comp. Neurol. 410, 320–341.

11. Ford, T.W., Bennett, J.A., Kidd, C., and McWilliam, P.N. (1990). Neurones in the dorsal motor vagal nucleus of the cat with non-myelinated axons projecting to the heart and lungs. Exp. Physiol. 75, 459–473. https:// doi.org/10.1113/expphysiol.1990.sp003423.

12. Jones, J.F., Wang, Y., and Jordan, D. (1995). Heart rate responses to selective stimulation of cardiac vagal C fibres in anaesthetized cats, rats and rabbits. J. Physiol. 489, 203–214. https://doi.org/10.1113/jphysiol.1995. sp021042.

13. Nosaka, S., Yamamoto, T., and Yasunaga, K. (1979). Localization of vagal cardioinhibitory preganglionic neurons with rat brain stem. J. Comp. Neurol. 186, 79–92. https://doi.org/ 10.1002/cne.901860106. 14. Taylor, E.W., Leite, C.A.C., Sartori, M.R., Wang, T., Abe, A.S., and Crossley, D.A., 2nd (2014). The phylogeny and ontogeny of autonomic control of the heart and cardiorespiratory interactions in vertebrates. J. Exp. Biol. 217, 690–703. https://doi.org/10. 1242/jeb.086199.

15. Taylor, E.W., Wang, T., and Leite, C.A.C. (2022). An overview of the phylogeny of cardiorespiratory control in vertebrates with some reflections on the 'Polyvagal Theory'. Biol. Psychol. 172, 108382. https://doi.org/10. 1016/j.biopsycho.2022.108382.

16. Laughton, W.B., and Powley, T.L. (1987). Localization of efferent function in the dorsal motor nucleus of the vagus. Am. J. Physiol. 252, R13–R25. https://doi.org/10.1152/ ajpregu.1987.252.1.R13.

17. Machhada, A., Marina, N., Korsak, A., Stuckey, D.J., Lythgoe, M.F., and Gourine, A.V. (2016). Origins of the vagal drive controlling left ventricular contractility. J. Physiol. 594, 4017–4030. https://doi.org/10. 1113/JP270984.

18. Machhada, A., Hosford, P.S., Dyson, A., Ackland, G.L., Mastitskaya, S., and Gourine, A.V. (2020). Optogenetic Stimulation of Vagal Efferent Activity Preserves Left Ventricular Function in Experimental Heart Failure. JACC. Basic Transl. Sci. 5, 799–810. https:// doi.org/10.1016/j.jacbts.2020.06.002.

19. Falvey, A., Palandira, S.P., Chavan, S.S., Brines, M., Tracey, K.J., and Pavlov, V.A. (2023). Electrical stimulation of the dorsal motor nucleus of the vagus regulates inflammation without affecting the heart rate. Preprint at bioRxiv. https://doi.org/10.1101/ 2023.05.17.541191.

20. Sporton, S.C., Shepheard, S.L., Jordan, D., and Ramage, A.G. (1991). Microinjections of 5-HT1A agonists into the dorsal motor vagal nucleus produce a bradycardia in the atenolol-pretreated anaesthetized rat. Br. J. Pharmacol. 104, 466–470. https://doi.org/10. 1111/j.1476-5381.1991.tb12452.x.

21. Thompson, D.A., Tsaava, T., Rishi, A., Nadella, S., Mishra, L., Tuveson, D.A., Pavlov, V.A., Brines, M., Tracey, K.J., and Chavan, S.S. (2023). Optogenetic stimulation of the brainstem dorsal motor nucleus ameliorates acute pancreatitis. Front. Immunol. 14, 1166212. https://doi.org/10.3389/fimmu. 2023.1166212.

22. Ottaviani, M.M., Vallone, F., Micera, S., and Recchia, F.A. (2022). Closed-Loop Vagus Nerve Stimulation for the Treatment of Cardiovascular Diseases: State of the Art and Future Directions. Front. Cardiovasc. Med. 9, 866957. https://doi.org/10.3389/fcvm.2022. 866957

23. Shivaswamy, T., Souza, R.R., Engineer, C.T., and McIntyre, C.K. (2022). Vagus Nerve Stimulation as a Treatment for Fear and Anxiety in Individuals with Autism Spectrum Disorder. J. Psychiatr. Brain Sci. 7, e220007. https://doi.org/10.20900/jpbs.20220007.

24. Groves, D.A., and Brown, V.J. (2005). Vagal nerve stimulation: a review of its applications and potential mechanisms that mediate its clinical effects. Neurosci. Biobehav. Rev. 29, 493–500. https://doi.org/10.1016/j. neubiorev.2005.01.004.

25. Pen˜ a, D.F., Engineer, N.D., and McIntyre, C.K. (2013). Rapid remission of conditioned fear expression with extinction training paired with vagus nerve stimulation. Biol. Psychiatry 73, 1071–1077. https://doi.org/10.1016/j. biopsych.2012.10.021.

26. Souza, R.R., Powers, M.B., Rennaker, R.L., McIntyre, C.K., Hays, S.A., and Kilgard, M.P. (2022). Timing of vagus nerve] stimula tion during fear extinction determines efficacy in a rat model of PTSD. Sci. Rep. 12, 16526.https://doi.org/10.1038/s41598-022-20301-9.

27. George, M.S., Ward, H.E., Jr., Ninan, P.T., Pollack, M., Nahas, Z., Anderson, B., Kose, S., Howland, R.H., Goodman, W.K., and Ballenger, J.C. (2008). A pilot study of vagus nerve stimulation (VNS) for treatment- resistant anxiety disorders. Brain Stimul. 1, 112–121. https://doi.org/10.1016/j.brs.2008. 02.001.

28. Lange, C.G., and James, W. (1967). The Emotions (Hafner Pub. Co.).

29. Hsueh, B., Chen, R., Jo, Y., Tang, D., Raffiee, M., Kim, Y.S., Inoue, M., Randles, S., Ramakrishnan, C., Patel, S., et al. (2023). Cardiogenic control of affective behavioural state. Nature 615, 292–299. https://doi.org/ 10.1038/s41586-023-05748-8.

30. McAllen, R.M., and Spyer, K.M. (1978). Two types of vagal preganglionic motoneurones projecting to the heart and lungs. J. Physiol. 282, 353–364. https://doi.org/10.1113/ jphysiol.1978.sp012468.

31. Mendelowitz, D. (1996). Firing properties of identified parasympathetic cardiac neurons in nucleus ambiguus. Am. J. Physiol. 271, H2609–H2614. https://doi.org/10.1152/ ajpheart.1996.271.6.H2609.

32. Browning, K.N., Renehan, W.E., and Travagli, R.A. (1999). Electrophysiological and morphological heterogeneity of rat dorsal vagal neurones which project to specific areas of the gastrointestinal tract. J. Physiol. 517, 521–532. https://doi.org/10.1111/j.1469- 7793.1999.0521t.x.

33. Jones, J.F., Wang, Y., and Jordan, D. (1998). Activity of C fibre cardiac vagal efferents in anaesthetized cats and rats. J. Physiol. 507, 869–880. https://doi.org/10.1111/j.1469- 7793.1998.869bs.x.

34. Cheng, Z., Zhang, H., Guo, S.Z., Wurster, R., and Gozal, D. (2004). Differential control over postganglionic neurons in rat cardiac ganglia by NA and DmnX neurons: anatomical evidence. Am. J. Physiol. Regul. Integr. Comp. Physiol. 286, R625–R633. https://doi. org/10.1152/ajpregu.00143.2003.

35. Cauley, E., Wang, X., Dyavanapalli, J., Sun, K., Garrott, K., Kuzmiak-Glancy, S., Kay, M.W., and Mendelowitz, D. (2015). Neurotransmission to parasympathetic cardiac vagal neurons in the brain stem is altered with left ventricular hypertrophy-induced heart failure. Am. J. Physiol. Heart Circ. Physiol. 309, H1281–H1287. https://doi. org/10.1152/ajpheart.00445.2015.

36. Madisen, L., Mao, T., Koch, H., Zhuo, J.M., Berenyi, A., Fujisawa, S., Hsu, Y.W.A., Garcia, A.J., 3rd, Gu, X., Zanella, S., et al. (2012). A toolbox of Cre-dependent optogenetic transgenic mice for light-induced activation and silencing. Nat. Neurosci. 15, 793–802. https://doi.org/10.1038/nn.3078.

37. McGovern, A.E., and Mazzone, S.B. (2010). Characterization of the vagal motor neurons projecting to the Guinea pig airways and esophagus. Front. Neurol. 1, 153. https://doi. org/10.3389/fneur.2010.00153.

38. Gee, M.M., Hornung, E., Gupta, S., Newton, A.J.H., Cheng, Z.J., Lytton, W.W., Lenhoff, A.M., Schwaber, J.S., and Vadigepalli, R. (2023). Unpacking the multimodal, multi- scale data of the fast and slow lanes of the cardiac vagus through computational modelling. Exp. Physiol. https://doi.org/10. 1113/EP090865.

39. Takanaga, A., Hayakawa, T., Tanaka, K., Kawabata, K., Maeda, S., and Seki, M. (2003). Immunohistochemical characterization of cardiac vagal preganglionic neurons in the rat. Auton. Neurosci. 106, 132–137. https:// doi.org/10.1016/S1566-0702(03)00127-9.

40. Kang, B.J., Chang, D.A., Mackay, D.D., West, G.H., Moreira, T.S., Takakura, A.C., Gwilt, J.M., Guyenet, P.G., and Stornetta, R.L. (2007). Central nervous system distribution of the transcription factor Phox2b in the adult rat. J. Comp. Neurol. 503, 627–641. https:// doi.org/10.1002/cne.21409.

41. Tao, J., Campbell, J.N., Tsai, L.T., Wu, C., Liberles, S.D., and Lowell, B.B. (2021). Highly selective brain-to-gut communication via genetically defined vagus neurons. Neuron 109, 2106–2115.e4. https://doi.org/10.1016/j. neuron.2021.05.004.

42. Christmas, A.J., and Maxwell, D.R. (1970). A comparison of the effects of some benzodiazepines and other drugs on aggressive and exploratory behaviour in mice and rats. Neuropharmacology 9, 17–29. https://doi.org/10.1016/0028-3908(70) 90044-4.

43. Crawley, J.N. (1985). Exploratory behavior models of anxiety in mice. Neurosci. Biobehav. Rev. 9, 37–44. https://doi.org/10. 1016/0149-7634(85)90030-2.

44. Lister, R.G. (1987). The use of a plus-maze to measure anxiety in the mouse. Psychopharmacology (Berl) 92, 180–185. https://doi.org/10.1007/BF00177912.

45. Doods, H., Entzeroth, M., and Mayer, N. (1991). Cardioselectivity of AQ-RA 741, a novel tricyclic antimuscarinic drug. Eur. J. Pharmacol. 192, 147–152. https://doi.org/10. 1016/0014-2999(91)90081-z.

46. Cohen, V.I., Jin, B., Gitler, M.S., Delacruz, R.A., Boulay, S.F., Sood, V.K., Zeeberg, B.R., and Reba, R.C. (1995). Novel Potent and M(2)- Selective Antimuscarinic Compounds Which Penetrate the Blood-Brain-Barrier. Eur. J. Med. Chem. 30, 61–69. https://doi.org/10. 1016/0223-5234(96)88210-9.

47. Travagli, R.A., Gillis, R.A., Rossiter, C.D., and Vicini, S. (1991). Glutamate and GABA- mediated synaptic currents in neurons of the rat dorsal motor nucleus of the vagus. Am. J. Physiol. 260, G531–G536. https://doi.org/10. 1152/ajpgi.1991.260.3.G531.

48. Travagli, R.A., and Gillis, R.A. (1994). Hyperpolarization-activated currents, IH and IKIR, in rat dorsal motor nucleus of the vagus neurons in vitro. J. Neurophysiol. 71, 1308– 1317. https://doi.org/10.1152/jn.1994.71. 4.1308.

49. Coverdell, T.C., Abraham-Fan, R.J., Wu, C., Abbott, S.B.G., and Campbell, J.N. (2022). Genetic encoding of an esophageal motor circuit. Cell Rep. 39, 110962. https://doi.org/ 10.1016/j.celrep.2022.110962.

50. Veerakumar, A., Yung, A.R., Liu, Y., and Krasnow, M.A. (2022). Molecularly defined circuits for cardiovascular and cardiopulmonary control. Nature 606, 739–746. https://doi.org/10.1038/s41586- 022-04760-8.

51. Ko¨ nig, P., Engel, A.K., and Singer, W. (1996). Integrator or coincidence detector? The role of the cortical neuron revisited. Trends Neurosci. 19, 130–137. https://doi.org/10. 1016/s0166-2236(96)80019-1.

52. Swoap, S.J., Overton, J.M., and Garber, G. (2004). Effect of ambient temperature on cardiovascular parameters in rats and mice: a comparative approach. Am. J. Physiol. Regul. Integr. Comp. Physiol. 287, R391–R396. https://doi.org/10.1152/ajpregu.00731.2003. Carnevali, L., and Sgoifo, A. (2014). Vagal modulation of resting heart rate in rats: the role of stress, psychosocial factors, and physical exercise. Front. Physiol. 5, 118. https://doi.org/10.3389/fphys.2014.00118. Marmerstein, J.T., McCallum, G.A., and Durand, D.M. (2021). Direct measurement of vagal tone in rats does not show correlation to HRV. Sci. Rep. 11, 1210. https://doi.org/10. 1038/s41598-020-79808-8.

53. Standish, A., Enquist, L.W., Escardo, J.A., and Schwaber, J.S. (1995). Central neuronal circuit innervating the rat heart defined by transneuronal transport of pseudorabies virus. J. Neurosci. 15, 1998–2012. https://doi. org/10.1523/JNEUROSCI.15-03-01998.1995. Beker, F., Weber, M., Fink, R.H.A., and Adams, D.J. (2003). Muscarinic and nicotinic ACh receptor activation differentially mobilize Ca2+ in rat intracardiac ganglion neurons. J. Neurophysiol. 90, 1956–1964. https://doi.org/10.1152/jn.01079.2002.

54. Ford, T.W., and McWilliam, P.N. (1986). The effects of electrical stimulation of myelinated and non-myelinated vagal fibres on heart rate in the rabbit. J. Physiol. 380, 341–347. https:// doi.org/10.1113/jphysiol.1986.sp016289. James, W. (1884). What is an emotion? Mind 9, 188–205.

55. Black, J.W., Crowther, A.F., Shanks, R.G., Smith, L.H., and Dornhorst, A.C. (1964). A New Adrenergic Betareceptor Antagonist. Lancet 1, 1080–1081. https://doi.org/10. 1016/s0140-6736(64)91275-9.

56. Gorman, A.L., and Dunn, A.J. (1993). Beta- adrenergic receptors are involved in stress- related behavioral changes. Pharmacol. Biochem. Behav. 45, 1–7. https://doi.org/10. 1016/0091-3057(93)90078-8.

57. Wohleb, E.S., Hanke, M.L., Corona, A.W., Powell, N.D., Stiner, L.M., Bailey, M.T., Nelson, R.J., Godbout, J.P., and Sheridan, J.F. (2011). beta-Adrenergic receptor antagonism prevents anxiety-like behavior and microglial reactivity induced by repeated social defeat. J. Neurosci. 31, 6277–6288. https://doi.org/10.1523/JNEUROSCI.0450- 11.2011.

58. Repova, K., Aziriova, S., Krajcirovicova, K., and Simko, F. (2022). Cardiovascular therapeutics: A new potential for anxiety treatment? Med. Res. Rev. 42, 1202–1245. https://doi.org/10.1002/med.21875. Critchley, H.D., Wiens, S., Rotshtein, P., Ohman, A., and Dolan, R.J. (2004). Neural systems supporting interoceptive awareness.

64. Khalsa, S.S., Rudrauf, D., Feinstein, J.S., and Tranel, D. (2009). The pathways of interoceptive awareness. Nat. Neurosci. 12, 1494–1496. https://doi.org/10.1038/nn.2411.
65. Hassanpour, M.S., Simmons, W.K., Feinstein, J.S., Luo, Q., Lapidus, R.C., Bodurka, J., Paulus, M.P., and Khalsa, S.S. (2018). The Insular Cortex Dynamically Maps Changes in Cardiorespiratory Interoception. Neuropsychopharmacology 43, 426–434. https://doi.org/10.1038/npp.2017.154.
66. Woodman, R., Student, J., Miller, C., and Lockette, W. (2023). Ivabradine-Induced Bradycardia is Accompanied by Reduced Stress-Related Anxiety. Am. J. Hypertens. 36, 316–323. https://doi.org/10.1093/ajh/ hpad019.

67. Saternos, H.C., Almarghalani, D.A., Gibson, H.M., Meqdad, M.A., Antypas, R.B., Lingireddy, A., and AbouAlaiwi, W.A. (2018). Distribution and function of the muscarinic receptor subtypes in the cardiovascular system. Physiol. Genomics 50, 1–9. https:// doi.org/10.1152/physiolgenomics. 00062.2017.

68. Fisher, J.T., Vincent, S.G., Gomeza, J., Yamada, M., and Wess, J. (2004). Loss of vagally mediated bradycardia and bronchoconstriction in mice lacking M2 or M3 muscarinic acetylcholine receptors. FASEB J 18, 711–713. https://doi.org/10.1096/fj.03- 0648fje.

69. Ehlert, F.J., Ostrom, R.S., and Sawyer, G.W. (1997). Subtypes of the muscarinic receptor in smooth muscle. Life Sci. 61, 1729–1740. https://doi.org/10.1016/s0024-3205(97) 00433-5.

70. Jiang, Y., Greenwood-Van Meerveld, B., Johnson, A.C., and Travagli, R.A. (2019). Role of estrogen and stress on the brain-gut axis. Am. J. Physiol. Gastrointest. Liver Physiol. 317, G203–G209. https://doi.org/10.1152/ ajpgi.00144.2019.

71. Coverdell, T.C., Abbott, S.B.G., and Campbell, J.N. (2024). Molecular cell types as functional units of the efferent vagus nerve. Semin. Cell Dev. Biol. 156, 210–218. https:// doi.org/10.1016/j.semcdb.2023.07.007.

72. Bourane, S., Grossmann, K.S., Britz, O., Dalet, A., Del Barrio, M.G., Stam, F.J., Garcia- Campmany, L., Koch, S., and Goulding, M. (2015). Identification of a spinal circuit for light touch and fine motor control. Cell 160, 503–515. https://doi.org/10.1016/j.cell.2015. 01.011.

73. National Research Council (US) Committee for the Update of the Guide for the Care and Use of Laboratory Animals (2011). Guide for the Care and Use of Laboratory Animals. https://doi.org/10.17226/12910.

74. Strain, M.M., Espinoza, L., Fedorchak, S., Littlejohn, E.L., Andrade, M.A., Toney, G.M., and Boychuk, C.R. (2023). Early central cardiovagal dysfunction after high fat diet in a murine model. Sci. Rep. 13, 6550. https://doi. org/10.1038/s41598-023-32492-w.

75. Littlejohn, E.L., Espinoza, L., Lopez, M.M., Smith, B.N., and Boychuk, C.R. (2019). GABA(A) receptor currents in the dorsal motor nucleus of the vagus in females: influence of ovarian cycle and 5alpha- reductase inhibition. J. Neurophysiol. 122, 2130–2141. https://doi.org/10.1152/jn. 00039.2019.

76. Daigle, T.L., Madisen, L., Hage, T.A., Valley, M.T., Knoblich, U., Larsen, R.S., Takeno, M.M., Huang, L., Gu, H., Larsen, R., et al. (2018). A Suite of Transgenic Driver and Reporter Mouse Lines with Enhanced Brain- Cell-Type Targeting and Functionality. Cell 174, 465–480.e22. https://doi.org/10.1016/j. cell.2018.06.035.

77. Golden, S.A., Covington, H.E., Berton, O., and Russo, S.J. (2011). A standardized protocol for repeated social defeat stress in mice. Nat. Protoc. 6, 1183–1191. https://doi. org/10.1038/nprot.2011.361.

78. La-Vu, M., Tobias, B.C., Schuette, P.J., and Adhikari, A. (2020). To Approach or Avoid: An Introductory Overview of the Study of Anxiety Using Rodent Assays. Front. Behav. Neurosci. 14, 145. https://doi.org/10.3389/fnbeh.2020. 00145.

79. Schneider, C.A., Rasband, W.S., and Eliceiri, K.W. (2012). NIH Image to ImageJ: 25 years of image analysis. Nat. Methods 9, 671–675. https://doi.org/10.1038/nmeth.2089.